Imperial College London

Guided waves for power plant applications

by

Sam Fletcher

A thesis submitted to Imperial College London for the Degree of

Engineering Doctorate

Department of Mechanical Engineering

Imperial College London

London, SW7 2AZ

October 2011

Abstract

This study explores the possibility of using the guided wave non-destructive testing technique for power plant applications. Guided waves are already used extensively in the petrochemical industry, however the nature of pipework in a power station has meant that guided waves have not been studied for use in this environment. Power station pipework is more challenging to inspect than petrochemical pipework using guided waves because the pipelines tend to be shorter, and the feature density is much higher, with welds, hangers, supports and bends all contributing to make analysis of results more difficult.

A particular focus of the study was detecting axially aligned defects in pipes, a problem that emerged in the UK coal power station fleet in 2006. Guided waves provided a desirable inspection technique because large volumes of pipework can be screened quickly, this being particularly advantageous due to the high volume of pipework that requires inspection.

Two guided wave approaches to detecting axial cracks in pipes were pursued. Long-range guided waves were initially examined as they are able to examine large quantities of pipework in a short amount of time. Unfortunately, long-range guided waves are sensitive to the change in cross-sectional-area of a pipe, and axially aligned defects produce only a very small change in cross-section. Therefore guided waves were not sensitive enough to detect a critically sized axial crack. The sensitivity of long-range guided waves was improved using a synthetic focusing algorithm, although this was still insufficient to detect a critically sized defect.

The second guided wave approach was to utilise circumferential guided waves to detect axial cracks in pipes. Although many of the advantages of long-range guided waves are lost, using circumferential guided waves is much faster than an alternative manual ultrasonic inspection. The results of circumferential guided wave experiments suggest that they would be capable of detecting a critically sized axial crack in a pipe.

Besides attempting to detect axial cracks guided waves have been tested on a small number of other power station pipework systems. These systems were tested as a way

to examine the viability of using guided waves as a general inspection tool at a power station. Although guided waves are not suitable for every application, there are a good number of potential applications due to the wide variety of pipework systems at a power station.

Acknowledgements

First and foremost I would like to acknowledge my supervisors, Professor Mike Lowe and Dr Colin Brett, who have provided invaluable support throughout my studies. I would also like to thank Professor Chris Scruby for introducing me to the course and offering encouragement for the last four years.

The members of the Imperial College NDT laboratory and the NDT section at E.ON New Build and Technology have my sincerest thanks for the help they have provided, from helping me to get started when I first began my course, to showing me around various power stations and teaching me what performing an inspection on site is really like. In particular Professor Peter Cawley from the Imperial College NDT laboratory and John Trelawny from E.ON New Build and Technology have given me plenty of assistance.

I do not think I could have completed the course without the support of the other members of my EngD cohort, Robin, Keith, Chris, Gabriel and Kit, and other members of the EngD scheme. Every time we met I was thoroughly entertained and I could not have asked for a nicer group of people to work with.

Finally I would like to thank both the RCNDE and E.ON New Build and Technology, for providing the financial support necessary to complete the course, and the resources for me to complete my work.

Contents

List of Figures **9**

List of Tables **20**

1 Introduction **22**

1.1 Background 22

1.2 Guided waves in a power station environment 25

1.3 Outline of thesis 26

1.4 Notes on units and terminology 28

2 Guided wave properties and their exploitation **29**

2.1 History of guided waves 29

2.1.1 Differences between guided wave ultrasonic testing and standard ultrasonic testing 30

2.2 Guided waves in free plates 32

2.2.1 Dispersion curves 35

2.2.2 Multi-modal nature of guided waves 37

2.3 Guided waves in free pipes 39

2.3.1 Mode families of guided waves in pipes 40

2.3.2 Effect of bends 41

2.4 Circumferential guided waves in free pipes 42

2.5 Scattering of guided waves from material discontinuities 44

2.5.1 Defect-like discontinuities in plates 45

2.5.2 Defect-like discontinuities in pipes 48

2.5.3 Other discontinuities 52

2.6 Generating guided waves for the purpose of non-destructive testing . . . 53

2.7 Use of guided waves in non-destructive evaluation 55

2.8 Conclusions 60

3 Axially aligned defects in pipes **61**

3.1 Introduction 61

3.2 Mode choice 64

3.3 Finite element modelling 65

3.4 Experimental procedure 67

3.5 Results and discussion 69

3.5.1 Crack length - through-thickness crack 74

3.5.2 Crack length - Part-depth crack 77

3.5.3 Toneburst frequency 80

3.5.4 Crack Depth 82

3.5.5 Crack Width 84

3.6 Conclusions 86

4 Focused guided waves **88**

4.1 Introduction 88

4.2 Benefits of focusing 88

4.2.1 Synthetic focusing algorithms 89

4.3 Focusing Using Common Source Method 91

4.4 Modelling and experimental procedure 94

4.5 Results and Discussion 95

4.5.1 Reflection Amplitude as a Function of Crack Length 95

4.5.2 Frequency Dependence 97

4.5.3 Crack Depth 99

4.6 Conclusions 100

5 Circumferential guided waves **102**

5.1 Introduction 102

5.2 Principles of circumferential guided wave inspection 104

5.3 Mode selection 113

5.3.1 $S0_C$ Mode 113

5.3.2 $A0_C$ Mode 113

5.3.3 $SH0_C$ Mode 114

5.4 Finite element modelling 115

5.5 Experimental procedure 118
5.6 Results and discussion 121
5.6.1 Crack Length 123
5.6.2 Crack Depth 125
5.6.3 Smallest detectable critical defect 130
5.7 Conclusions 132

6 Guided wave inspection of sootblower pipework 135

6.1 Introduction 135
6.2 Wavemaker G3 137
6.3 Sootblower system description 139
6.4 Proposed pipework classification system 142
6.5 Experimental procedure 143
6.5.1 Guided wave procedure 143
6.5.2 Surface scanning procedure 146
6.6 Results and discussion 148
6.7 Conclusions 156

7 Other applications 158

7.1 Port of Liverpool steam line 159
7.1.1 Introduction 159
7.1.2 Pipeline description 159

7.1.3 Inspection procedure 162

7.1.4 Results 164

7.1.5 Conclusions 168

7.2 Fiddler's Ferry oil line 169

7.2.1 Introduction 169

7.2.2 Pipeline description 169

7.2.3 Inspection procedure 170

7.2.4 Results 171

7.2.5 Conclusions 174

8 Conclusions and future work **176**

8.1 Axial cracking in pipes 177

8.2 Sootblower pipework 178

8.3 Discussion of use of guided wave testing for power plant applications . . 179

8.4 Discussion of potential of guided wave testing for future power plant applications 180

8.5 Key findings 181

8.6 Recommendations 182

References **183**

List of Publications **193**

List of Figures

1.1 Picture of cold-formed bend after an axial crack resulted in the pipe rupturing. 23

1.2 Sectioned 4" pipe with longitudinally aligned pitting. Axial cracks have a tendency to develop at the bottom of these pits when they are aligned in this way. Note the pitting is highly localised to one circumferential position with the rest of the pipe remaining relatively smooth. 23

1.3 Profile of axial crack in a pipe. The view is along the axis of the pipe. . . 24

1.4 Some examples of pipework found in a power station. 26

2.1 Figure illustrating the difference between standard ultrasonic testing and guided waves. Arrangement in both cases is pulse-echo and arrows indicate direction of wave propagation. 32

2.2 Diagram of plate in a Cartesian coordinate system. The dashed line represents the midpoint at which the origin of z is defined. 34

2.3 Phase velocity dispersion curves for a steel plate. The x-axis is the frequency-thickness product so the curves scale with plate thickness and signal frequency. 36

2.4 Group velocity dispersion curves for a steel plate. The x-axis is the frequency-thickness product so the curves scale with plate thickness and signal frequency. 37

2.5 Mode shapes of the fundamental symmetric S0, left, and fundamental antisymmetric A0, modes. In this figure the y direction is into the page. . 38

2.6 Group velocity dispersion curves for a 5 inch schedule 120 steel pipe with an outer diameter of 141.3mm and a wall thickness of 12.7mm. The axisymmetric modes have been highlighted in bold. 40

2.7 Phase velocity dispersion curve for circumferential guided waves in a 5 inch schedule 120 steel pipe with an outer diameter of 141.3mm and a wall thickness of 12.7mm. The radius-thickness ratio for this pipe is approximately 5.7. 44

2.8 (Reproduced from [71]) Predicted A0 reflection coefficient from a crack in a plate versus crack depth, for various frequencies. 46

2.9 (Reproduced from [69]) Measured and predicted reflection coefficients for a through-thickness notch in a 76-mm (nominal 3-inch) diameter, 5.5-mm wall thickness pipe at 70 kHz as a function of the percentage circumferential extent of the notch. 50

2.10 (Reproduced from [36]) Variation of reflection ratio with defect depth for zero axial length at various frequencies, axisymmetric defect. Results are from axisymmetric model with $T(0,1)$ incident in 3 inch (solid lines) and 24 inch pipes (dashed lines). The empty circles indicate the depth value for which ka=1 at each frequency. 51

2.11 Picture of commercial guided wave equipment produced by Guided Ultrasonics Ltd. This is the G3 instrument attached to a low-profile 5 inch solid transducer ring. 56

2.12 (Reproduced from [92]) Schematic snapshot of Creeping and Head wave generation from a probe at the ultrasonic critical angle. Illustrated are the Creeping wave (C), Head wave (H), direct compression waves (P) and shear waves (S) generated due to the finite size of the probe. 59

3.1 Schematic diagram of transducer layout and defect location on pipe. . . 62

3.2 Demonstration of how overlapping signals can prevent calculation of reflection coefficient in the frequency domain. The time signal is in blue and a Hilbert transform in red. 63

3.3 Demonstration of how finite element mesh is modified to include a crack. a) The mesh is shown in plan view and b) The 3D solid mesh is shown looking axially along the pipe. 67

3.4 Picture of experimental set up. The pipe is mounted on a milling machine and a transducer ring can be seen on the near end of the pipe. 68

3.5 Picture of FE pipe model with $T(0,1)$ wave mode reflecting from an axial crack. The crack nodes are highlighted in red and the colour scale represents amplitude on a linear scale. The amplitudes have been artificially increased to make the reflected wave more visible. The incident toneburst has a centre frequency of 50 kHz and the crack length is equal to the wavelength of the incident toneburst. 70

3.6 Typical time traces for FE and experimental data showing the reflection of guided waves from an axial crack. 71

3.7 Finite element time trace data focusing on the crack reflection 72

3.8 Time trace of reflection from a crack with a longer spatial length than the incident toneburst. The reflections from the near tip and far tip of the crack are spatially separated demonstrating that the reflection from the far tip of the crack is of much higher amplitude than the reflection from the near tip of the crack. 73

3.9 Diagram of reflection of the $T(0,1)$ mode from an axial crack in a pipe. The numbers represent individual processes and are explained in detail in the main text. 73

3.10 Comparison of finite element and experimental data for the reflection coefficient as a function of crack length for a through-thickness crack in a pipe, over a range of frequencies. The crack length is scaled with wavelength. 75

3.11 FE results displaying reflection coefficient as a function of crack length over a range of incident toneburst frequencies. 77

3.12 Comparison of finite element and experimental data for the reflection coefficient as a function of crack length for a part depth crack of 80% through-thickness extent in a pipe, over a range of frequencies. The crack length is scaled with the wavelength of the incident toneburst. . . . 78

3.13 FE time-trace of reflection from a crack with a through-thickness extent of 80% and a length of 6λ, demonstrating the difference in amplitude between the near tip and far tip reflections for a part depth crack. 79

3.14 Effect of incident toneburst centre frequency on reflection coefficient from a through-thickness axial crack in a pipe with a radius of 70mm. The crack length is half the wavelength of the incident toneburst at all frequencies, close to the crack length of the first peak in reflection coefficient seen in Figure 3.10. 80

3.15 Reflection coefficient as a function of both toneburst centre frequency and pipe diameter, with a constant frequency-diameter product of 7 MHz-mm. The crack length is equal to the wavelength of the incident toneburst. 81

3.16 Effect of crack depth on the reflection coefficient from an axial crack in a pipe. Data is presented for toneburst frequencies of 30 kHz, 40 kHz and 50 kHz and reflection amplitudes are normalised to the reflection amplitude of a through-thickness crack. In all cases the crack length was equivalent to the wavelength of the incident toneburst. 83

3.17 FE results displaying reflection coefficient as a function of crack depth for incident toneburst frequencies of 30 kHz, 40 kHz and 50 kHz. In all cases the crack length was equivalent to the wavelength of the incident toneburst. 84

3.18 Effect of crack width on the reflection coefficient from an axial crack in a pipe with incident toneburst centre frequencies of 30 kHz, 40 kHz and 50 kHz. Crack width is scaled with wavelength of incident toneburst and crack length is equal to the wavelength of the incident toneburst. 85

4.1 Group velocity dispersion curves for a nominal 5" schedule 120 steel pipe with an outer diameter of 141mm and a wall thickness of 12.5mm. Important modes are highlighted in bold. The figure was generated using the software Disperse [86]. 90

4.2 Unrolled pipe display images produced using CSM algorithm. Images are of a through-wall crack with an axial extent of 32mm with both (a) FE data , and (b) experimental data shown . The grey scale is linear with the images normalised to the peak amplitude of the defect signal. Crack location is indicated by white line with width exaggerated. The centre frequency of the incident toneburst was 50kHz. 93

4.3 Comparison of FE data and experimental measurements showing how reflection coefficient depends on crack length. Focused and unfocused results are shown for a through-thickness crack. FE data is shown as a dashed line and experimental data is shown as a solid line. 96

4.4 Comparison of FE data and experimental measurements showing how reflection coefficient depends on crack length. Focused and unfocused results are shown for an 80% deep crack. FE data is shown as a dashed line and experimental data is shown as a solid line. 96

4.5 Results of FE models indicating how incident toneburst frequency affects reflection coefficient for both focused and unfocused guided waves. In all cases the crack length was equal to half the wavelength of the incident toneburst. 98

4.6 Results of FE models indicating how crack depth affects reflection coefficient for both focused and unfocused guided waves with a centre frequency of 50kHz. The crack length is equal to half the wavelength of the incident toneburst. 100

5.1 Schematic diagram illustrating a circumferential guided wave inspection. 105

5.2 Phase velocity dispersion curves for circumferential guided waves in a steel pipe scaled with frequency-thickness product. The ratio of outer diameter to inner diameter is 1.22. The dashed vertical line indicates the cut-off frequency of the $A1_C$ and $SH1_C$ modes at 1.63 MHz-mm. 108

5.3 View of cross-section of pipe representing the dead-zones when conducting a circumferential guided wave inspection. 110

5.4 Length of dead zone in millimetres as a function of Frequency-thickness for the three fundamental circumferential guided wave modes. Dead-zone calculations in this figure are only valid for pipework with a ratio of outer diameter to pipe thickness of 11.2. 111

5.5 Minimum size of dead-zone for the $SH0_C$ mode as a function of ratio between outer diameter and wall thickness. The particular case of a five inch schedule 120 pipe is marked. The ranges of ratios for certain schedules are also displayed. 112

5.6 Image of finite element model used to study circumferential guided waves. Crack nodes and monitoring nodes are highlighted. The excitation node is at the centre of the array of receiver nodes. The $SH0_C$ wave propagating circumferentially and the $S0_C$ mode propagating axially are also labelled. 116

5.7 Experimental set-up for circumferential guided wave experiments. A 1m section of six inch pipe is mounted on a milling machine to cut axial slots. An aluminium bar used to hold the transducer in place is visible in front of the pipe. 119

5.8 Image of equipment used to attach transducers to pipe. a) shows the aluminium bar holding transducers in place with transducer cables protruding from the centre of the bar. b) is a side view of the bar with both transducers shown held against the pipe. 120

5.9 Function generator and oscilloscope used to generate and monitor circumferential guided wave signals. The function generator is on the bottom and the oscilloscope on the top. 121

5.10 Typical time trace data from both a finite element model and a laboratory experiment. Defect signal is from an axial notch with 60mm axial extant and 50% through-thickness extent. Toneburst centre frequency is 65 kHz. 122

5.11 Typical time trace data from finite element modelling for $A0_C$ and $S0_C$ modes. Defect signal is from an axial crack infinite axial extant and 50% through-thickness extent. Toneburst centre frequency in both cases is 90 kHz. 123

5.12 Comparison between FE and experimental data showing the reflection coefficient of the $SH0_C$ mode from an axial crack in a pipe as a function of crack length. The crack has a through-thickness extent of 50% and the incident toneburst centre frequency is 65 kHz. 124

5.13 Finite element data for reflection coefficient as a function of crack length extending to full length of pipe section. Cracks are through-thickness and toneburst centre frequency is 75 kHz. 125

5.14 Comparison between FE and experimental data showing the reflection coefficient of the $SH0_C$ mode from an axial crack in a pipe as a function of crack depth. The crack has an axial length of 120mm and the incident toneburst centre frequency is 65 kHz. 126

5.15 FE results plotting reflection coefficient as a function of crack depth with incident $A0_C$ mode. Results are presented for separate cases of cracks emanating from the inner surface and outer surface. 128

5.16 FE results plotting reflection coefficient as a function of crack depth with incident $S0_C$ mode. Results are presented for separate cases of cracks emanating from the inner surface and outer surface. 129

5.17 Values of circumferential stress and displacement for $S0_C$ mode as a function of position in pipe wall. Radial position of 0mm represents inner surface and radial position of 12.7mm represents outer surface. Displacement is displayed in blue and stress in red. 130

5.18 FE data showing reflection coefficient of the $SH0_C$ and $A0_C$ modes as a function of crack length for a crack with a through-wall extent of 20%. The centre frequency of the incident toneburst is 90 kHz. 131

6.1 Schematic of sootblower supply pipework on A side of a boiler at Kingsnorth power station. The primary distribution line is highlighted in blue and inspection locations are indicated with red circles. The black dots represent where the sootblower supply system is attached to individual sootblowers, with the associated numbers being the sootblower designations. 140

6.2 Schematic of sootblower supply pipework on B side of a boiler at Kingsnorth power station. The primary distribution line is highlighted in blue and inspection locations are indicated with red circles. The black dots represent where the sootblower supply system is attached to individual sootblowers, with the associated numbers being the sootblower designations. 141

6.3 Photograph showing reducer connecting 2 inch supply to sootblower B29 with 2.5 inch main supply pipework 142

6.4 Expanded view of sootblower pipework on 'A-side' of boiler centred on inspection locations. Arrows indicate direction of steam flow. Red circles indicate inspection positions. 144

6.5 Schematic diagram of sootblower pipework where inspections were performed on 'B-side' of unit 4. Red and black circles indicate inspection locations and black circles indicate where pipework enters individual sootblowers. Arrows indicate direction of steam flow. 145

6.6 White light scanner used to scan the inner surface of a pipe section and provide quantitative data about the condition of it. 147

6.7 Guided Wave results for a brand new section of 2 inch pipe intended to replace existing sootblower pipework. Because there are no welds the end-wall reflections are used to calibrate the DAC curves. The noise level is 32 dB below the weld DAC, in the section between 0m and the first end-wall reflection 149

6.8 Guided Wave results for supply line to sootblower 29B. 150

6.9 Guided wave results for sootblower 29B with expanded y-axis. 150

6.10 Logarithmic plot of guided wave results from sootblower pipework illustrating the difference between coherent noise and electronic noise. The blue dashed line indicates the noise level. 151

6.11 Unrolled pipe image (a) and inner surface profile (b) of sootblower section 29-2. The colour scale in the pipe image indicates displacement from nominal pipe bore with red being further from the centre of the pipe. The surface profile diagram also displays the nominal position of the outer surface of the pipe, at 4.5mm, to provide a sense of scale. 153

7.1 Schematic diagram of process steam lines where they leave Port of Liverpool power station. The northern line is to the left of the diagram and the southern line to the right. Welds are indicated with circled numbers. 160

7.2 Picture of steam lines leaving Port of Liverpool power station with northern and southern lines labelled. A road crossing can be seen on the northern line. 161

7.3 Picture of clamp used to hold steam line in place at Port of Liverpool power station. 161

7.4 Picture of inflatable transducer ring used to perform guided wave inspections at Port of Liverpool power station. 163

7.5 Guided wave results from Port of Liverpool power station demonstrating the reflection amplitude of clamped support. 165

7.6 Guided wave time trace for a section of pipe on a Port of Liverpool steam line over a range of frequencies, with clamped supports and welds labelled. The number in parentheses in the sub-figure description is the frequency regime as stated when using the Wavemaker G3 system. Amplitude is scaled for clarity. 166

7.7 Guided wave results from a long straight section of main steam line at Port of Liverpool power station. 167

7.8 Picture of section of Fiddler's Ferry BUFO oil line taking a curved path around a cooling tower. 170

7.9 Ring of transducers in use for guided wave inspection. 171

7.10 Pipe layout of fuel oil line at Fiddler's Ferry power station. Pipeline is colour coded according to condition of pipework based on guided wave inspections. (Not to scale). 173

7.11 Sample guided wave result for a good piece of pipe. 174

7.12 Sample guided wave result for a medium piece of pipe. 174

7.13 Sample guided wave result for a poor piece of pipe. 175

List of Tables

3.1 Rate of increase of reflection coefficient from an axial crack in a pipe with respect to crack width at 30 kHz, 40 kHz and 50 kHz. Crack widths are presented relative to the wavelength of the incident toneburst and as an absolute value. 86

6.1 Table displaying the RMS, noise level and ultrasonic attenuation for sections of sootblower pipework. The RMS was measured using a white light scanning device and the noise level and attenuation were measured using guided wave results. The RMS value for the clean pipe has not been measured, but is assumed to be very small as the pipe has not been in service. 154

Chapter 1

Introduction

1.1 Background

In 2006 a steam pipe at a coal-fired power station ruptured causing a large amount of damage [81], with a picture of the pipe after the rupture presented in Figure 1.1. The cause of the rupture was found to be an axial crack that had developed in a cold-formed bend at a location where pitting occurs, with the crack subsequently found to be emanating from the bottom of a group of aligned pits. Cold-formed bends are created by bending a piece of straight pipe after it has been manufactured, rather than during manufacture. They are typically smooth large radius bends with the radius being around five times larger than the diameter of the pipe.

Due to the nature of the UK electricity market many power stations that were designed for base load are now used intermittently. Standing water within pipes is therefore common and this in turn causes pitting to develop on the internal surface of the pipe. The pits tend to form in a line along the axis of the pipe at the water line and if this happens cracking can develop from the bottom of the pits. A picture of this type of pitting is presented in Figure 1.2. Here pits have aligned longitudinally along the pipe at a very specific circumferential position, leaving the rest of the pipe defect free. When pitting occurs in this way there is a greatly increased risk of axial cracking. If crack growth is allowed to continue the pipe eventually ruptures, as happened in 2006, causing a lot of

Figure 1.1: Picture of cold-formed bend after an axial crack resulted in the pipe rupturing.

damage and potential loss of life.

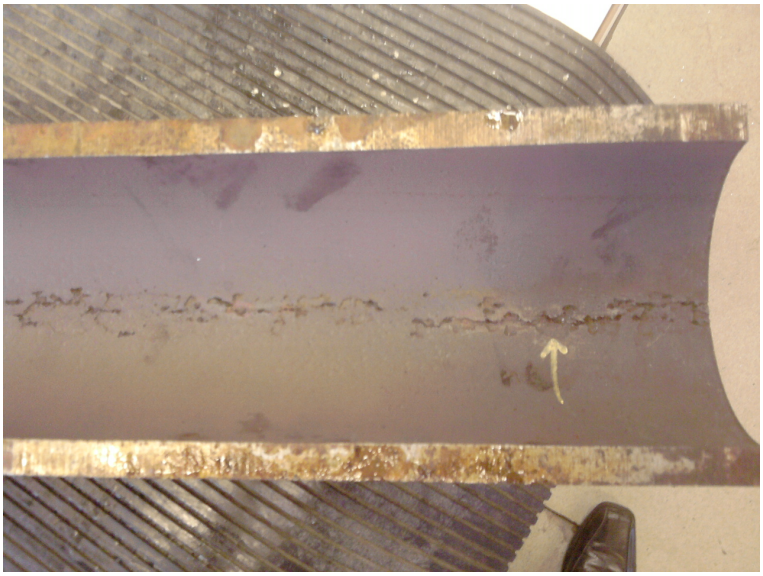

Figure 1.2: Sectioned 4" pipe with longitudinally aligned pitting. Axial cracks have a tendency to develop at the bottom of these pits when they are aligned in this way. Note the pitting is highly localised to one circumferential position with the rest of the pipe remaining relatively smooth.

In Figure 1.3 the profile of an axial crack can be seen as viewed along the axis of the pipe. In the picture the crack has a through-wall extent of over 50% and would thus be

considered extremely dangerous. For a guided wave inspection to be viable it would be necessary to detect an axial crack with a through-wall extent of 20%.

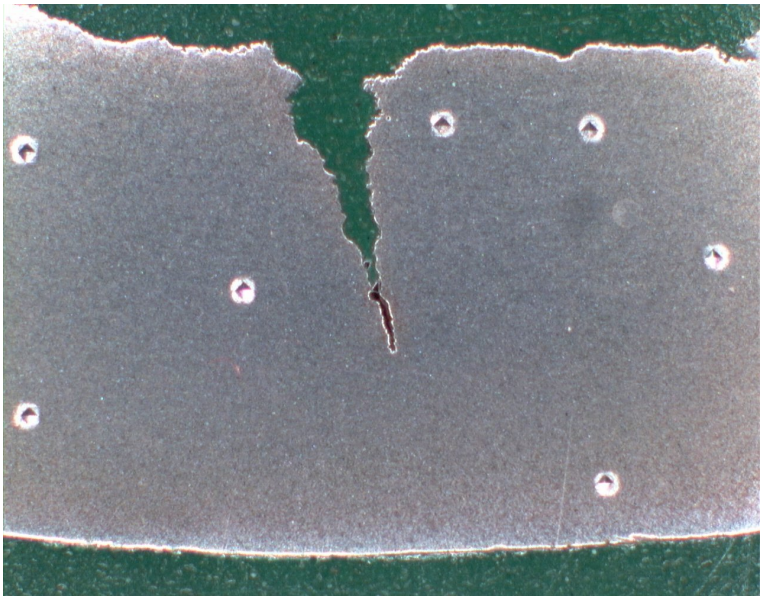

Figure 1.3: Profile of axial crack in a pipe. The view is along the axis of the pipe.

As a result of the rupture a large inspection program was instigated to inspect the condition of all cold-formed bends within the power station using Non Destructive Testing (NDT). Also, because many coal-fired power stations built in the 1960's share the same design it was necessary to extend the inspections nationwide. The inspections were carried out using standard ultrasonic testing ultrasonics with an angled beam used to find indications of pitting and/or cracking on the inner bore of the pipe. This is an extremely laborious process taking approximately one hour to inspect a single bend. With 3000-4000 bends in a typical station it becomes clear that it is a very lengthy process to inspect them all.

Although the inspections were initially limited to pipe-bends, as these were thought to be the highest risk areas, it is clear from Figure 1.2 that the same problem can also appear on straights. This dramatically increases the quantity of inspections that have to be conducted thus making this a daunting inspection task.

The primary aim of this thesis is to investigate whether guided waves can be used as a screening tool that can rapidly inspect long lengths of pipework. Any wave that propagates in a bounded medium where the structure of the component guides the

wave, for instance where the wave reverberates between the surfaces, can be considered a guided wave. Typical structures that can support guided waves are plates and pipes with a low frequency ultrasonic wave that has a wavelength that is of the order or longer than the thickness of the component. Using guided waves it should be possible to inspect an entire pipe run from a single remote location - covering 4-6 bends [27]. Being able to inspect bends this quickly would obviously have advantages over standard ultrasonic inspections in terms of speed. Using guided waves also offers the advantage of being able to inspect inaccessible or difficult to access pipework. The intention is to use guided waves as a screening tool that can indicate which areas of pipework need further inspections, as it is very unlikely that guided waves are sensitive enough to accurately size any potential crack.

The reason that guided waves may not be sensitive enough to detect axial cracks is that the amplitude of the response to a pipe feature is proportional to the change in cross-section of a pipe caused by that feature [36]. An axial crack represents a very small change in cross-section so provides a very small response.

1.2 Guided waves in a power station environment

In addition to investigating whether guided waves can be used to screen pipes for axial cracking, other potential guided wave applications in a power station environment are examined. Guided waves are already used routinely in the petrochemical industry [15] but are rarely used in the power industry. Established guided wave testing techniques are mostly used to detect corrosion, with only a limited amount of research related to cracking in pipes. The structures used by the petrochemical industry lend themselves to guided wave inspection, with long straight pipes and large featureless containers being common. When guided wave inspections are carried out on these components the received signal is relatively simple so it is not as difficult to identify areas of concern.

In contrast, the components in a power station have a very high feature density with bends, hangers, T-pieces etc all very close to each other, for example see Figure 1.4.

The received guided wave signal is therefore complicated by many reflections and mode conversions that make signal interpretation difficult. In a challenging environment such as this it is necessary to be very careful when analysing results, and accurately mapping out pipework, so it is essential to know the location of these features beforehand. Good knowledge about how guided waves interact with various features and the signals they are expected to produce would also help greatly when trying to detect a defect in a component.

Figure 1.4: Some examples of pipework found in a power station.

Guided waves have been trialled on many different components within power stations, and not all of them are suitable for a guided wave inspection. Many applications are discussed in this thesis, along with many other potential areas of interest that have not been investigated yet. Due to the large number of components and systems in a power station it is likely that guided wave inspections can be utilised in a meaningful way.

1.3 Outline of thesis

In Chapter 2 of this thesis an overview of guided waves is presented. The overview focuses on the properties of guided waves and a range of current applications. Guided waves in plates are discussed as well as long-range guided waves in pipes and circumfer-

ential guided waves in pipes with particular attention on wave propagation in defect-free material and interactions between guided waves and material discontinuities. A summary of available commercial guided wave inspection equipment is also presented.

In Chapter 3 the interaction between the $T(0,1)$ mode and axial cracks in pipes is studied. Cracks are characterised by plotting the reflection coefficient of the incident wave as a function of various parameters such as crack depth, crack length and incident toneburst centre frequency. It is demonstrated that the $T(0,1)$ mode is not sensitive enough to detect critical sized axial defects.

The idea of focusing guided waves to increase sensitivity to axial defects is explored in Chapter 4. Synthetic focusing was achieved using an algorithm applied in post-processing that could be used on previously collected data. Although the focusing algorithm did increase sensitivity, it was not sufficient to detect critical sized defects.

After determining that it was too challenging to detect shallow axial cracks in pipes using long-range guided waves, circumferential guided waves were studied, with the work reported in Chapter 5. Although many of the advantages of long-range guided wave were lost, the approach still offers significant advantages over manual ultrasonic inspections. It is possible to detect an axial crack with a critical depth using circumferential guided waves, but only if it has sufficient axial extent. This makes even circumferential guided waves unsuitable in many areas to detect axial cracking.

In addition to attempting to detect axial cracking in pipes using guided waves, in Chapter 6 a system to classify pipework according to its general condition using guided waves is described. The aim is to quantify the guided wave signal according to factors such as noise and attenuation, and use the information to classify a section of pipe as being in 'good', 'medium', or 'poor' condition. Guided wave measurements and surface roughness scans are conducted on sootblower pipework in order to validate the system.

In Chapter 7 a small number of other potential guided wave applications are examined, including a steam line at a combined heat and power station and a fuel oil line. It is important to investigate how many power station applications are suitable for guided wave inspection. Although commercial guided wave systems and established techniques

are used to conduct these inspections, the results must be interpreted in novel ways to account for the nature of the different power station components. Conclusions from the thesis are presented in Chapter 8.

1.4 Notes on units and terminology

For historical reasons in the power industry both metric and imperial units are used, and therefore units stated in this thesis are a mixture of metric and imperial. This particularly applies when describing pipe diameters and wall thicknesses where both inches and millimetres are used. The conversion ratio is 1 inch = 25.4mm.

The terms "schedule" and "nominal diameter" of a pipe are used frequently in this thesis to describe pipework. The nominal diameter is representative of the inner diameter (bore) of a pipe, and the schedule refers to the ratio between the pipe diameter and the wall thickness. A higher schedule indicates a thicker-walled pipe. The majority of pipework used in this study was a mixture of five inch and six inch nominal diameter with schedule 120. Schedule 120 is relatively thick-walled pipework, especially when compared to the pipework used in the petrochemical industry, which typically is closer to schedule 40.

Chapter 2

Guided wave properties and their exploitation

2.1 History of guided waves

One of the earliest mentions of what would now be considered guided waves was by Lord Rayleigh in 1888 [94], where he discussed vibrations in an infinite plate. This followed his earlier work that concerned waves on the surface of an infinite half space [93], which are now referred to as Rayleigh waves. Further work on waves in elastic plates was published by Lamb in 1917 [64] and provided mathematical descriptions of both symmetric and antisymmetric wave modes in plates. The equations allowed the dispersion curves for guided wave modes in free plates to be calculated. However, it was impossible to solve the equations analytically and numerical solutions were difficult to formulate because computers were unavailable at the time.

Gazis extended the description of guided waves from plates to pipe structures [51, 52], where equations to calculate dispersion curves in pipes, analogous to the plate equations of Lamb, were described. It was not until after this, in 1961, that experimental evidence of Lamb waves was produced by Worlton [111]. It was at this time that it became possible to consider Lamb waves for non-destructive testing.

From the 1990's and continuing until today much work has been done researching the use of guided waves in non-destructive testing. For his thesis, Alleyne [17] showed that it was possible to use Lamb waves for non-destructive testing. The use of guided waves in pipeline testing was also demonstrated by Alleyne and Cawley [10]. Work has also been done to calculate dispersion curves for guided waves in rail by Gavric [50], Rose et al. [95] and Cawley et al. [27] in order to perform long range inspections on railway rails. In industry guided waves are now used routinely, particularly in the petrochemical industry [16]. The application of guided waves to non-destructive testing is currently a very active area of research, and an overview of the state-of-the-art of the subject (as of 2006) can be found here [70].

2.1.1 Differences between guided wave ultrasonic testing and standard ultrasonic testing

Here a brief overview of the differences between guided waves and standard ultrasonic testing is presented. The term 'standard ultrasonic testing' refers to high frequency ultrasonic testing utilising bulk waves. Standard ultrasonic testing is employed extensively in industry as an NDT technique and a good reference text for ultrasonic techniques is provided by Krautkramer and Krautkramer [60].

As has been mentioned, in standard ultrasonic testing bulk waves are used to detect and classify defects. There are two bulk modes - longitudinal and shear. Particle motion is parallel to the direction of wave propagation for the longitudinal mode and perpendicular to the direction of wave propagation for the shear mode. The longitudinal mode velocity tends to be approximately double the velocity of the shear mode, for example in steel the longitudinal mode velocity is in the range $5900ms^{-1}$ to $6100ms^{-1}$, and the shear mode velocity is in the range $3100ms^{-1}$ to $3300ms^{-1}$. In most applications the frequencies of these waves range from around 0.5MHz to 20MHz and therefore have wavelengths between 0.3mm and 12mm for a longitudinal wave in steel.

The ability to resolve features is determined by the wavelength of the ultrasonic wave, so when conducting standard ultrasonic testing with a short wavelength it is possible to

accurately determine the size of a defect. Typically the accuracy is equivalent to the wavelength of the incident wave. However, the attenuation of the wave also increases with frequency, so an improved ability to resolve defects leads to reduced range of inspections. Guided waves use much lower frequencies than standard ultrasonic testing, typically in the range 20kHz - 100kHz, with wavelengths of the order 30mm-300mm. This makes them unsuitable for locating and characterising small defects, such as a 1mm crack in a weld, but very good for locating large corrosion defects a long way from the inspection location, by virtue of having low attenuation.

In general standard ultrasonic testing is capable of inspecting an area directly below the transducer. In contrast, guided waves can perform a long range inspection. This is illustrated in Figure 2.1. In this figure both types of ultrasonic inspection are demonstrated in a pulse-echo configuration, where the same transducer is used to both transmit and receive the ultrasonic signal. A pulse-echo configuration is used to measure the reflection of the ultrasonic wave off defects and component geometry. Transducers can also be arranged in a pitch-catch configuration, requiring a separate transmitter and receiver. In this arrangement the transmission coefficient is measured and a defect can be measured by, for instance, the extent to which it blocks the ultrasonic wave and reduces the amplitude of the transmitted signal.

An important point to note is the area labelled 'dead-zone' on Figure 2.1. A dead-zone occurs in the pulse-echo configuration because the transducer cannot receive any useful information whilst it is still transmitting the signal. In standard ultrasonic testing this often means that defects close to the surface are difficult to locate using this method. The dead-zone for guided waves is much larger than for standard ultrasonic testing, because guided waves are used at a much lower frequency. Therefore any defects close to the inspection location will not be detected. However, guided waves are capable of detecting near-surface defects because they interrogate the entire cross-section of the component.

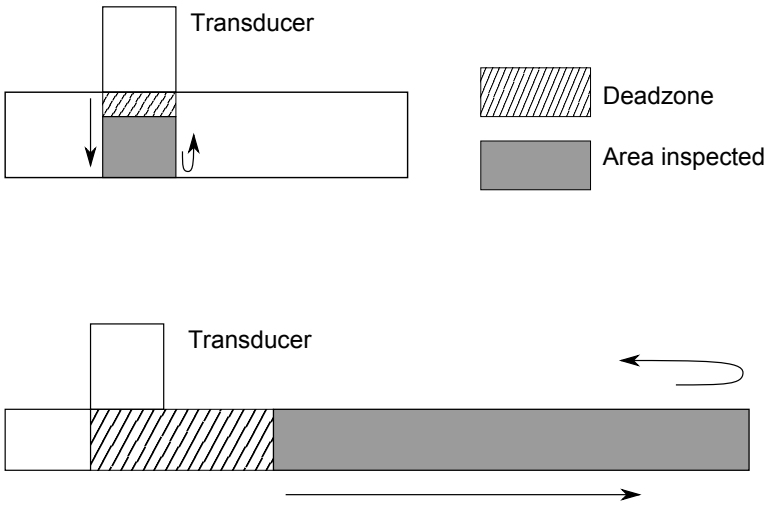

Figure 2.1: Figure illustrating the difference between standard ultrasonic testing and guided waves. Arrangement in both cases is pulse-echo and arrows indicate direction of wave propagation.

2.2 Guided waves in free plates

A surface wave in an infinite half-space, also called a Rayleigh wave [93], is considered to be a guided wave because it is guided by the surface of the half-space. Although no real half-spaces can exist, Viktorov [105] showed that a plate thicker than $5\lambda_R$, where λ_R is the Rayleigh wavelength, can be approximated as a half-space. In a plate with a thickness below $5\lambda_R$ a wave would be bound by both surfaces and the plate would act as a waveguide. Waves in this latter configuration were first described by Lamb [64] and are thus known as 'Lamb waves'.

To describe Lamb waves mathematically we first need to consider the wave equations for a plane elastic wave in an infinite isotropic solid. Many authors have derived the wave equations, for example Brekhovskikh and Goncharov [25]. In a material of density ρ, and using Cartesian coordinates, the wave equations are as follows:

$$\rho\frac{\partial^2 u_x}{\partial t^2} = (\lambda+\mu)\frac{\partial}{\partial x}\left(\frac{\partial u_x}{\partial x}+\frac{\partial u_y}{\partial y}+\frac{\partial u_z}{\partial z}\right)+\mu\left(\frac{\partial^2}{\partial x^2}+\frac{\partial^2}{\partial y^2}+\frac{\partial^2}{\partial z^2}\right)u_x$$
$$\rho\frac{\partial^2 u_y}{\partial t^2} = (\lambda+\mu)\frac{\partial}{\partial y}\left(\frac{\partial u_x}{\partial x}+\frac{\partial u_y}{\partial y}+\frac{\partial u_z}{\partial z}\right)+\mu\left(\frac{\partial^2}{\partial x^2}+\frac{\partial^2}{\partial y^2}+\frac{\partial^2}{\partial z^2}\right)u_y$$
$$\rho\frac{\partial^2 u_z}{\partial t^2} = (\lambda+\mu)\frac{\partial}{\partial z}\left(\frac{\partial u_x}{\partial x}+\frac{\partial u_y}{\partial y}+\frac{\partial u_z}{\partial z}\right)+\mu\left(\frac{\partial^2}{\partial x^2}+\frac{\partial^2}{\partial y^2}+\frac{\partial^2}{\partial z^2}\right)u_z \qquad (2.1)$$

where u represents particle displacement in the subscript direction, and λ and μ are the $Lamé$ stiffness constants [19], and t represents time.

Malvern [74] showed that it is possible to separate any vector field into a rotational component, $\nabla \times \mathbf{H}$, and an irrotational component, $\nabla\phi$, using a Helmholtz decomposition [77]. In the decomposition $\mathbf{H}$ is a vector potential and ϕ is a scalar potential, and using the potential functions allows the equations 2.1 to be rewritten as:

$$\rho\frac{\partial^2\phi}{\partial t^2} = (\lambda+2\mu)\nabla^2\phi$$
$$\rho\frac{\partial^2\mathbf{H}}{\partial t^2} = \mu\nabla^2\mathbf{H} \qquad (2.2)$$

These equations are commonly known as the Helmholtz differential equations. Like the equations 2.1, the equations 2.2 apply to elastic waves in an infinite solid. In an infinite free plate there are boundary conditions at the two surfaces of the plate that provide constraints to wave propagation. Consider an infinite plate in a Cartesian coordinate system, as depicted in Figure 2.2, with the plate in the $x-y$ plane and z normal to the plate surface. The origin of z is at the mid-point of the plate, which has a thickness d. For a plane wave propagating in the x direction, with zero particle displacement in the y direction, rotation can only occur about the $y-axis$, meaning $\mathbf{H}_x = \mathbf{H}_z = 0$. Zero displacement in the y direction also explicitly implies that $\frac{\partial}{\partial y} = 0$ and $u_y = 0$. With these conditions, and substituting:

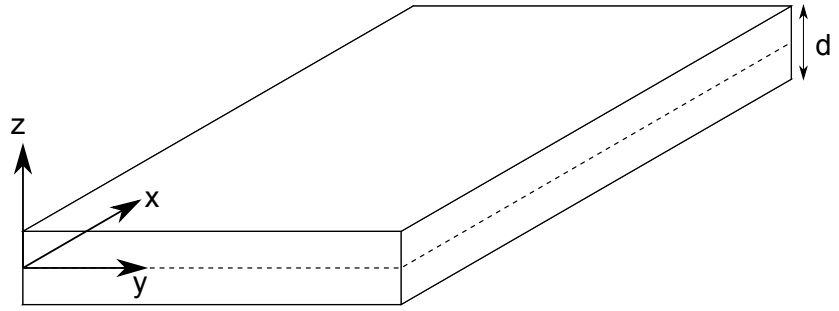

Figure 2.2: Diagram of plate in a Cartesian coordinate system. The dashed line represents the midpoint at which the origin of z is defined.

$$c_L = \left(\frac{\lambda + 2\mu}{\rho}\right)^{1/2}$$
$$c_T = \left(\frac{\mu}{\rho}\right)^{1/2} \tag{2.3}$$

with c_L and c_T being the longitudinal and transverse phase velocities respectively, equation 2.2 reduces to:

$$\frac{\partial^2 \phi}{\partial t^2} = c_L\left(\frac{\partial^2 \phi}{\partial x^2} + \frac{\partial^2 \phi}{\partial z^2}\right)$$
$$\frac{\partial^2 \mathbf{H_y}}{\partial t^2} = c_T\left(\frac{\partial^2 \mathbf{H_y}}{\partial x^2} + \frac{\partial^2 \mathbf{H_y}}{\partial z^2}\right) \tag{2.4}$$

These are the Lamb wave equations for waves in plates. Similarly, if we assume that all particle displacements are in the y direction, then equation 2.2 reduces to:

$$c_T\left(\frac{\partial^2 \mathbf{H}}{\partial x^2}\right) = \frac{\partial^2 \mathbf{H}}{\partial t^2} \tag{2.5}$$

Equation 2.5 describes the motion of shear horizontal (SH) waves in a plate.

2.2.1 Dispersion curves

The longitudinal and transverse velocities described in equation 2.3 apply only to waves in infinite media, and these waves are non-dispersive, meaning the velocity is not dependent on wave frequency. In general guided waves in bounded media are dispersive, that is the velocity is dependent on the frequency of the wave. This gives rise to a difference in phase and group velocities for guided waves that is not present in bulk waves in an isotropic material.

Phase velocity indicates the velocity of wave peaks in a toneburst and group velocity indicates the velocity with which the energy in a wave packet propagates through a material. Group velocity is very useful because it determines the time a signal is expected to arrive at a transducer. The phase velocity is also important when trying to excite a specific wave mode.

The equations 2.3 describe the phase velocity in terms of material density and the $Lamé$ stiffness constants. By solving the wave equation, phase velocity can be expressed in terms of the wavenumber, k, and the angular frequency, ω, of the wave, as can the group velocity.

$$\begin{aligned} v_{ph} &= \frac{\omega}{k} \\ v_{gr} &= \frac{\partial \omega}{\partial k} \end{aligned} \tag{2.6}$$

Dispersion gives rise to dispersion curves that plot the wave velocity against frequency. Examples of both phase velocity and group velocity dispersion curves for 1mm thick steel plate are presented in Figure 2.3 and Figure 2.4 respectively. These dispersion curves are generated using the software Disperse [86], software written at Imperial College to calculate dispersion curves. Because the frequency scales with plate thickness the scale on the x-axis is frequency-thickness product, so the curves can be generalised to any plate thickness.

In Figures 2.3 and 2.4 all modes that exist below 10 MHz-mm are shown. It is obvious

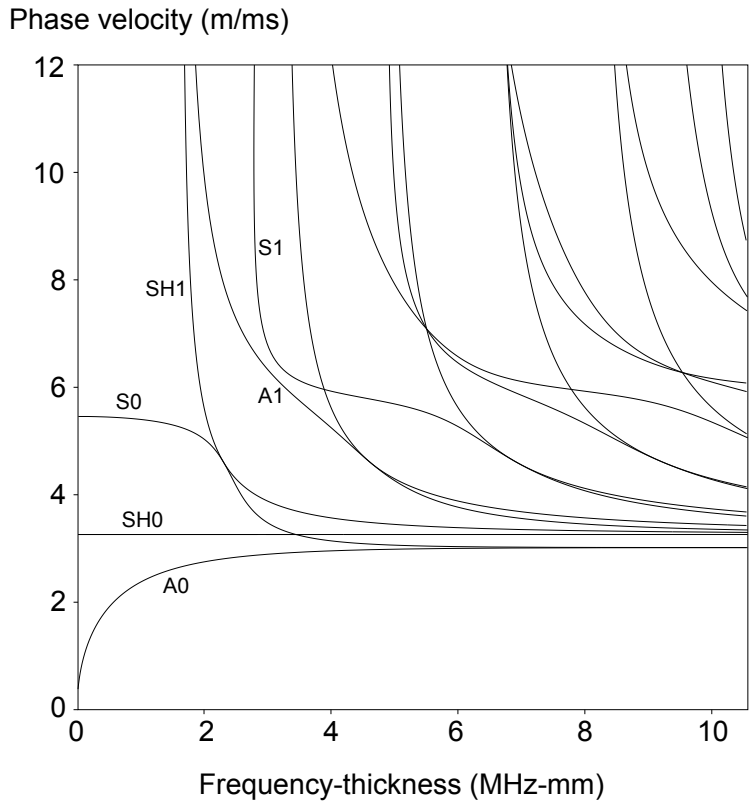

Figure 2.3: Phase velocity dispersion curves for a steel plate. The x-axis is the frequency-thickness product so the curves scale with plate thickness and signal frequency.

from the figure how dispersive the majority of modes are, particularly near the cut-off frequency. However, it is possible to select modes and excite them at frequencies where dispersion is minimal. Most NDT is conducted in the region of the dispersion curves below the cut-off frequency for the A1 mode at 1.6 MHz-mm. This ensures that only the fundamental guided wave modes can propagate and ensures waves cannot mode convert to higher order modes - thus simplifying the analysis of the results.

If the S0 mode is selected the least dispersive region of this curve is at very low frequencies, however at low frequencies the ability to resolve defects is reduced [72]. It has been shown by Wilcox et al. [109] that an optimum frequency exists that balances these two requirements. At very low frequencies the A0 mode is very dispersive so it is not desirable to use this frequency regime. A frequency-thickness above 1 MHz-mm is usually sufficient at minimising the effects of dispersion [71]. The fundamental shear horizontal

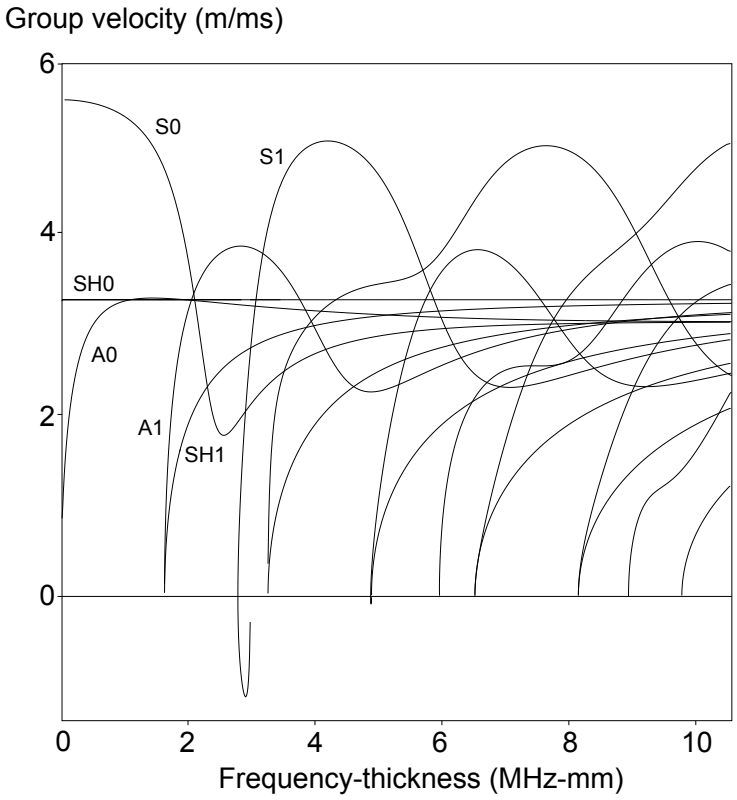

Figure 2.4: Group velocity dispersion curves for a steel plate. The x-axis is the frequency-thickness product so the curves scale with plate thickness and signal frequency.

mode is unusual in that it is completely non-dispersive across the entire frequency range. Therefore dispersion is not a consideration when using this mode for non-destructive testing.

2.2.2 Multi-modal nature of guided waves

Bulk waves have only two modes - longitudinal and shear. Lamb waves have an infinite number of modes that are arranged into two mode families - the symmetric (Sn) modes and the antisymmetric (An) modes. Here the symmetry refers to particle motion relative to the midpoint of the plate in the $x - y$ plane, as presented in Figure 2.5 [6]. As well as Lamb modes there are also shear horizontal (SHn) modes that have particle motion in the y direction. For all guided wave mode families in a plate the letter n represents

the order of the mode in question, starting at 0 for the fundamental mode.

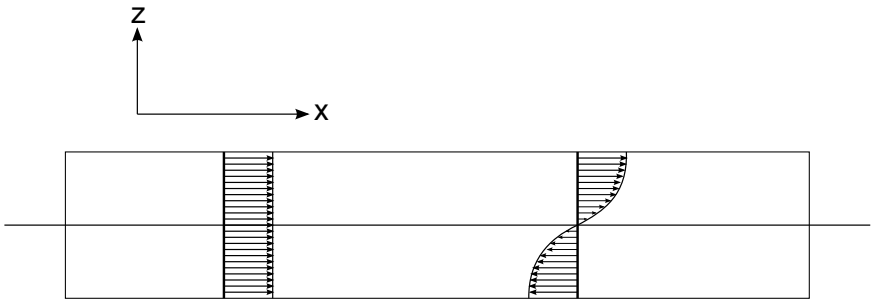

Figure 2.5: Mode shapes of the fundamental symmetric S0, left, and fundamental anti-symmetric A0, modes. In this figure the y direction is into the page.

As has been previously mentioned, there are an infinite number of guided wave modes. All except the three fundamental modes have cut-off frequencies below which they do not propagate. The cut-off frequencies are dependent on the material and inversely proportional to the thickness of the plate, such that for any given material the frequency-thickness product for a given mode is constant. For instance, in steel the A1 mode cut-off is at a frequency-thickness product of 1.6 MHz-mm.

The multi-modal nature of guided waves can make the analysis of inspection results difficult when compared to bulk waves, because different modes can propagate at different velocities and reflect off defects and geometric boundaries, producing a very complicated signal. It is difficult - often impossible - to ensure that a signal originating from a defect is separated from the geometric signals generated by the plate. The effects of dispersion compound this issue as the velocities of the modes are also dependent on frequency, and therefore the distance between the transducer and a defect can affect the measured signal [107]. To minimise this problem inspections are often carried out at low frequencies where fewer modes are present and specific modes are excited [9].

A method for separating modes in a multi-modal time history was developed by Alleyne and Cawley [7]. The method involves performing a two-dimensional Fourier transform (2D-FFT) where a Fourier transform of the time history is performed in both the frequency domain and the spatial domain, in order to produce results in the frequency-

wavenumber domain. To perform the spatial Fourier transform measurements of the time history must be taken at several locations along the direction of beam propagation. The output of the 2D-FFT is a three-dimensional plot of amplitude-frequency-wavenumber with the modes separated, allowing the amplitude and dispersion relationships of each mode to be measured.

The mode shapes of the different modes need to be considered when discussing guided waves. The local stresses and displacements for each mode vary differently through the thickness of the plate, and this affects the sensitivity of these modes to discontinuities. For instance, higher order modes will have a node at a point through the thickness of the material, where the stress and strain values are zero. If a defect is located at this node the mode will have a very low reflection amplitude.

2.3 Guided waves in free pipes

Work on sound propagation in pipes has been conducted by many authors [51, 83, 84, 99], who have calculated dispersion relationships for guided waves in pipes. Equations 2.2 are separable in cylindrical coordinates so the solution may be divided into the product of each of the spatial dimensions.

$$\phi, \mathbf{H} = \Gamma_1(r)\Gamma_2(\theta)\Gamma_3(z)e^{i(\mathbf{kr}-\omega t)} \tag{2.7}$$

Here, $\Gamma_1(r)$, $\Gamma_2(\theta)$ and $\Gamma_3(z)$ describe the field variation in each cylindrical direction and $\mathbf{k}$ is a vector wavenumber. If it is assumed that there is no propagation in the r direction, and there is harmonic variation of the displacement field in the axial and circumferential directions, then equation 2.7 reduces to:

$$\phi, \mathbf{H} = \Gamma_1(r)e^{i\nu\theta}e^{i(kz-\omega t)}, \tag{2.8}$$

where ν is the circumferential order, and must be a whole number, and k is the wavenum-

ber in the axial z direction. Pavlakovic [85] generated a system of differential equations by substituting this expression into equation 2.2 (not reproduced here) and used the differential equations to calculate dispersion curves in a hollow cylinder.

The group velocity dispersion curves for a 5 inch steel pipe are presented in Figure 2.6. Many of the guided wave modes in a pipe are analogous to Lamb modes in a plate, although an additional set of 'flexural' modes exist that are analogous to Lamb modes propagating in a helical direction around the pipe.

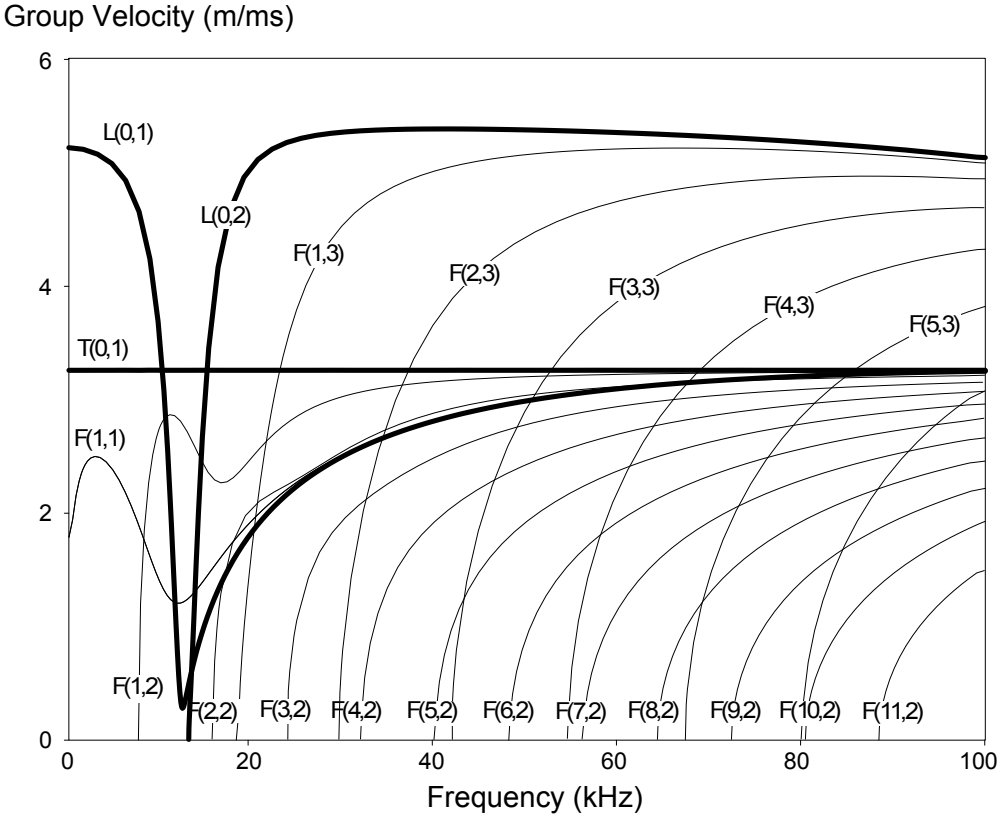

Figure 2.6: Group velocity dispersion curves for a 5 inch schedule 120 steel pipe with an outer diameter of 141.3mm and a wall thickness of 12.7mm. The axisymmetric modes have been highlighted in bold.

2.3.1 Mode families of guided waves in pipes

As in plates there are families of wave modes in pipes. These are the torsional, flexural and longitudinal mode families. The system for naming pipe guided wave modes is

described by Silk and Bainton [99]. Mode names in pipes are of the form $X(n,m)$. The X is either L, T or F to indicate longitudinal, torsional of flexural. The value of n represents the harmonic order of circumferential variation and describes the number of cycles of variation of displacement around the circumference, with $n = 0$ signifying an axially symmetric mode. The harmonic order through the thickness of the pipe is indicated by m and has a value $m = 1$ for the fundamental harmonic. Torsional and longitudinal modes all have zero order circumferential variation, $n = 0$, and are therefore all axially symmetric, whereas no flexural modes have zero order circumferential variation.

The torsional modes can be thought of as a 'twisting' motion in a pipe, with particle displacements and stresses primarily in the tangential direction. This is analogous to shear horizontal modes in a plate. Longitudinal modes are compression modes along the axis of the pipe and are analogous to S0 Lamb modes in a plate. Flexural modes have a 'bending' motion in a pipe and do not have direct plate analogies as they display circumferential variation, which cannot exist in a plate. It is more helpful to think of them as Lamb modes or shear horizontal modes propagating in a helical direction along the pipe.

2.3.2 Effect of bends

Dispersion curves for toroidal structures were calculated numerically by Demma [37] using finite element analysis. A numerical method was necessary because it was impossible to calculate dispersion curves in such a structure analytically. This was followed up with extensive work by Demma et al. [35] to determine the effect that bends have on a guided wave inspection. The additional factor of bend radii, relative to curvature in the pipe-wall, was shown to have an increasing effect on the dispersion curves as the bend radius was reduced.

Any pipework that forms a bend is by definition not axisymmetric. Therefore the axisymmetric torsional and longitudinal modes cannot exist in their standard forms through a bend. This leads torsional and longitudinal modes to have a non-uniform shape when propagating in a bend, and new notation in the form $T(0,n)_T$ and $L(0,n)_T$ is used to

indicate that this is the case.

In the case of flexural wave modes propagating in a bend the dispersion curve for a particular mode in effect becomes two separate modes through a bend. If a flexural $F(n,m)$ mode is propagating in a straight section of pipe the notation used for the two related modes in a bend are $F(n,m)_S$ and $F(n,m)_A$, where the subscripts indicate whether the mode is symmetric or antisymmetric.

Demma considered an inspection on a straight beyond a bend, rather than an inspection of the bend itself. This was achieved by exciting the $L(0,2)$ mode and the $T(0,1)$ mode, as these are commonly used modes used in non-destructive testing, and measuring the mode shapes on a section of straight pipe after the bend. Measurements were also made to verify whether or not a reflection of either mode took place at the bend. The results showed that there was only a negligible reflection of either mode at the bend, and that there was significant mode conversion beyond the bend. The $L(0,2)$ partially converted to an $F(1,3)$ mode and the $T(0,1)$ mode partially mode converted to the $F(1,2)$ mode. Other mode conversions that took place were small enough that they could be neglected in a first approximation.

The implication of the mode conversions is that additional propagating modes have to be considered in any inspection beyond a bend. The scattering of the excited modes, usually $L(0,2)$ and $T(0,1)$, from defects as well as mode converted flexural modes will affect any results.

2.4 Circumferential guided waves in free pipes

A circumferential guided wave in a pipe propagates in the circumferential direction around a pipe. The wave modes are similar to those in a plate and therefore the same mode naming convention is used as for plates. The dispersion curves and mode shapes are altered slightly by the fact that the inner and outer surfaces of the pipe are different shapes, the inner surface having a higher curvature than the outer surface. Because the propagation is in the circumferential direction, only a single slice of a pipe at the

transducer is inspected, so circumferential guided waves do not provide a long-range inspection. However, because the direction of wave propagation is perpendicular to the crack, it is likely to be more sensitive to axial cracks in a pipe.

Guided waves in curved plates were investigated by Wilcox [110] as part of a PhD thesis. He found that in curved structures, guided waves did not have the elegant dispersion relations found in the flat plate equivalent. An infinitely long cylinder with an angular direction extending from zero to infinity was considered in order to calculate the dispersion relations in curved structures. This was achieved and phase velocity-frequency dispersion curves were plotted for curved structures with varying radius-thickness ratio, ranging from 10:1 (low curvature) to 1:1 (high curvature). The phase velocity dispersion curves for circumferential guided waves in a 5 inch steel pipe are presented in Figure 2.7. As curvature increases mode pairs (e.g. S2 and A2) exchanged positions, no longer crossing over as in the case of a flat plate. Higher order mode pairs exchanged position as the curvature increased further. Wilcox found that the solutions break down at low frequency, due to an artefact in the calculations. If the wavenumber is small the order of the Bessel function used to evaluate the dispersion relationship becomes negative, which makes performing these calculations impossible.

Fong [44] also described guided waves within a curved structure, in this case a curved bar. The wave equation in cylindrical coordinates is considered in order to formulate dispersion relations for curved structures. Exact analytical solutions were found to be unstable at high frequency and high curvature, therefore asymptotic solutions were found. The asymptotic solutions were found to compare favourably with the analytical results allowing dispersion relations to be calculated for all frequencies and geometries.

The aim of Fong was to try and limit the effect that curvature had on dispersion by monitoring how phase velocity and mode shape varied between a flat and a curved structure. Understanding how to limit the effects of curvature would allow for guided wave inspections to be carried out on components that may or may not be bent. Differing curvatures between the inner surface and outer surface of a curved structure affect particle motion within the structure and it is important to consider the degree of curvature in such situations. The difference in phase velocity between a flat and curved plate

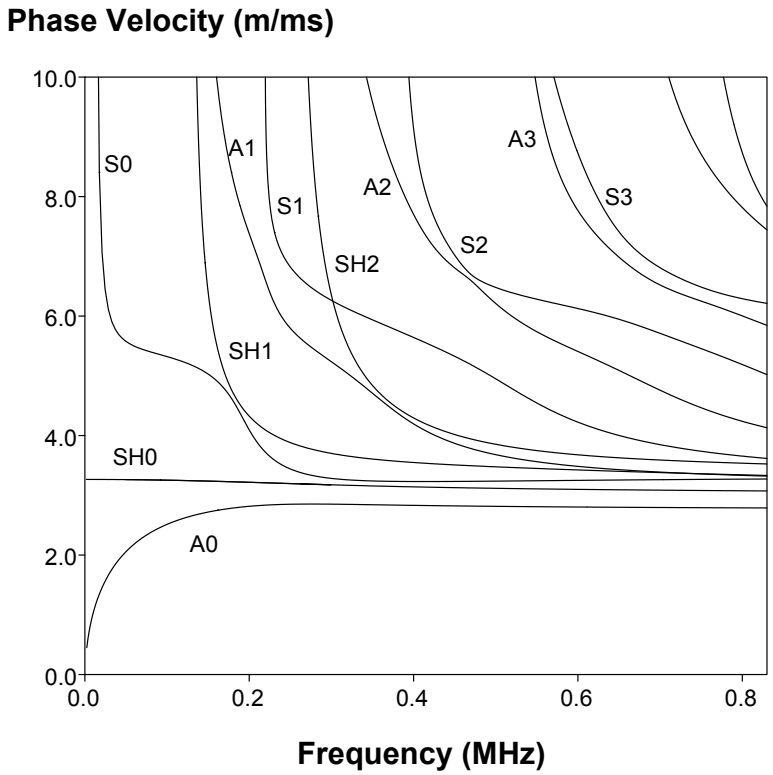

Figure 2.7: Phase velocity dispersion curve for circumferential guided waves in a 5 inch schedule 120 steel pipe with an outer diameter of 141.3mm and a wall thickness of 12.7mm. The radius-thickness ratio for this pipe is approximately 5.7.

was plotted as a function of frequency and curvature for different modes. From this an 'optimal frequency' could be established at which the difference in phase velocity was minimised. The changes in phase velocity directly cause variation in the mode shapes within a curved structure, and the variation in mode shapes can be quantified using the "S-factor".

2.5 Scattering of guided waves from material discontinuities

Determining the manner in which guided waves scatter from component discontinuities is a very important aspect of performing guided wave inspections. Discontinuities can in-

clude defects, such as cracks or corrosion, and other features such as welds and supports. Being able to distinguish between different features is obviously essential to conducting a successful inspection.

Defects usually take the form of either a large area of thinned material (such as a corrosion patch), cracking, or pitting. Pitting is a very localised form of wall loss in a pipe that can often lead to more generalised wall loss, resembling a corrosion patch, or cracking. The size, orientation and profile of a defect can all have major effects on the reflection coefficient of guided waves. A crack or notch type defect with a very sudden change in wall loss would produce a different response to a corrosion patch, which has a more gradual change in wall loss.

2.5.1 Defect-like discontinuities in plates

The scattering of Lamb waves from defects in plates was investigated by Alleyne and Cawley [8]. In this case the defects took the form of notches which are simple to model using finite element software, and to machine into a plate. Using the 2D-FFT method [7] the transmission and reflection amplitudes for the A0, S0 and A1 modes were measured. The transmission and reflection amplitudes were shown to be dependent on the frequency-thickness product, mode, and notch geometry. In particular it was shown that the ability to detect a defect did not depend on the absolute size, but rather the through-thickness extent in the plate relative to the thickness of the plate. This statement held even when the notch was tilted relative to the normal of the plate surface, with the through-thickness extent rather than notch length determining the transmission and reflection amplitudes.

More detailed work examining the scattering of the three fundamental guided wave modes, S0, A0, and SH0, from notches and steps in plates was conducted by Lowe and Diligent [72], Lowe et al. [71], and Demma et al. [34] respectively. The papers examine in detail the effects that input frequency, notch depth and notch width have on the amplitude of a reflected guided wave. All three fundamental nodes are shown to have a reflection amplitude that is dependent on the notch width in a non-linear manner,

with the SH0 and A0 modes exhibiting a roughly sinusoidal shape and the S0 mode a roughly cosinusoidal shape. These effects are explained by interference phenomena, with the reflection from a step down in the plate interfering with the reflection from a step up. For the A0 and S0 modes an S-parameter approach [19] was used to analyse the interference effect at low frequency (quasistatic) and found to be applicable for small cracks and notches. At higher cracks sizes and frequencies ray theory predictions proved more accurate. For the SH0 mode simply superimposing the reflections from the start of the notch and the end of the notch proved accurate for all notch sizes and frequencies.

An interesting feature of the work presented in [71] is how the reflection coefficient of the A0 mode varies with crack depth, with the reflection coefficient decreasing with increasing crack depth at certain crack depths. The pattern is attributed to axial and shear crack opening displacements (COD) and their relative importance for different crack depths according to mode shape. At low crack depths the reflection coefficient increase with crack depth with the behaviour controlled by the axial component of the COD. At medium depths the shear component of the COD begins to take over and there is relatively little change in reflection coefficient. Behaviour is also dominated by the near surface parts of the crack also reducing the effect of depth. At high depths the reflection coefficient rises rapidly with crack depth, with shear COD dominating.

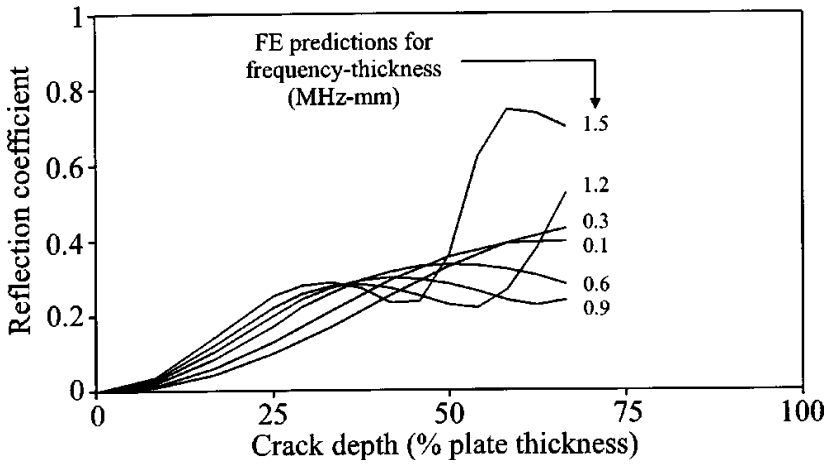

Figure 2.8: (Reproduced from [71]) Predicted A0 reflection coefficient from a crack in a plate versus crack depth, for various frequencies.

Rajagapol and Lowe have produced numerous papers [87–89] studying the scattering

of SH0 guided waves from through-thickness and part-depth cracks in plates. A wave normally incident on a through-thickness crack was studied in [87], variable incidence angle on a through-thickness crack in [88] and variable incidence angle on a part-depth crack in [89]. For waves normally incident on a crack, the reflection coefficient was plotted as a function of crack length. There was a distinct maximum when the crack length was equivalent to twice the wavelength of the incident wave, caused by interference from crack-tip diffractions. The reflection coefficient is shown to be highest in a narrow angular band close to the specular direction. The oblique incidence study showed that the specular reflection is strongest at the normal position and reduces rapidly as the incidence angle approaches the critical angle. The reflection coefficient for part-depth cracks is similar to that for through-thickness cracks except that it is modified by a frequency dependent scale factor.

The scattering of the S0 Lamb wave mode from circular defects has been studied, with through holes investigated by Diligent et al. [38] and flat-bottomed holes investigated by Diligent and Lowe [39]. For through holes the reflection coefficient was measured as a function of hole diameter, with hole diameters up to 2.5 wavelengths of the incident wave, and found to generally increase with hole diameter. There are small undulations in the reflection function that are accounted for by secondary reflections from the hole, in particular the reflection of the mode converted SH0 wave. The reflection coefficient was also found to decrease as the distance between the hole and monitoring position was increased. Polar plots were presented with the amplitude of the scattered S0 mode and the mode converted SH0 mode.

Some key differences between the two-dimensional problem of a through hole, and the three-dimensional problem of a part depth hole, are the mode conversion to the A0 mode and the propagation of modes across the ligament material for the part-depth hole [39]. The reflection coefficient as a function of hole diameter is more complicated for a flat-bottomed hole than for a through hole, displaying maxima when the hole diameter is at odd multiples of the wavelength, and minima when at even multiples of the wavelength. The maxima and minima are the result of interference of reflections from the near-side and far-side of the hole. The effect of distance between the hole and monitoring position

is not greatly affected for a flat-bottom hole compared to a through hole.

Other authors [41, 97] have also examined the scattering of the SH modes from discontinuities in a plate. Ditri [41] considered the case where multiple modes are propagating in the plate. By expanding the wave fields on either side of a discontinuity, which could consist of either a step change in thickness or a change in material properties, and imposing a 'non-coupling' condition it was shown why certain modes are not generated during a scattering event. Rose and Zhao [97] used a boundary element numerical analysis of discontinuities and compared them to experimental results, with good agreement.

The work discussed previously considered notches and cracks oriented in a perpendicular direction to the direction of propagation of the incident wave. A crack-like defect oriented parallel to the direction of wave propagation presents a much smaller cross-section and is therefore more difficult to detect. Ratassepp et al. [91] studied the scattering of the SH0 mode from such a crack in a plate and found that the reflection amplitude of the SH0 mode was indeed low. The incident SH0 wave is also diffracted strongly in a direction perpendicular to the direction of the incident wave.

2.5.2 Defect-like discontinuities in pipes

The majority of research concerning discontinuities in pipes considers either circumferential cracks [14, 20, 36, 40, 69] or corrosion-like patches [26, 28, 33, 112]. Ditri [40] analysed the scattering of guided waves from a circumferential crack using the S-parameter, modified for use in a pipe. The S-parameter allowed for the calculation of the amplitude of a mode of arbitrary circumferential order assuming an incident axisymmetric mode, thereby providing the possibility of sizing cracks.

Bai et al. [20] describe a numerical method to model the reflection of guided waves from circumferential cracks in pipes. A three-dimensional problem is reduced to two quasi one-dimensional problems by employing wave function expansion in the axial direction and decomposing the problem into a symmetry problem and an antisymmetry problem. From this reflection and transmission coefficients from an arbitrary circumferential crack

are calculated. The numerical method is less computer intensive than equivalent finite element calculations and allowed more scenarios to be modelled in a shorter time. The model was experimentally validated for multiple incident modes.

The reflection of the longitudinal $L(0,2)$ mode from circumferential notches in pipes was investigated by Alleyne et al. [14]. The primary variables investigated in the study were the circumferential extent of the notch and the through-thickness extent of the notch. It was demonstrated through finite element analysis and experimental work that the reflection amplitude varied almost linearly with circumferential extent and had a stronger function with respect to through-thickness extent. The study involved pipes of varying diameter showing similar results, thereby demonstrating that the results are general to all pipe sizes.

Mode conversion takes place with an incident $L(0,2)$ wave and has been studied by Lowe et al. [69]. The reflection amplitudes of the incident mode and the $F(1,3)$, $F(2,3)$ modes have been measured as the function of the circumferential extent of a notch in a pipe, and the results are reproduced in Figure 2.9. The reflection amplitude of the zero order $L(0,2)$ mode increased linearly with the circumferential extent of the notch. Both the first order $F(1,3)$ and second order $F(2,3)$ modes varied roughly sinusoidally with circumferential extent with the $F(1,3)$ mode peaking at 50% circumferential extent and the $F(2,3)$ mode peaking at 25% and 75% circumferential extent with a minimum at 50% circumferential extent. At low circumferential extent the reflection amplitudes of the mode converted higher order modes is of a similar magnitude to the incident $L(0,2)$ mode and at 100% circumferential extent, i.e. an axisymmetric discontinuity, no mode conversion takes place.

Similar work examining the reflection and mode conversion of the torsional $T(0,1)$ mode from circumferential notches in pipes was carried out by Demma et al. [36]. As well as studying the effect of circumferential extent and through-thickness extent this paper investigated the effect that the axial extent of a notch has on reflection coefficient. Another aspect of the work was the effect of mode conversion, by also measuring the reflection amplitudes of the flexural $F(1,2)$, $F(2,2)$ and $F(1,3)$ modes. The reflection of the $T(0,1)$ mode is a linear function of the circumferential extent of the notch, but

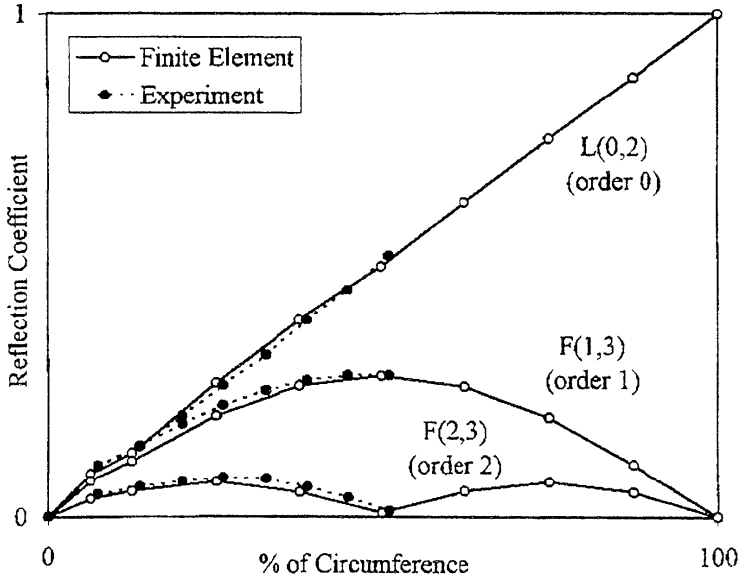

Figure 2.9: (Reproduced from [69]) Measured and predicted reflection coefficients for a through-thickness notch in a 76-mm (nominal 3-inch) diameter, 5.5-mm wall thickness pipe at 70 kHz as a function of the percentage circumferential extent of the notch.

the reflection amplitudes of the mode-converted $F(1,2)$ and $F(2,2)$ modes vary in a roughly sinusoidal manner, with the $F(1,2)$ mode reflection amplitude peaking at 50% circumferential extent and the $F(2,2)$ mode peaking at 25% circumferential extent. Mode conversion is a significant effect when considering non-axisymmetric discontinuities. When the circumferential extent of a discontinuity is low the reflection amplitudes for the flexural modes are almost as high as the reflection amplitude of the $T(0,1)$ mode, but they never exceed it. With an axisymmetric discontinuity no mode conversion takes place.

The effect that the through-thickness extent has on reflection amplitude is dependent on the frequency of the incident toneburst and is not a linear relationship. Figure 2.10 (reproduced from [36]) presents the reflection coefficient of the fundamental torsional mode as a function of crack depth over a range of frequencies. For a fixed pipe diameter increasing the frequency of the incident toneburst will increase the reflection amplitude. As the axial extent of the notch is increased the reflection amplitude of the $T(0,1)$ mode varies in a roughly sinusoidal manner, similar to the equivalent SH0 mode in a plate.

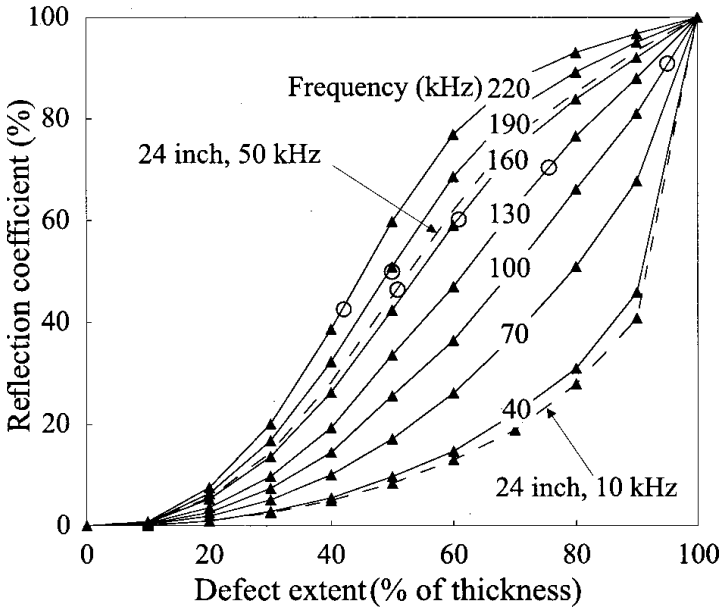

Figure 2.10: (Reproduced from [36]) Variation of reflection ratio with defect depth for zero axial length at various frequencies, axisymmetric defect. Results are from axisymmetric model with $T(0,1)$ incident in 3 inch (solid lines) and 24 inch pipes (dashed lines). The empty circles indicate the depth value for which ka=1 at each frequency.

The reflection of guided waves from corrosion type defects has been studied by several authors [26, 28, 33, 112]. Corrosion defects differ from notches in that they have both axial and circumferential extent, and the depth tends to increase gradually rather than as a single step. Carandante et al. [26] studied the effect of a tapered circumferential notch by plotting the reflection coefficient as a function of the axial extent of the notch and the taper angle of the notch. The reflection angle increased with taper angle with the highest reflection coefficient in the limiting case of a standard straight-sided notch.

Although many of the individual factors had been considered independently as described previously, Cawley et al. [28] considered the effect of several factors together, in order to provide predictions about defect characteristics from a guided wave measurement using the $L(0,2)$ mode. Factors included defect geometry, frequency and pipe size and results were generalised in an effort to predict the response from an arbitrarily sized defect.

Demma et al. [33] completed a similar exercise to Cawley et al. [28], including the $T(0,1)$ mode, and provided a guide for interpreting guided wave measurements to determine the

characteristics of a defect when performing a non-destructive examination. The relative reflection amplitudes of the incident mode and mode converted flexural modes can be used to estimate the circumferential extent of a defect, as the expected ratio of reflection amplitudes is known. The total cross-sectional loss can also be estimated from the reflection amplitude of the incident axisymmetric mode, and these two measurements combined provide an estimate of through wall loss. The axial extent of a discontinuity can be estimated by varying the frequency of the incident toneburst and monitoring the frequencies at which peaks in the reflection amplitude occur.

2.5.3 Other discontinuities

Other component features that are not defects are also classified as discontinuities and can strongly reflect guided waves, in fact often more strongly than the defect signals it is desirable to locate. A weld will often have a weld cap increasing the local wall thickness, and the effect this has on guided waves needs to be understood. In pipes, the vast majority of welds are very close to axisymmetric discontinuities and therefore an incident guided wave will not undergo a mode conversion after reflecting from one. As most defects are not axisymmetric, it is possible to identify welds by the lack of mode conversion upon reflection [27]. Weld caps in the 3-12 inch range of pipe sizes also usually have approximately the same change of cross-sectional area of around 20-25% [73] compared to the cross-sectional area of the pipe, and their response is not highly dependent on frequency [27].

Supports are very common structures on engineering components and have a variety of styles. There may be simple supports where a pipe is merely resting on the support, or a clamped support or welded support where that pipe is physically attached to the support. To date very little research has been conducted into the scattering of guided waves from supports. By calculating the dispersion curves in a supported pipe Galvagni and Cawley [48] show that below a certain cut-off frequency the $T(0,1)$ mode no longer propagates, and therefore at low frequencies there is a very large reflection of the $T(0,1)$ mode. The reflection amplitude of the $T(0,1)$ mode rapidly reduces as the frequency is

increased beyond the cut-off.

2.6 Generating guided waves for the purpose of non-destructive testing

Ultrasonic waves are generated using some form of transducer. The most common type of transducer currently in use is the piezoelectric transducer (PZT) where a piezoelectric material is electrically excited to produce mechanical vibrations, which can then be transmitted into a component. Other methods of exciting ultrasonic waves include electromagnetic acoustic transducers (EMATs) [47] or laser ultrasonics [98].

In early guided wave research angled, water-coupled PZT compression probes were used to generate Lamb waves in plates using the coincidence rule [17, 111]. This method allowed for favourable excitation of desired modes by choosing the correct angle for the transmitter and receiver transducers relative to the plate to selectively excite particular modes. In the case of water coupling the equation to determine the correct transducer angle is described by Freedman [45]:

$$\theta_p = \sin^{-1}\left(\frac{c_L}{c_p}\right) \tag{2.9}$$

In Equation 2.9, θ_p is the transducer angle, c_L is the longitudinal wave velocity in water, and c_p is the Lamb wave phase velocity in the plate. The process matches the wavelength of ultrasound in the water to the wavelength of Lamb waves in the plate, as determined by the phase velocity. Only a mode with the correct phase velocity will be strongly excited allowing for single mode excitation.

A water-coupled piezoelectric transducer is only sensitive to out-of-plane displacements on the surface of a plate so careful consideration of mode shape is required when selecting an appropriate mode. The A0 mode has high amplitude out-of-plane displacements so exciting this mode is a relatively simple task. In contrast, the S0 mode has high amplitude

in-plane displacement and low amplitude out-of-plane displacements, making excitation of this mode with angled transducers rather more difficult. To negate this difficulty, Lowe et al. [71] employed a compression transducer directly on the end of the plate. However, in many cases it is not feasible to do this.

An alternative to water-coupled transducers is to use dry-coupled transducers, and this is possible because of the relatively low frequencies used in guided wave testing. Alleyne and Cawley [12] developed a dry-coupled transduction system for pipes using shear piezoelectric transducers aligned axially along the pipe to excite the $L(0,2)$ mode. Shear transducers have a piezoelectric crystal orientated so that particle motion is parallel to the surface of the transducer, unlike a compression probe where particle motion if perpendicular to the transducer surface. This allows shear transducers to excite and receive shear motion. The dry-coupled transducers were compared to fully bonded transducers and the performance of the two types was similar. Rotating the transducers so that they are aligned circumferentially around the pipe allows for the excitation of the $T(0,1)$ mode [16], a popular mode for guided wave pipe inspections [27].

By employing a ring of transducers around the pipe it is possible to suppress non-axisymmetric modes and excite only the desired axisymmetric modes. The number of transducers needed in the ring is determined by the dispersion curves in a pipe, and with N transducers it is possible to suppress up to the $N-1$ order flexural modes [16].

Ultrasound pulses can also be generated in conductive or magnetostrictive materials using electromagnetic acoustic transducers. EMATs utilise an alternating electromagnetic coil and a permanent magnetic field to induce eddy currents in a component, causing the surface to expand or contract due to the Lorentz force. By arranging the coils it is possible to excite compression, shear vertical and shear horizontal ultrasound waves in the material [55].

The advantages of EMATs compared to piezoelectric transducers is that they are non-contact and therefore do not have any coupling issues. It also possible to excite a shear horizontal wave mode which is almost impossible with PZT. The primary disadvantage is that EMATs will generally produce much lower amplitude signals, and can therefore

be less sensitive than PZTs [42].

A method to improve the signal amplitude achieved using EMATs is to make use of the magnetostrictive effect. Compared to a purely conductive material, a magnetostrictive material will interact much more strongly with a magnetic field so higher amplitude ultrasound can be achieved. The steel used to construct power station boilers is not naturally magnetostrictive, however when they are exposed to high temperatures magnetite forms which is magnetostrictive. For this reason EMATs can be used on any plant component that is exposed to high temperatures, but not components that are not [101]. A magnetostrictive strip can be artificially created by bonding a strip of magnetostrictive material to the outside of a pipe, a method utilised by Kwun et al. [62]. For a fuller description of the application of EMATs in a power station environment please see Section 5.2.

Lasers can be used to generate ultrasound in a material by using a high-power pulsed laser to alternately heat and cool the material, causing it to expand and contract. A second receiving laser can then monitor vibrations in the material by interferometry. Laser ultrasound systems are not widely used for guided wave inspections because of their expense and the fact that they can be unwieldy for on-site applications [98].

2.7 Use of guided waves in non-destructive evaluation

Since the mid 1990's guided wave inspections have become routine in industry, particularly in the petrochemical industry. Currently the most common application area is the detection of corrosion under insulation in pipes [70]. Guided waves are well suited to this task as the pipes are often long and straight, and guided waves reflect strongly from corrosion defects. The advantage of guided waves when trying to locate corrosion under insulation is that full coverage of long lengths of pipe is possible without having to expensively remove lagging. A guide for interpreting corrosion measurements is provided by Demma et al. [33]. Other guided wave pipe inspections are advantageous if any pipework is inaccessible, for instance buried under a road.

Several commercial applications of guided wave pipe inspection systems are available. Systems that use piezoelectric transducers are available from Guided Ultrasonics Ltd [1], a spin-off from Imperial College (pictured Figure 2.11), and TWI who provide the Teletest®system [78]. Magnetostrictive guided wave sensors are also available from SWRI in the USA [63]. Both of the PZT systems can address the transducers individually, allowing for the monitoring of non-axisymmetric flexural modes so an assessment can be made as to whether a reflected signal is from an axisymmetric or non-axisymmetric discontinuity. The magnetostrictive system does not use individually addressable transducers so this function is not possible.

Figure 2.11: Picture of commercial guided wave equipment produced by Guided Ultrasonics Ltd. This is the G3 instrument attached to a low-profile 5 inch solid transducer ring.

The most popular mode for pipe inspections is the fundamental torsional $T(0,1)$ mode [16] because it is non-dispersive over the entire frequency range, and it is a simple task to excite a single mode. Previously the $L(0,2)$ mode was considered most suitable for long-range testing, but the difficulty of achieving single mode excitation, due to the presence of the $L(0,1)$ mode at low frequencies, has led to it being less widely used now. The $T(0,1)$ mode also has the advantage that it is less affected by fluids in the pipe than the $L(0,2)$ mode [16].

The maximum range of a guided wave inspection system depends heavily on the condition

and layout of the pipe. In ideal conditions an inspection range up to 100m from the inspection location is possible. Pipe features such as welded supports, bends, welds and T-pieces will reduce this distance, and it is impossible to inspect beyond a flange. Bonded coatings such as bitumen can cause extreme attenuation due to guided waves leaking into the bitumen [100]. General corrosion in a pipe also reduces inspection range because of small ultrasound reflections caused by the corrosion. For a clean pipe Alleyne et al. [15] determined that a practical testing limit is either two bends or six welds.

The detection limit for a defect in a real pipe is stated as 5% [73] loss of cross-section. This is averaged over the full pipe circumference, so the reflection amplitude would be the same for a defect with a 5% depth extending around the whole circumference, and a through-thickness defect extending around 5% of the circumference. This applies to both circumferential cracks and corrosion defects. It is however possible to discriminate between a defect extending around the whole circumference and a much more localised defect by measuring the amplitude of the mode-converted signal.

Laboratory systems, some of which have undergone field trials, have been developed for Lamb wave inspections of plates [46, 108]. These systems use the principles described by Alleyne and Cawley [9] to optimise the inspections. Guided wave inspections have been conducted on rail [27, 106] using prototype equipment, and inspections of rock-bolts have also been conducted [21–23].

Research is currently being conducted on the use of circumferential guided waves for NDT applications and a small number of commercial suppliers are developing inspection systems that utilise circumferential guided waves. Valle et al. [104] used circumferential guided waves to inspect a helicopter component. The component was a rotor hub consisting of an inner and outer cylinder where fatigue cracks may form on the interface, although the study examined the more general case of multi-layered cylinders. Circumferential guided wave dispersion relations were calculated numerically for three scenarios: a solid cylinder; a hollow cylinder; and the two layer cylinder.

The work on inspecting cylindrical structures was expanded on by Valle et al. [103] in a paper that described how cracks can be located and characterised using circumferential

guided waves. The method relies on measuring the reflection consisting of a complicated multi-mode broadband signal in the frequency range of 0.2-2 MHz. Advanced signal processing techniques are then implemented to gain information about defects. It is possible to size defects using this technique by measuring the energy of the reflected signal, although this relies on the fact that the crack is over the full axial extent of the inspected component. The modelling in the study was limited to 2D, assuming a crack with an infinite axial extent. No attempt was made to investigate the effect of varying the axial extent of the crack, as this was not relevant for the application. Using this method it is possible to detect axial cracks with a 10% through-wall extent in a rotor hub component, sufficient to detect a critical size axial crack in a power station. It remains to be determined how the axial extent of such a crack would affect the detectability.

Cheong et al. [29] describe an inspection technique to locate axial defects in feedwater pipes in a pressurised heavy water nuclear reactor. A standard 500 kHz angled transducer is used to generate the circumferential waves. Because it is difficult to achieve the exact incident angle on a curved surface and the critical angle is required to perform the inspection, a rocking method is employed. This involves rocking the transducer on the pipe to ensure waves are incident at the critical angle.

An inspection method called CHIME that can utilise circumferential guided waves currently exists and is used for industrial applications [92]. The system consists of two transducers in a pitch-catch configuration and the transducers can be placed up to one metre apart on a flat or curved surface. The entire zone between the transducers is inspected. The technique makes use of a compression 'Creeping' wave along the surfaces of the sample and associated transverse 'Head' waves between the surfaces of the sample.

A schematic of the Creeping and Head waves, along with bulk P and S waves, is presented in Figure 2.12. The Creeping wave propagates along the surface and the Head waves skip between the two surfaces. To transmit the creeping and head waves the transducer must be angled to generate shear waves in the material at the critical angle. The combination of creeping/head waves creates ultrasonic peaks in the receiver and the peaks can be analysed to determine the location and extent of corrosion. The first peak is a direct

Creeping wave. The second peak is a Head wave that has undergone a full skip and then propagated the remaining distance as a Creeping wave. The third peak is produced by a Head wave that has undergone two full skips and propagated the remaining distance as a Creeping wave, and so on.

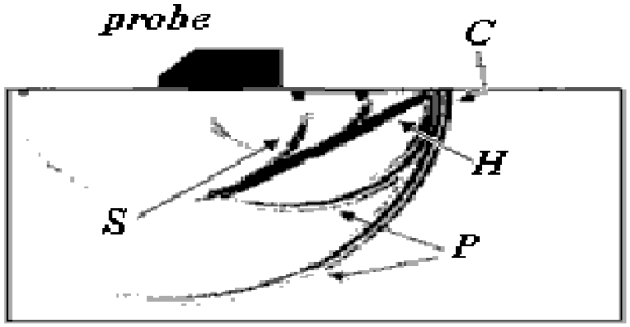

Figure 2.12: (Reproduced from [92]) Schematic snapshot of Creeping and Head wave generation from a probe at the ultrasonic critical angle. Illustrated are the Creeping wave (C), Head wave (H), direct compression waves (P) and shear waves (S) generated due to the finite size of the probe.

CHIME can only be used on structure with limited curvature; in a pipe the practical limit is an outer-radius:inner-radius ratio of 1.19:1. At curvatures higher than this the pipe walls may not be parallel enough for the Head wave to strike at the critical angle and convert to a creeping wave. Full coverage therefore cannot be guaranteed. For reference in the 5 inch pipework at Grain power station this ratio is 1.22:1, which is outside the range for CHIME.

Another technology using circumferential guided waves to detect corrosion in pipes is described by Fraunhofer IZFP [82] (in German). The system utilises two EMAT transducers and can detect corrosion by measuring the attenuation of the guided wave propagating across the corrosion. The amplitude of the guided wave propagating across the corrosion is compared to a direct signal that does not scatter from any pipe defects. A larger difference in amplitude between the two signals is caused by greater attenuation of the propagating signal and indicates corrosion may be present.

2.8 Conclusions

In this chapter the theory and current applications of guided waves have been described. A brief history of guided wave research was included along with the physics behind guided waves. The scattering of guided waves from discontinuities in plates and pipes was explored in the context of using guided waves for non-destructive testing.

Although guided waves are already an established technology for detecting corrosion in the petrochemical industry, little work has been done on detecting and characterising crack-like defects in pipes, particularly cracks oriented in the axial direction. The next chapters will investigate the scattering of guided waves from axial cracks in pipes in order to determine whether they represent a viable inspection technique for detecting axial cracks in power station pipework.

Chapter 3

Reflection of the fundamental torsional mode from axial cracks in pipes

3.1 Introduction

In this chapter the reflection characteristics of the fundamental torsional guided wave mode from axially aligned crack-like defects in pipes is studied. This alignment of cracks in pipes has not been previously studied because it is expected that an axial crack will only produce a very small reflected signal. For guided waves to become a useful tool for detecting axial cracks in a power station environment it will be necessary to detect a critical sized defect, determined to be 20% of the through-thickness extent of the pipe [43].

Finite element modelling (FEM) and laboratory experiments have been used to determine the nature of the reflection of guided waves from axial cracks in pipes. FEM is a very useful tool because its use allows a large quantity of data to be collected in a relatively short amount of time at low cost. Many different cracks geometries can be modelled, for instance crack length, crack depth and crack width, and other variables such as

incident toneburst frequency and pipe dimensions. It would prove difficult and time consuming to test all of these variables experimentally. Instead a small number of laboratory experiments are conducted in order to validate the FE results, and FEM is then relied upon to provide an accurate data for the scenarios that have not been tested experimentally.

A schematic of the pipe layout used for both the modelling and the experimental work in this study is presented in Figure 3.1. A ring of transducers is located at one end of a short length of pipe, with an axially aligned crack some arbitrary distance away. Shear transducers are used and are aligned to excite and receive particle motion in the circumferential direction. The transducers are excited simultaneously to produce a fundamental torsional $T(0,1)$ guided wave mode and the responses from all of the transducers are summed to measure the reflection of the $T(0,1)$ mode. Summing the responses ignores the effect of any mode-converted flexural modes that reflect off the defect.

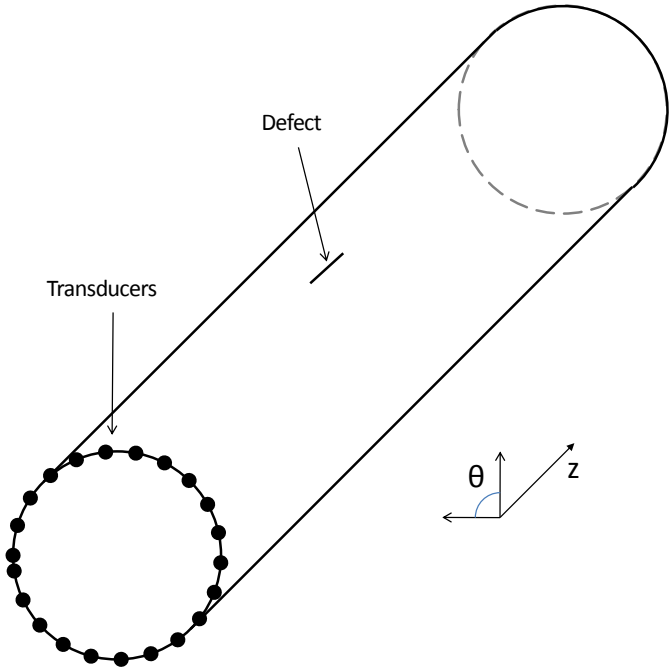

Figure 3.1: Schematic diagram of transducer layout and defect location on pipe.

To assess how strongly the incident torsional waves reflects from the defect the reflection coefficient is calculated using Equation 3.1, where R is the reflection coefficient.

$$R = \frac{\textit{Amplitude of reflected signal}}{\textit{Amplitude of incident toneburst}} \tag{3.1}$$

The reflection coefficient is calculated in the time domain rather than the frequency domain. Time domain calculations are based on the maximum amplitude of a Hilbert transform, whereas for a frequency domain calculation the signal needs to be windowed and Fourier transformed. However, it can be difficult to window the desired signal if there is signal overlap. Figure 3.2 presents two overlapping tonebursts in the time domain and includes a Hilbert transform of the signal. In this case it would be impossible to separate the two signals in order to perform a frequency domain reflection coefficient calculation, but the time domain amplitude is unaffected.

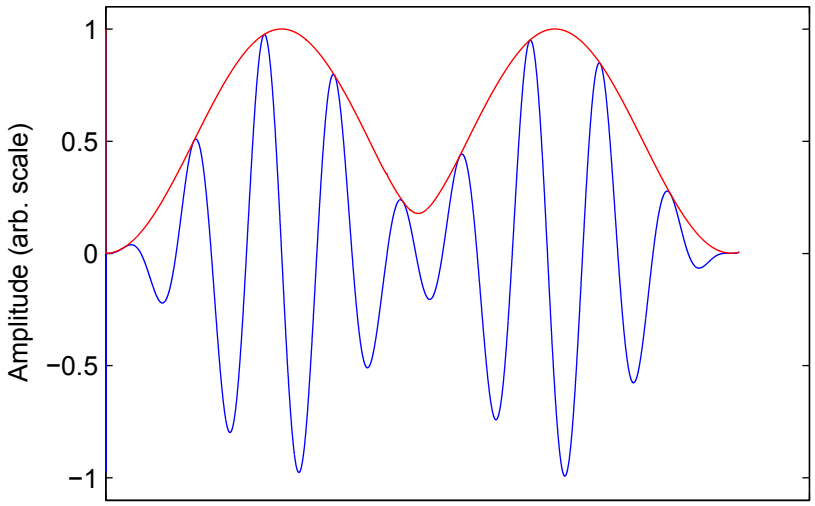

Figure 3.2: Demonstration of how overlapping signals can prevent calculation of reflection coefficient in the frequency domain. The time signal is in blue and a Hilbert transform in red.

Much of the work described in this chapter was conducted in collaboration with Madis Ratassepp, who had earlier completed research into the scattering of the SH0 guided wave mode from cracks aligned in the direction of propagation of the wave, in plates [91].

3.2 Mode choice

The dispersion curves presented in Figure 2.6 show that there are many modes that are able to propagate in the frequency range used in this study. The majority of the modes are non-axisymmetric flexural modes but there are also three axisymmetric modes, consisting of two longitudinal modes, $L(0,1)$ and $L(0,2)$, and the fundamental torsional mode $T(0,1)$. It is desirable to excite a single axisymmetric mode in order to ensure the measured signal is as simple as possible.

In this investigation the torsional $T(0,1)$ mode is used as this mode has several advantages over other modes. It is non-dispersive over the entire frequency spectrum making signal interpretation less complicated, and it is possible to achieve pure mode excitation due to the high cut-off frequency of the next torsional mode, which is 130kHz for a 5 inch diameter pipe with a wall thickness of 12.7mm. The dominant particle displacements of the $T(0,1)$ mode are perpendicular to the crack direction, as opposed to the longitudinal modes where the particle displacements are parallel to the crack direction. This is expected to make the $T(0,1)$ mode reflect more strongly from an axial crack than either of the longitudinal modes [76]. The $T(0,1)$ mode is also largely unaffected by fluid in a pipe which can be important in practical situations [33]. The $T(0,1)$ mode is a popular choice of mode in non-destructive testing and there is a large body of literature detailing its use in guided wave testing [27, 33, 36]

By using a ring of transducers placed around the circumference of the pipe it is possible to suppress all non-axisymmetric wave modes present at the desired frequencies [16]. By orienting the shear transducers in the circumferential direction only the torsional mode is excited and not the longitudinal modes. It is possible to excite the longitudinal modes by orienting the transducers in the axial direction, but it is difficult to selectively excite either of the two longitudinal modes without exciting the other. Multi-mode excitation is not an issue when considering torsional modes because the cut-off frequency of the $T(0,2)$ mode is outside the frequency range used in this study.

3.3 Finite element modelling

The reflection of guided waves from circumferential notches in pipes has been successfully studied in the past using the finite element method [14, 36]. Finite element analysis was conducted using the ABAQUS software with its explicit time stepping procedure [5]. Both membrane and full 3D models [14] were used for this study.

Membrane models have the advantage that they are computationally inexpensive, but they are limited to the modelling of through-thickness cracks. Membrane models are constructed using four-node linear "membrane" elements that are arranged to form the shape of a pipe. The elements are placed at the mid-wall radius of the pipe. Each node of an element has three degrees of freedom, displacements in the axial, circumferential or radial direction. Because a membrane element has no depth, only modes that have uniform particle displacements through the thickness of the pipe wall can be modelled using a membrane model. The $T(0,1)$ mode does have uniform particle displacements through the thickness of the pipe wall so membrane models can be used to study the reflection of the $T(0,1)$ mode from through-thickness axial defects

To model a part-depth crack or notch it is necessary to use a full 3D model, where the whole volume of the pipe is discretized using eight-node linear "brick" elements. Each node of the element has three degrees of freedom (displacements in x, y and z directions) and, although computationally expensive, such elements permit full 3D analysis of the pipe, with part-thickness notches.

The size of the elements in a mesh is determined by the need to satisfy the condition of eight elements per wavelength, which was found to produce reliable results by Lowe et al. [69]. Conversely the maximum frequency when using a model with a given element size can also be determined.

The 3D models used in this study have the same dimensions as two real pipes used in experiments (see Section 3.4), in order to provide a direct comparison between finite element and experimental results. The 3.7 m long pipe, with an outer diameter of 141.3mm and inner diameter of 115.9mm, was modelled using a mesh with 925 elements

along the length, 128 elements around the circumference, and 5 elements through the wall thickness. As a result each element was 4 mm long, 2.5mm deep and 3.47mm around the circumference on the outer surface of the pipe. With elements of these dimensions, and using the criteria stated above, the maximum ultrasonic frequency is limited to 80 kHz, sufficient for this part of the study.

When modelling pipes with through-thickness cracks a membrane model of a steel pipe 3.7m long and with a diameter of 140mm was used. A mesh with 925 elements along the length and 128 elements around the circumference gave an element size of 4mm along the length and 3.43mm around the circumference. Certain aspects of the study required simulations using relatively high ultrasonic frequencies, with an incident toneburst centre frequency of up to 160 kHz. A finer mesh membrane model was used, the model pipe having a length of 3.7m and a radius of 0.07m and consisting of 3700 elements along the length and 440 elements around the circumference, giving element dimensions of 1mm square.

Notches of small width were used to represent the cracks, in order to best simulate experimental conditions. They ranged in through-wall extent from 100% to 20% depth. Figure 3.3 shows how the mesh was modified to produce a notch, with both a plan view and a view looking axially along the pipe for the case of a full 3D model. In a membrane model the width of a notch is a single value, as the model has no variation through the thickness. In a 3D model the width of the notch varied through the thickness of the pipe wall due to the curvature of the pipe. To model the experimental data as accurately as possible the width of the notch in the 3D pipe models had an average opening of 3mm (notches were created in the real pipe with a width of 3mm, see Section 3.4. On the outer surface of the pipe the opening displacement was 3.29 mm and on the inner surface the opening displacement was 2.70 mm. This notch profile was the same in all 3D pipe models. The notches were formed by varying the shape of the elements in the region around the defect.

The axisymmetric torsional mode $T(0,1)$ was generated by prescribing identical tangential displacement time histories at all nodes at the end of the pipe. Numerous simulations were performed in which the central frequency of the tone burst ranged from 15 kHz to

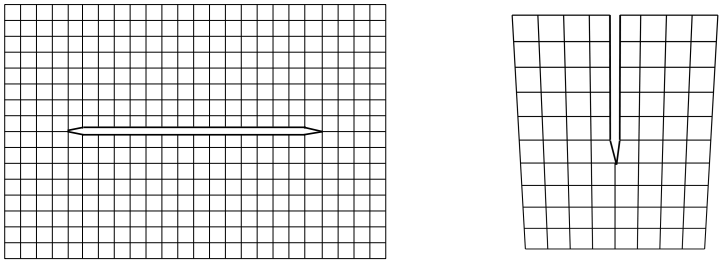

(a) Plan view **(b)** Front view

Figure 3.3: Demonstration of how finite element mesh is modified to include a crack. a) The mesh is shown in plan view and b) The 3D solid mesh is shown looking axially along the pipe.

160 kHz with the majority of the work using a 5-cycle toneburst modified with a Hanning window. Part of the study investigates how varying the incident frequency affects the reflection coefficient, and for this work a narrow band signal consisting of a 10-cycle toneburst modified with a Hanning window was used. The monitoring was performed by measuring the circumferential displacements at 16 nodes, simulating the receivers, equally spaced around the circumference at the end of the pipe.

3.4 Experimental procedure

Experiments were performed on two nominal 5 inch diameter steel pipes with an outer diameter of 141.3mm and wall thickness 12.7mm. The pipes were 3.7m long. Figure 3.4 shows the experimental set-up with the pipe ends labelled 'A' and 'B', and a transducer ring attached to end A of the pipe. The pipes were mounted on a milling machine for the duration of the experiment to enable the accurate cutting of axial notches without having to disturb the transducer ring. Two pipes were available so it was possible to experiment with two different notch depths. The notches were milled *in-situ* with the transducers remaining in place whilst the cutting was taken place. This was to ensure that there was no variation in transducer coupling or position that could affect the results. The notches were 3mm wide and their length was increased by increments of 8mm up to 120mm. Due to the shape of the drill-bit the ends of the notch were rounded and the

part depth notch was flat bottomed. They were aligned axially along the pipe. The cut was started 1.8m from the end A of the pipe and extended away from the transducer ring. One of the notches was through-thickness, the other was a part depth notch with a through-thickness extent of 80%, so had a depth of 10mm. The pipes were supported on 'v' blocks which have been found to produce a minimal reflected signal [11].

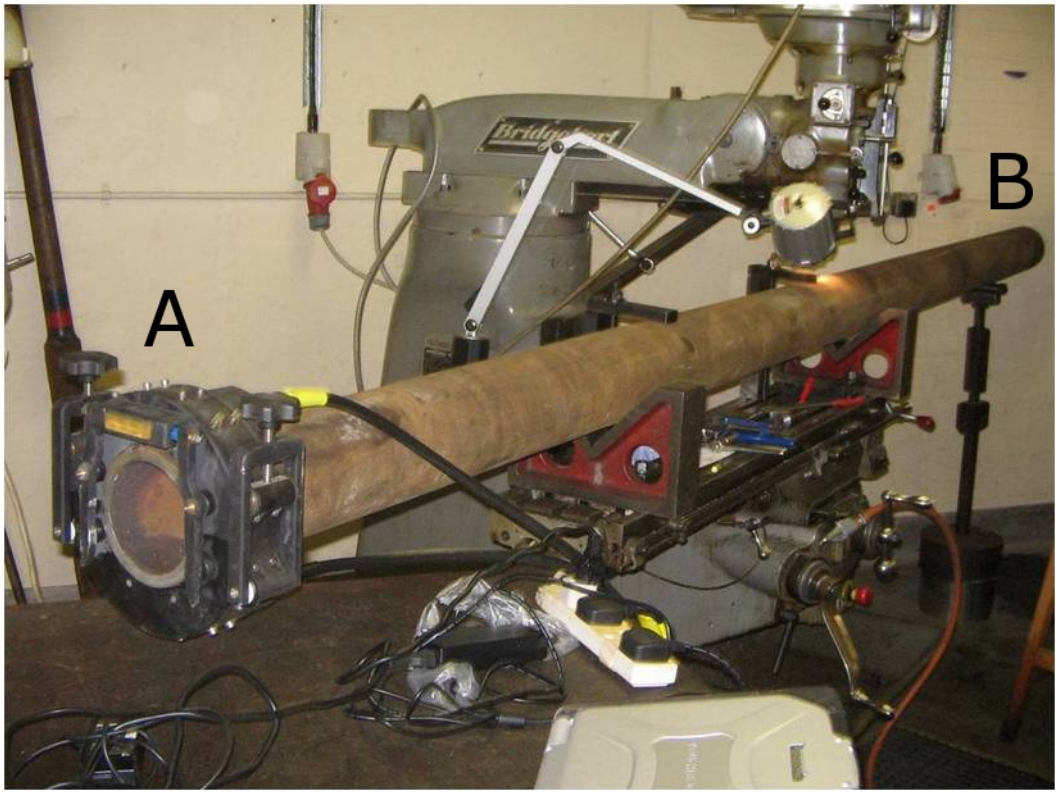

Figure 3.4: Picture of experimental set up. The pipe is mounted on a milling machine and a transducer ring can be seen on the near end of the pipe.

In order to produce the torsional $T(0,1)$ mode required for this experiment a ring of transducers needed to be clamped to the pipes. The transducer ring was produced by Guided Ultrasonics Ltd [1], and can be seen at end A of the pipe in Figure 3.4. In fact two rings of transducers are contained within the clamp as the hardware supports directionality in the sound wave by delaying excitation of one of the rings. Directionality was not important in this investigation so only the transducers from one of the rings were excited, with the transducers in the second ring not activated. Each ring is made up of 16 shear transducers oriented in such a way as to impart force in the circumferential direction around the pipe, so that only the $T(0,1)$ mode was excited. The transducers

are arranged in pairs with each pair controlled by a single channel from the generation equipment, with a total of eight channels for each ring of transducers. The pairs are arranged so that both transducers are in the same ring within the transducer housing, meaning it is possible to excite a single ring. Also, by summing all of the received signals it was possible to only monitor the reflected $T(0,1)$ mode and disregard mode converted signals.

The transducer ring was placed as close to end A of the pipe as possible in order to eliminate echoes from end A of the pipe. A reflection from end A of the pipe would interfere with the excitation wave propagating towards the crack and produce unpredictable results. The distance between the transducer ring and end A of the pipe was much less than the wavelength of the excited toneburst, thus the problem was minimised.

The equipment used to control the transducers was a Wavemaker G3 instrument produced by Guided Ultrasonics Ltd [1]. For this experiment the signal produced was a 5-cycle toneburst modulated by a Hanning window. The centre frequency of the tonebursts ranged from 20kHz to 65kHz in increments of 5kHz. Each individual 'shot' was performed at a specific centre frequency. Therefore there was a shot at each increment of crack length and at each increment of frequency. Measurements were also taken before any milling had started in order to get a clean reference signal. Each shot consisted of 256 averages in order to improve the signal to noise ratio. This was very important due to the expected very small signals.

3.5 Results and discussion

In this section results are presented illustrating how various parameters affect the reflection coefficient of the $T(0,1)$ mode from an axial notch/crack in a pipe. The majority of the parameters are investigated using finite element analysis, with experimental validation of FE results in the case of the crack length investigation. Figure 3.5 presents an image of an FE model after the incident toneburst has reflected from the crack. The

incident toneburst has a centre frequency of 50 kHz and the crack length is equal to the wavelength of the incident toneburst. A reflected wave is visible, however it is of low amplitude. It was necessary to artificially increase the amplitudes in the model in order for the reflected signal to be clearly visible. In Figure 3.5 it is also possible to identify a diffracted wave propagating in the circumferential direction.

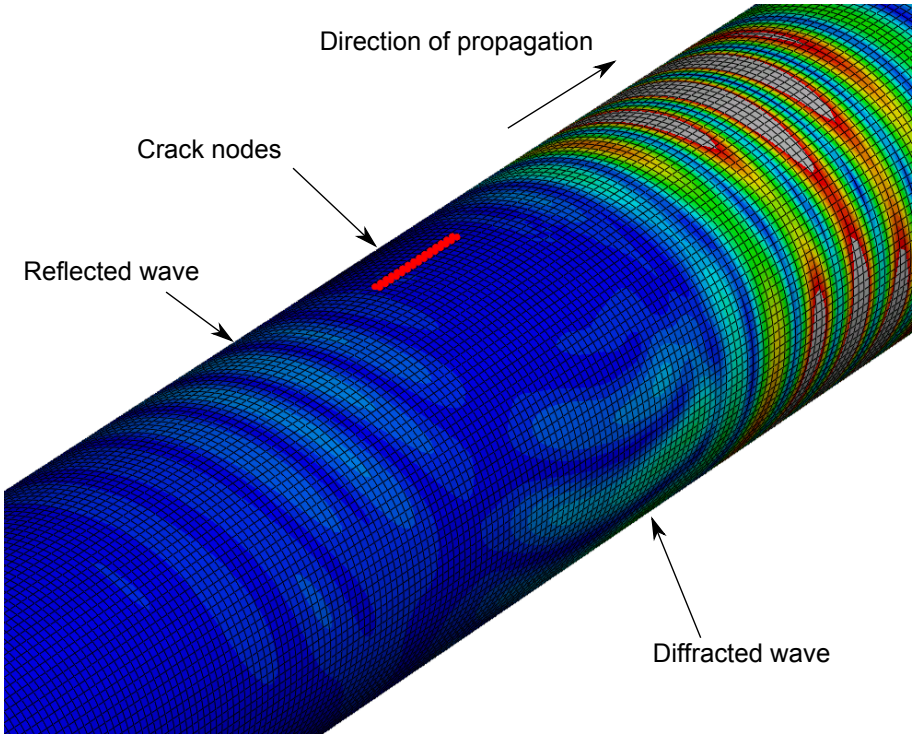

Figure 3.5: Picture of FE pipe model with $T(0,1)$ wave mode reflecting from an axial crack. The crack nodes are highlighted in red and the colour scale represents amplitude on a linear scale. The amplitudes have been artificially increased to make the reflected wave more visible. The incident toneburst has a centre frequency of 50 kHz and the crack length is equal to the wavelength of the incident toneburst.

Typical time traces displaying the transducer response for both FE and experimental data are presented in Figure 3.6, with the incident toneburst; reflection from crack; and endwall reflection all labelled, with the endwall representing a 100% reflection from the end of the pipe section. As the only mode of interest is the $T(0,1)$ mode the time signals from each individual transducer in the transducer ring are summed to produce the results in Figure 3.6. It should be noted that in the FE time trace presented in Figure 3.6a the signal indicating the endwall reflection is significantly larger in amplitude than the signal representing the incident toneburst. The reason for this is the proximity

of the monitoring points to the end of the pipe. This sets up constructive interference as the wave reflects from the end of the pipe where the transducers are located [24].

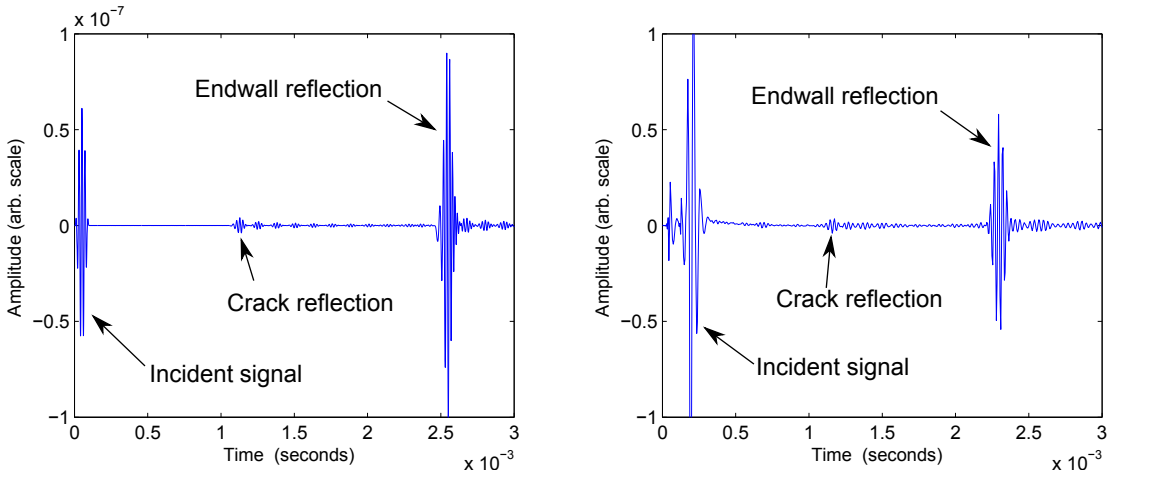

(a) Time trace produced in FE modelling **(b)** Time trace produced in laboratory experiments

Figure 3.6: Typical time traces for FE and experimental data showing the reflection of guided waves from an axial crack.

The reflection from the crack has a pattern specific to axially aligned defects in pipes, which can be seen clearly in Figure 3.7. It consists of a series of pulses with gradually decaying amplitudes. The length of time between the start of each pulse corresponds to the time it would take an SH0 wave mode to propagate around the circumference of the pipe. This behaviour can be explained by the scattering of the incident $T(0,1)$ off the crack in the circumferential direction and propagating around the circumference of the pipe. After propagating around the full circumference the wave is then scattered off the crack again, back towards the receiving transducers. This happens repeatedly as the sound wave continues to propagate around the circumference of the pipe, giving the characteristic signal.

Modelling has shown that the primary reflection and diffraction events occur at the far end of the crack relative to the direction of the incident toneburst. This becomes obvious for very long cracks, where the length of the cracks is higher than the spatial length of the incident 5-cycle toneburst. Figure 3.8 presents a time trace for a through-thickness crack with a length approximately equal to six wavelengths of the incident toneburst. In this case the reflections from the start of the crack and end of the cracks are spatially

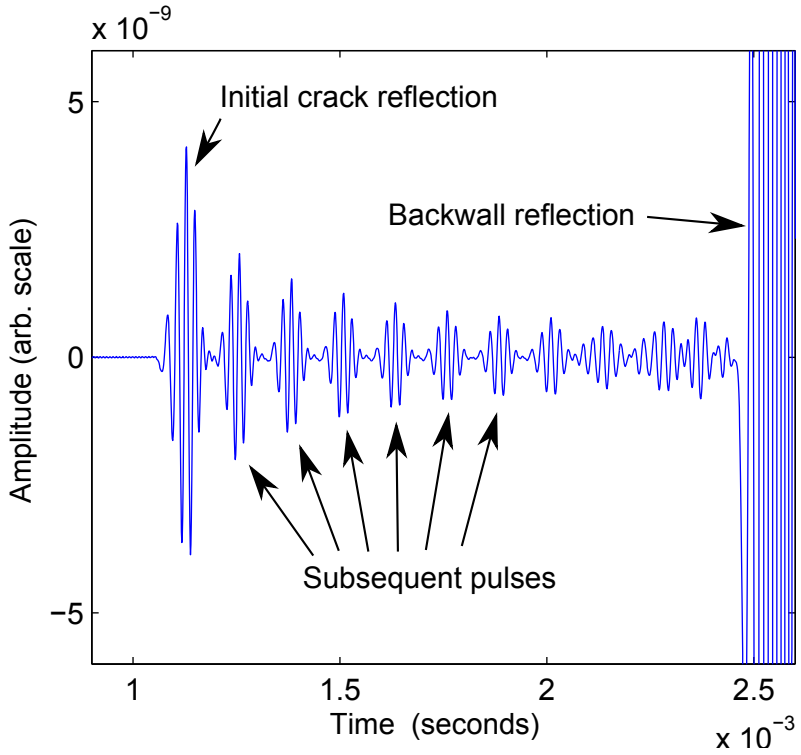

Figure 3.7: Finite element time trace data focusing on the crack reflection

separated, and it can be seen that the amplitude of the reflection from the far end of the crack is much larger than the amplitude of the reflection form the near end of the crack, with an amplitude 16dB higher than the amplitude of the near-tip reflection.

A diagram of the processes that take place when the $T(0,1)$ mode reflects from an axial crack in a pipe is presented in Figure 3.9. The numbered processes in the Figure are described below. In the descriptions the near tip refers to the end of the crack first encountered by the incident wave, and the far tip refers to the other end.

1. The $T(0,1)$ mode propagates along the pipe and until it encounters a discontinuity.
2. When the incident toneburst reaches an axial crack there is a small reflection from the near tip of the crack due to there being a discontinuity in the pipe.
3. A surface wave will propagate along the edge of the crack and will reflect off the far tip of the crack, propagating in the opposite direction back towards the transmitting transducers.

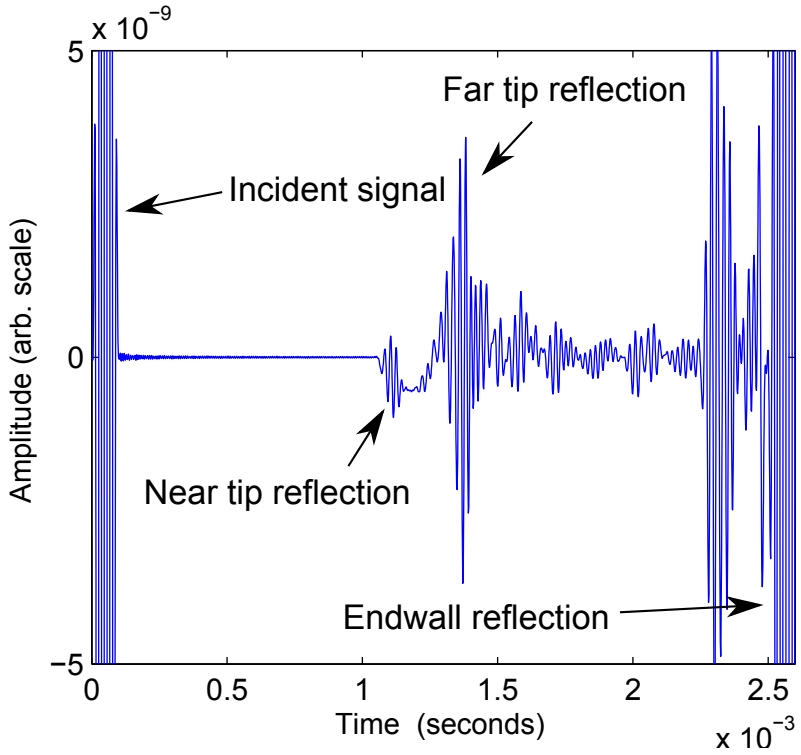

Figure 3.8: Time trace of reflection from a crack with a longer spatial length than the incident toneburst. The reflections from the near tip and far tip of the crack are spatially separated demonstrating that the reflection from the far tip of the crack is of much higher amplitude than the reflection from the near tip of the crack.

4. At the far tip diffraction takes place creating a wave that propagates in the circumferential direction around the pipe. Once this wave has propagated around the whole circumference it scatters off the crack again.

5. The wave reflected from the far tip of the crack propagates as a surface wave back

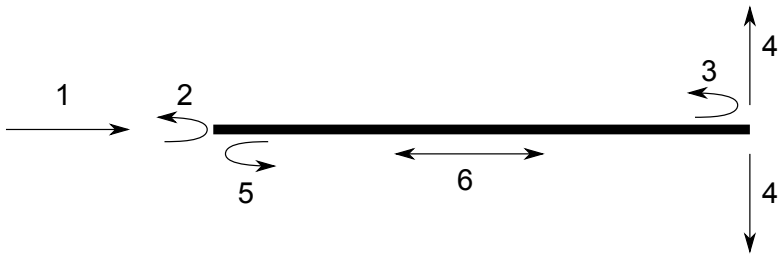

Figure 3.9: Diagram of reflection of the $T(0,1)$ mode from an axial crack in a pipe. The numbers represent individual processes and are explained in detail in the main text.

along the crack and reflects off the near tip.

6. The reflection from both crack tips cause reverberations along the surface of the crack. The reverberations are further complicated when the diffracted wave scatters off the crack. There are complicated interference phenomena occurring that lead to a complicated relationship between reflection coefficient and crack length.

3.5.1 Crack length - through-thickness crack

A comparison between FE predictions and experimental results for a through-thickness crack, as a function of crack length, is presented in Figure 3.10. Comparisons are presented over a range of toneburst centre frequencies - 30 kHz, 35 kHz, 40 kHz and 50 kHz. Finite element results are presented here for both 3D models and membrane models, which is possible because through-thickness cracks are being investigated. The purpose of presenting results for both types of model is to validate both model types with experimental data.

In general there is good agreement between FE modelling results and experimental results, with the exception of when the frequency was at 40 kHz. Here there was a marked difference between the FE and experimental results with the experimental results being consistently higher than the FE predictions. There was also a more pronounced cyclical nature to the experimental results relative to the FE data. There is a slight discrepancy between the membrane finite element predictions and 3D finite element predictions, with the membrane models having a consistently lower amplitude than the 3D models. The disparity in amplitudes between 3D and membrane FE models could potentially be due to subtle effects in the 3D models, such as variation in particle stress and displacement through the thickness of the pipe, or differences in the inner and outer radii of the pipe, that are not considered in a membrane model. However, as the data produce by the two types of model are similar it is possible to ascertain that both model types provide accurate predictions of guided wave reflection characteristics from axial cracks in pipes.

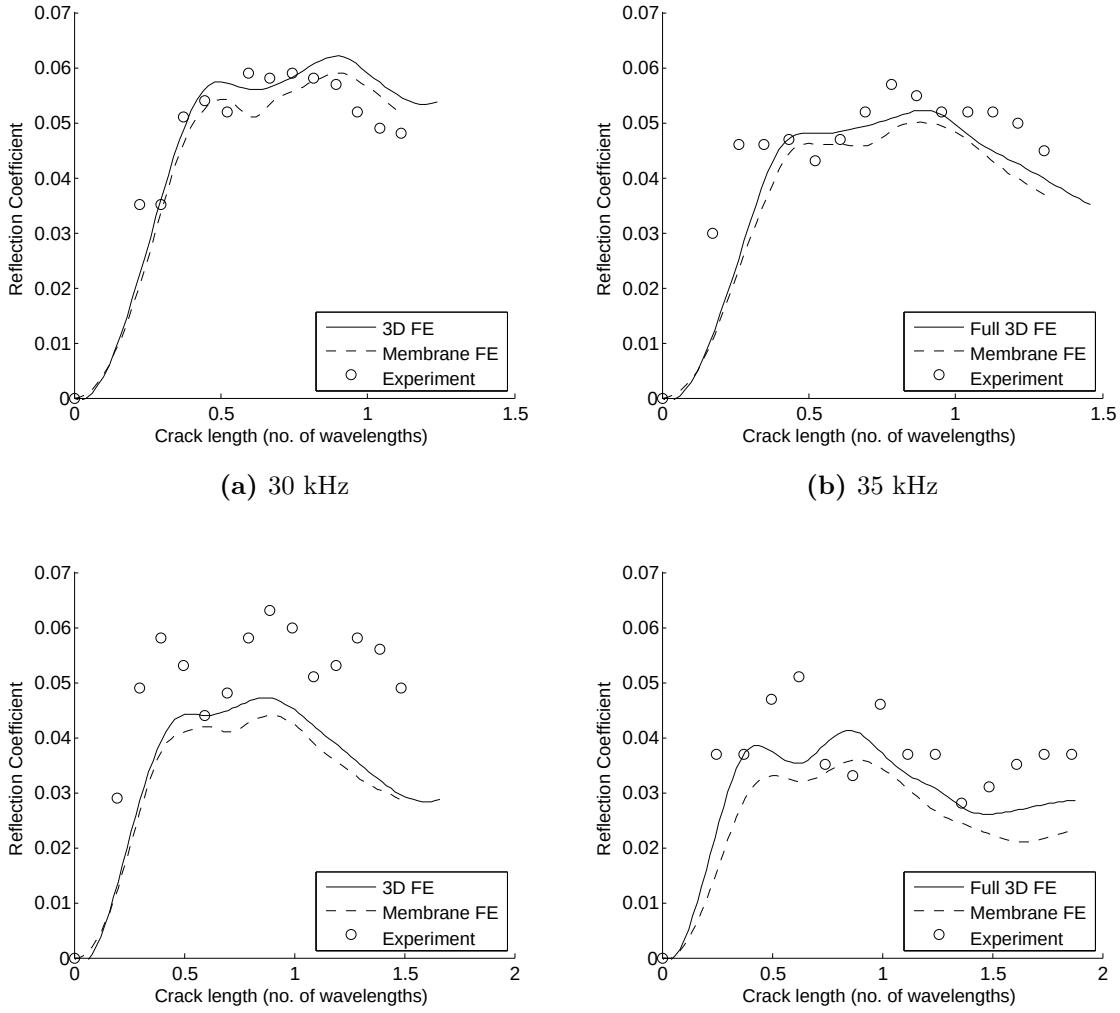

(a) 30 kHz **(b)** 35 kHz

(c) 40 kHz **(d)** 50 kHz

Figure 3.10: Comparison of finite element and experimental data for the reflection coefficient as a function of crack length for a through-thickness crack in a pipe, over a range of frequencies. The crack length is scaled with wavelength.

Differences in values between FE and experimental data can be accounted for in the 30 kHz, 35 kHz and 50 kHz cases by the presence of noise. Although low amplitude signals are being examined, in the best-case scenario for laboratory experiments, a good signal-to-noise ratio has been calculated, with a value of 22dB. This SNR value was calculated with an incident toneburst centre frequency of 30 kHz with a crack length of 64mm. Here the signal to noise ratio was calculated by measuring the root mean square of the crack reflection and comparing it to the root mean square of the same location in the time signal of the clean pipe.

It is more difficult to reconcile the difference in the 40 kHz case. The differences between FE and experiment are much larger and the cyclical interference pattern in the experimental data is much more exaggerated compared to the FE models. It is unlikely that random noise is a cause of this. It is likely that this effect is caused by a larger reflection from the front of the crack than predicted in the model. The shapes at the ends of the crack are necessarily different in the model and the experiment, with a V-notch in the model and a rounded end on the real pipe. The rounded end may be particularly sensitive to reflection at 40 kHz with a reduced effect at lower frequencies.

At all frequencies the reflection coefficient increases with crack length until the crack length is slightly less than half of the wavelength, λ, of the incident toneburst. As the crack length continues to increase there is a small reduction in reflection coefficient, an effect that is more exaggerated at certain frequencies. A maximum value of reflection coefficient occurs when the crack length is slightly shorter than the wavelength of the incident toneburst, with a length of approximately 0.9λ.

With crack lengths up to one wavelength it is predicted that the explanation for the peaks in reflection coefficient are caused by interference between the reflection from the beginning of the crack and the reflection from the end of the crack. This would be expected to produce peaks when the crack length is equal to a multiple of $\frac{1}{2}\lambda$, but it is observed that the peaks occur at slightly shorter crack lengths. Rayleigh [93] demonstrated that the velocity of propagation of a surface wave on an elastic solid is $0.9554c_s$, where c_s is the bulk shear velocity, equivalent to the $T(0,1)$ mode velocity. The surface wave propagating along the edge of the crack therefore has a shorter wavelength than the fundamental torsional mode in the pipe, and the peaks occur at shorter crack lengths than would be expected if the surface wave velocity was equivalent to the $T(0,1)$ mode velocity.

When the FE crack length results are presented for different frequencies (see Figure 3.11) it becomes clear that for a through-thickness crack the reflection coefficient is greater at lower frequency. This affects the choice of frequency when performing an inspection and suggests that axial defects should be more detectable at low frequencies. This issue is discussed more thoroughly in Section 3.5.3.

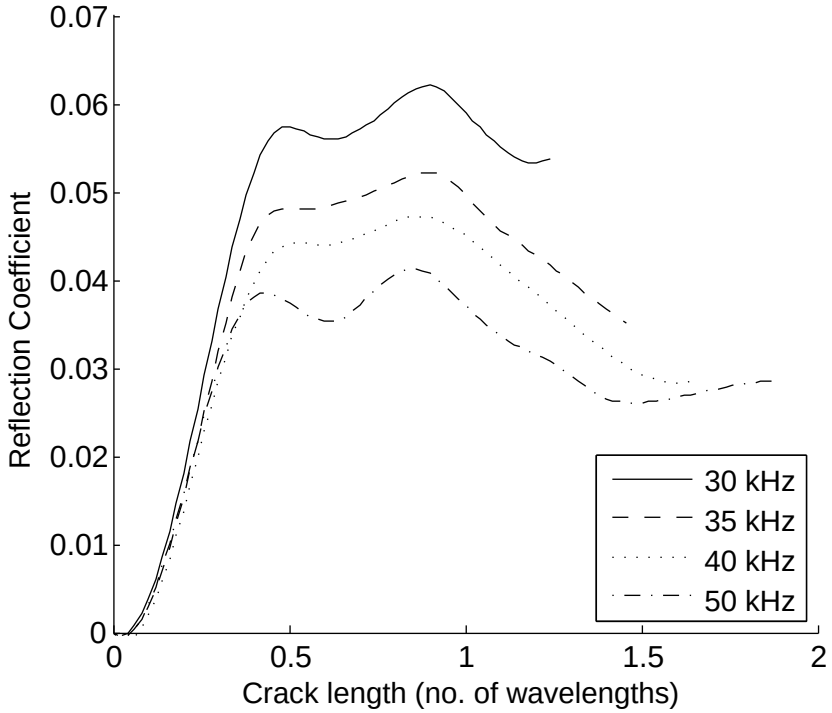

Figure 3.11: FE results displaying reflection coefficient as a function of crack length over a range of incident toneburst frequencies.

3.5.2 Crack length - Part-depth crack

A comparison between finite element predictions and experimental data is presented in Figure 3.12 showing how reflection coefficient changes as a function of crack length for a crack with a through-wall extent of 80%. Results are presented for incident toneburst frequencies of 35 kHz, 40 kHz and 50 kHz, and the agreement between FE and experimental data is excellent. Only 3D FE models are used when studying part depth cracks, because it is impossible to model a part depth crack using membrane elements. The reflection amplitude is around half the amplitude of the reflection amplitude of the through thickness crack at the same frequency for an equivalent length crack, suggesting a non-linear relationship between crack depth and reflection coefficient. It is not possible to identify the 'echoes' that were present in the time traces of the through-thickness crack experiments due to their amplitude being too low.

Similar to the through-thickness results, there is an interference pattern evident in the data. The effect is more pronounced for a part-depth crack than a through-thickness

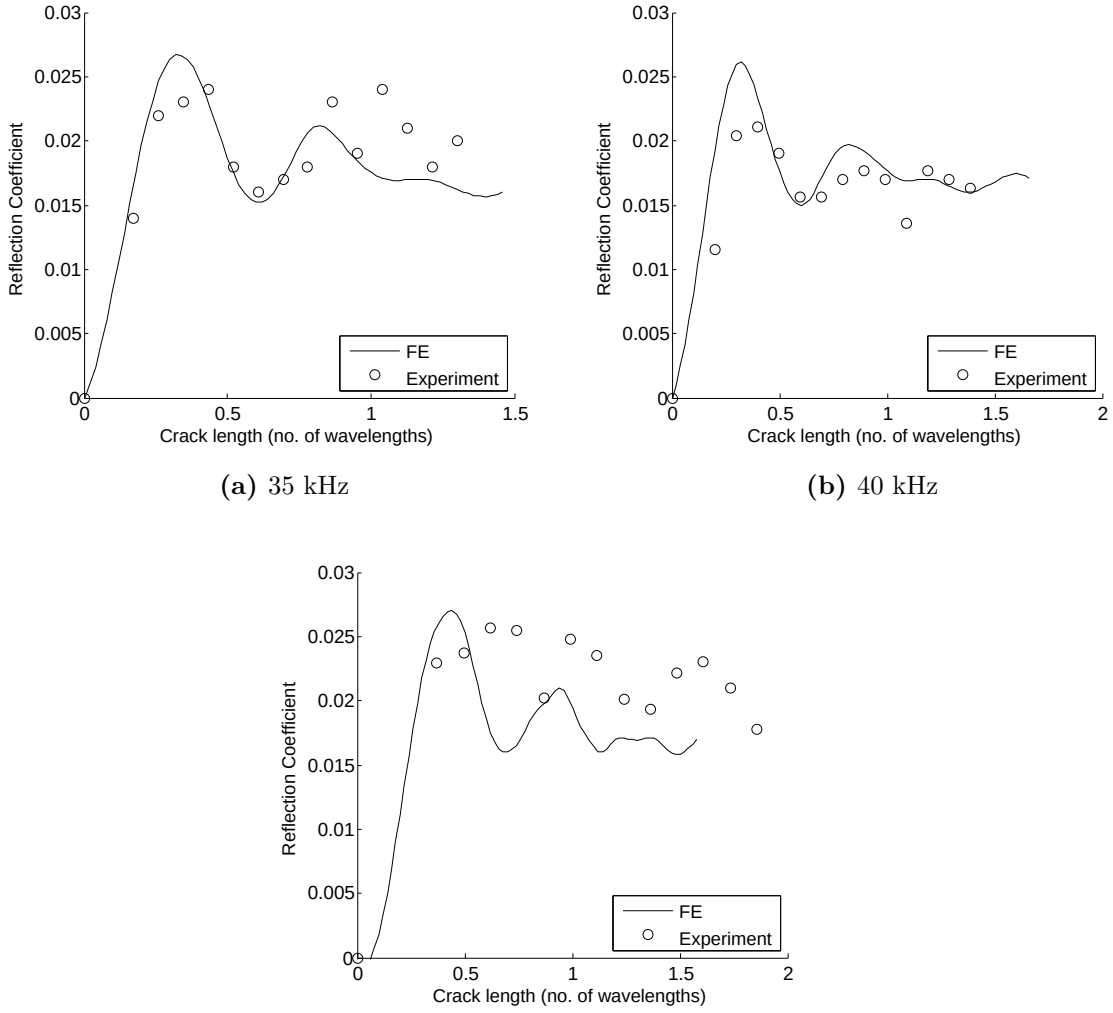

(a) 35 kHz

(b) 40 kHz

(c) 50 kHz

Figure 3.12: Comparison of finite element and experimental data for the reflection coefficient as a function of crack length for a part depth crack of 80% through-thickness extent in a pipe, over a range of frequencies. The crack length is scaled with the wavelength of the incident toneburst.

crack. The amplitude of the reflection from the start of the crack does not decrease as much as the amplitude of the reflection from the end of the crack as the through-thickness extent of the crack is reduced. This is shown in Figure 3.13 where there is a 10dB difference in amplitude between the near tip and far tip reflections, less than the 16dB difference observed for a through-thickness crack. The peaks in reflection amplitude again occur at crack lengths shorter than the half-integer wavelength values for the incident toneburst.

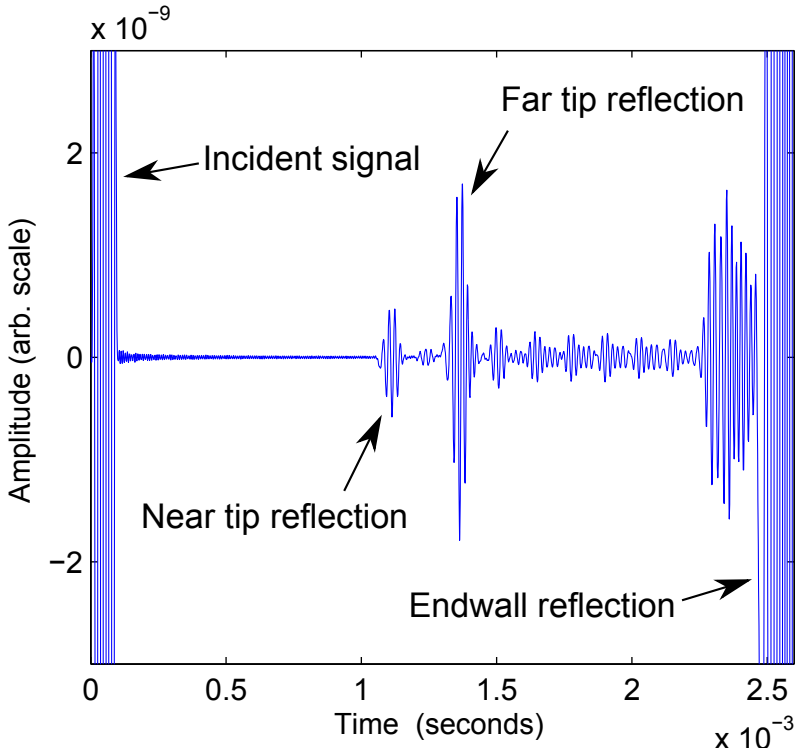

Figure 3.13: FE time-trace of reflection from a crack with a through-thickness extent of 80% and a length of 6λ, demonstrating the difference in amplitude between the near tip and far tip reflections for a part depth crack.

A reduction in crack depth would intuitively lead to a reduction in the amplitude of waves scattered from the crack. The cross-section of the crack is smaller, therefore reducing the reflection from the start of the crack. The mode conversion from the torsional mode to the surface wave on the crack is reduced because of the reduced free surface of the crack. There is also potential for ultrasound energy to leak from the crack surface into the main body of the pipe. The reduced free surface diminishes both the primary reflection from the end of the crack and the diffracted wave that propagates circumferentially around the pipe. The reduction in scattering energy of the circumferentially propagating wave causes the pulses subsequent to the primary reflection to have a very small amplitude, to the extent that they are no longer detectable, as described previously.

3.5.3 Toneburst frequency

The results presented in Figure 3.14 indicate how the frequency of the incident toneburst affects the amplitude of the reflection coefficient from a through-thickness axial crack in a pipe. The data was generated using membrane finite element pipe models and the toneburst centre frequency varied from 25 kHz to 160 kHz. In all cases the crack length was modelled to be equal to half the wavelength of the incident toneburst, to coincide with the first peak in the reflection coefficient in Figure 3.10. The crack length at which the first peak occurs is not constant with frequency, as can be seen in Figure 3.11, but is close to half the wavelength over the full frequency range.

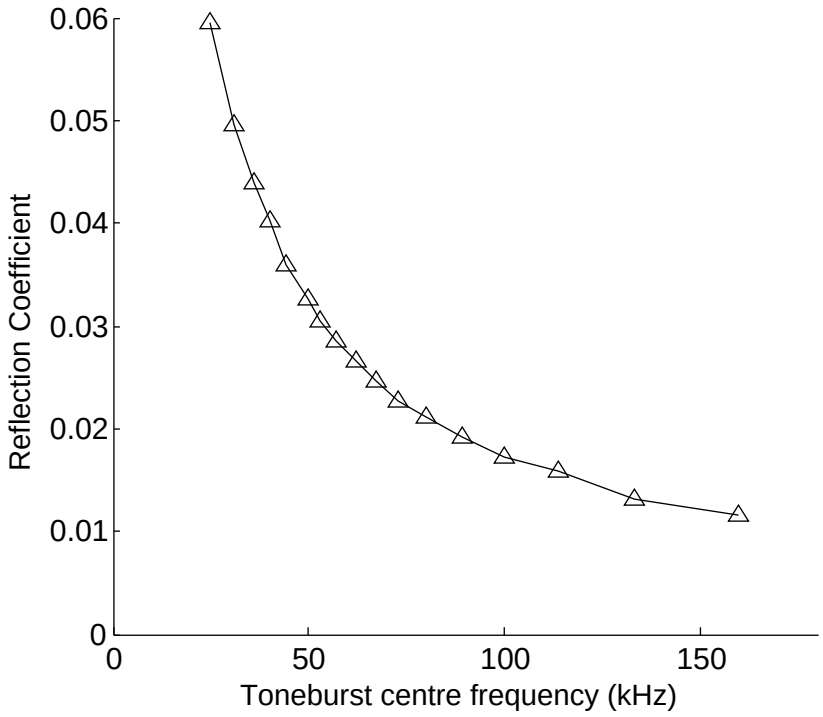

Figure 3.14: Effect of incident toneburst centre frequency on reflection coefficient from a through-thickness axial crack in a pipe with a radius of 70mm. The crack length is half the wavelength of the incident toneburst at all frequencies, close to the crack length of the first peak in reflection coefficient seen in Figure 3.10.

The reflection coefficient is highly dependent on the frequency of the incident toneburst, with a 14dB difference in signal amplitude over the frequency range studied. The frequency range was not extended below 25 kHz because below this frequency the cir-

cumferentially propagating wave was severely interfering with the signal reflecting off the crack, due to the circumference being less than approximately three wavelengths, and signal overlap occurring.

The inverse situation to varying frequency at a fixed pipe diameter is to vary pipe diameter at a fixed toneburst frequency. This produces a nearly identical curve and thus in fact the reflection coefficient is constant if the frequency-diameter product is kept constant. Figure 3.15 demonstrates this in a plot of reflection coefficient against toneburst centre frequency and pipe diameter, with a constant frequency-diameter product of 7 MHz-mm. The reflection coefficient is nearly constant, with small differences being accounted for by small rounding errors. Strictly the pipe-diameter–wall-thickness ratio should be constant for the frequency-diameter relationship to remain valid, and if pipes were modelled using a full 3D model this would have to be accounted for. In producing the results presented in Figure 3.15 however, membrane models with zero pipe-wall thickness were utilised, so this did not factor into the results.

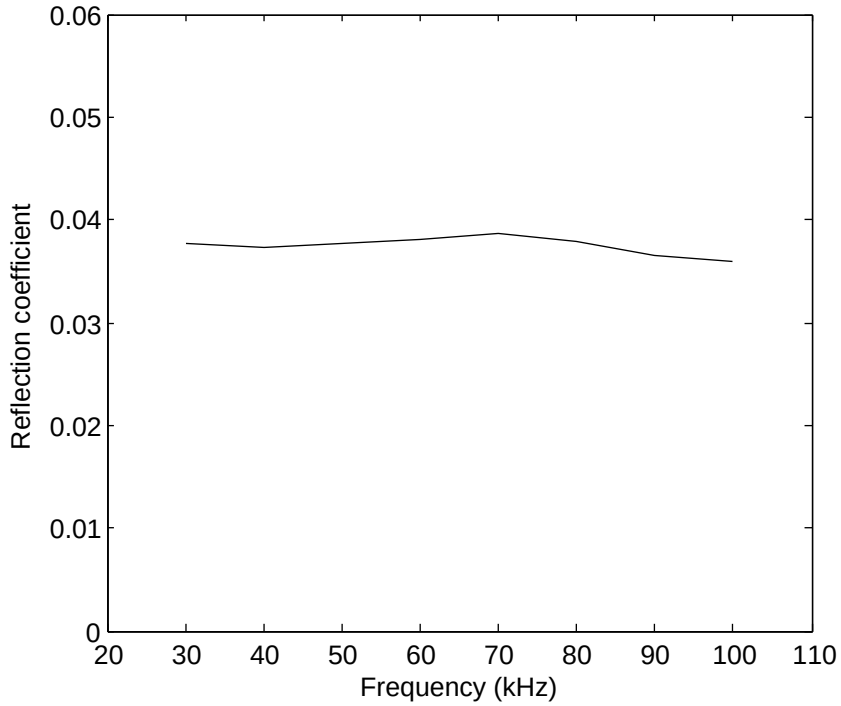

Figure 3.15: Reflection coefficient as a function of both toneburst centre frequency and pipe diameter, with a constant frequency-diameter product of 7 MHz-mm. The crack length is equal to the wavelength of the incident toneburst.

The results suggest that to maximise reflection coefficient from a through-thickness axial crack at a given pipe size the lowest frequency should be used that does not lead to interference effects between the primary crack reflection and the circumferential propagating wave. For a 5-cycle toneburst the circumference of the pipe should be approximately three wavelengths of the incident toneburst or longer.

3.5.4 Crack Depth

It is obvious from previous results that there is a non-linear relationship between crack depth and reflection coefficient. In Figure 3.16 FE results are plotted showing how the reflection amplitude varies depending on the depth of an axial crack. Results are presented for incident toneburst frequencies of 30 kHz, 40 kHz and 50 kHz and reflection amplitudes are all normalised to the reflection amplitude of a through-thickness crack at the same frequency. In all cases the crack length was equivalent to the wavelength of the incident toneburst.

The data shows that the relationship between crack depth and reflection amplitude is also dependent on frequency. As the frequency decreases the curves become increasingly concave. This would suggest that when trying to detect a shallow crack it may be beneficial to use a higher frequency, as opposed to a through-thickness crack that has a higher reflection coefficient at lower frequencies. However, the reflection coefficient from a part-depth axial crack of 20% through-thickness extent is exceptionally small and at 50 kHz has a value of 5.81×10^{-4}, two orders of magnitude below what is considered detectable in a practical situation [73].

Similar curves to those demonstrated in Figure 3.11 have been observed previously for cracks and notches aligned circumferentially around a pipe, with the reflection coefficient of both the $L(0,2)$ mode [14], and the $T(0,1)$ mode [36]. Demma et al. [36] noted that for a part-depth axisymmetric discontinuity there is a cut-off between a high frequency approximation and a low frequency approximation of the results. The cut-off between the two regimes occurs roughly when $ka = 1$, where k is the wavenumber and a is the characteristic dimension of the defect, in this case the crack depth. With an incident

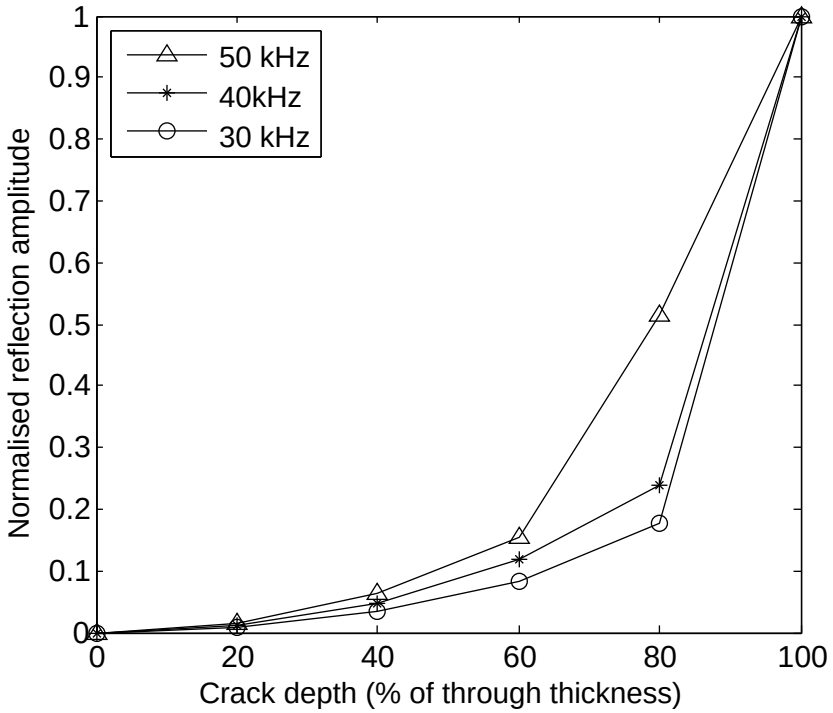

Figure 3.16: Effect of crack depth on the reflection coefficient from an axial crack in a pipe. Data is presented for toneburst frequencies of 30 kHz, 40 kHz and 50 kHz and reflection amplitudes are normalised to the reflection amplitude of a through-thickness crack. In all cases the crack length was equivalent to the wavelength of the incident toneburst.

toneburst frequency of 50 kHz and using the following to calculate the wavenumber;

$$k = \frac{2\pi f}{V} \tag{3.2}$$

where V is the phase velocity, a defect depth of 10.4mm gives a ka value of 1. This corresponds to a through-thickness extent of 83%, so the majority of work considered here is in the low frequency regime. In this frequency regime the reflection coefficient is below the linear curve making detection of part-depth axial cracks even more difficult.

It is not possible to merely increase frequency to improve the reflection coefficient and increase the detectability of axial cracks. A further consideration for this work compared to axisymmetric defects is that for through-thickness axial defects the reflection increases

as frequency is reduced. The absolute, rather than normalised, data from Figure 3.16 are presented in Figure 3.17 and show that there is a cross-over depth above which a lower frequency becomes more sensitive to a particular defect. The cross-over depth can also be affected by other factors such as pipe diameter and crack length so it is difficult to determine the optimum inspection frequency to use in order to maximise reflection coefficient. This argument is rendered moot however, when consideration is given to previous statements that critical sized axial cracks are well below a realistic detection threshold.

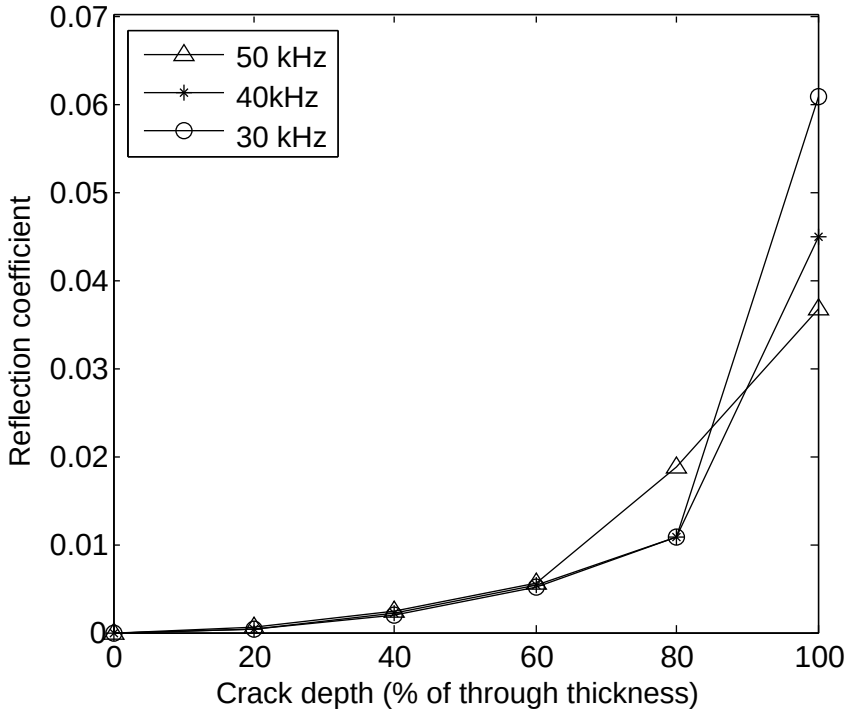

Figure 3.17: FE results displaying reflection coefficient as a function of crack depth for incident toneburst frequencies of 30 kHz, 40 kHz and 50 kHz. In all cases the crack length was equivalent to the wavelength of the incident toneburst.

3.5.5 Crack Width

A finite element study into the effect that crack width has on the reflection coefficient from an axial crack has been conducted. A through-thickness crack was modelled using membrane elements and the study covered incident toneburst centre frequencies of 30

kHz, 40 kHz and 50 kHz. In all cases the crack length was equal to the wavelength of the incident toneburst. The results are plotted in Figure 3.18 with the crack width scaled to the wavelength of the incident toneburst, the maximum crack width being 3mm. A maximum width of 3mm was deemed sufficient because that is the width of the notches created in the laboratory experiments, and is a greater value than any crack that is likely to be discovered in a real-life application.

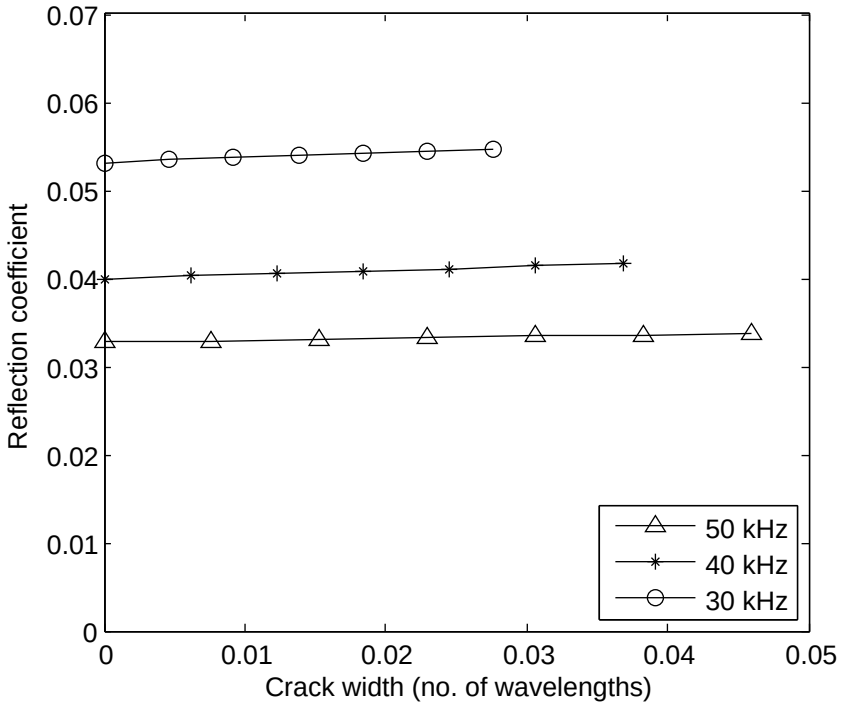

Figure 3.18: Effect of crack width on the reflection coefficient from an axial crack in a pipe with incident toneburst centre frequencies of 30 kHz, 40 kHz and 50 kHz. Crack width is scaled with wavelength of incident toneburst and crack length is equal to the wavelength of the incident toneburst.

It is clear that crack width has only a very weak effect on the amplitude of the reflection coefficient, and that this applies across the frequency range studied here. A linear relationship can be seen between crack width and reflection coefficient, for all frequencies studied. Table 3.1 presents the rate of increase of reflection coefficient, as a function of the crack width, measured in both wavelengths and millimetres. The numbers are very low demonstrating that crack width is not an important factor in determining the reflection coefficient.

Toneburst frequency	Rate of increase per wavelength	Rate of increase per mm
30 kHz	$0.0569\lambda^{-1}$	$5.23 \times 10^{-4} mm^{-1}$
40 kHz	$0.0454\lambda^{-1}$	$5.57 \times 10^{-4} mm^{-1}$
50 kHz	$0.0211\lambda^{-1}$	$3.23 \times 10^{-4} mm^{-1}$

Table 3.1: Rate of increase of reflection coefficient from an axial crack in a pipe with respect to crack width at 30 kHz, 40 kHz and 50 kHz. Crack widths are presented relative to the wavelength of the incident toneburst and as an absolute value.

The results presented in Table 3.1 suggest that the rate of increase of reflection coefficient with crack width is to some extent dependent on frequency. At 40 kHz the rate of increase of reflection coefficient is marginally higher than would be expected if this were not the case. This is evident when examining the third column of the table where the rate of increase of reflection coefficient is higher at 40 kHz than at 30 kHz. The rate would be expected to be higher with the frequency of the incident toneburst at 30 kHz because the reflection coefficient for a zero-width crack is higher at this frequency.

3.6 Conclusions

In this chapter the reflection characteristics of the fundamental torsional $T(0,1)$ guided wave mode from axial cracks in pipes has been studied. The reflection coefficient was measured to characterise axial cracks in terms of their length, depth and width over a range of frequencies. The work was conducted using finite element analysis with laboratory experiments used to validate the FE models. The feasibility of using guided waves to detect axial defects in practical situations at power stations has also been examined.

It has been found that the $T(0,1)$ guided wave mode is not sensitive enough to detect axial cracks that are considered to be a critical size in a power station, taken to be 20% of the through-thickness extent of the pipe. The reflection coefficient for a crack of this depth is minuscule across the full frequency spectrum and regardless of the crack length. It would likely be possible to detect a through-thickness crack in a practical situation,

but due to the reflection coefficient being strongly dependent on crack depth a part-depth crack would be difficult to detect in a practical situation. A crack below 80% through-thickness extent would be difficult to detect even in a laboratory environment.

The stated detection threshold for guided waves in a practical situation is 5% of the amplitude of an endwall reflection [73]. By this metric it would only be possible to detect through-wall cracks. However, if the pipework away from any cracking is clean it would be possible to identify defects with a smaller reflection coefficient. The pipes used in the laboratory experiment of this study are ex-service components and therefore are representative of pipes that would need inspecting.

Realistically, a signal-to-noise ratio of 6dB would be required to detect a defect, and the highest signal-to-noise ratio measured in the laboratory experiments was 22dB, for a through-thickness crack of the optimum length with a toneburst centre frequency of 30 kHz. Therefore a crack producing a reflection amplitude 14dB lower than a through-thickness crack could feasibly be detected. Figure 3.17 demonstrates that a crack with a through-wall extent of 20% has a reflection amplitude 43dB below the reflection amplitude of a through-thickness crack, meaning an increase to sensitivity of at least 29dB would be required in order to detect a critical defect.

There is a complicated relationship between reflection coefficient and crack length that can be explained by interference phenomena between guided wave reflections from both the start of the crack and the end of the crack. For longer cracks at low incident toneburst frequency diffracted waves that propagate circumferentially around the pipe can also have an effect on the reflection coefficient.

Chapter 4

Focused guided waves

4.1 Introduction

The previous chapter examined the reflection of the fundamental torsional guided wave mode from an axial crack in a pipe. The study determined that the reflection amplitude from an axial crack was heavily dependent on crack depth and that it was only possible in ideal circumstances, in practise, to detect an axial crack if the crack extended through 80% of the wall thickness. This was insufficient for the practical inspection being pursued as a crack extending through just 20% of the wall thickness would be considered critical.

The aim of this chapter is to investigate whether focused guided waves would offer an improved sensitivity to axial cracks in pipes. By focusing the guided waves it should be possible to increase the reflection amplitude, compared to unfocused guided waves, from an axial crack, and therefore detect shallower defects than was previously possible.

4.2 Benefits of focusing

When an axisymmetric wave in a pipe reflects from a non-axisymmetric discontinuity, mode conversion takes place [36]. Mode conversion will primarily take place to a specific 'family' of flexural modes, depending on the incident axisymmetric mode. For instance

the $L(0,1)$ mode will mode convert to the $F(n,1)$ mode family, with n representing the circumferential order, and the $T(0,1)$ mode will primarily mode convert to the $F(n,2)$ flexural mode family. The flexural mode families associated with an axisymmetric mode are analogous to plate modes with similar mode shapes to the axisymmetric modes propagating in a helical direction along a pipe, and at high frequency the dispersion curves for the flexural modes will converge on the associated axisymmetric mode [31].

Figure 4.1 shows the group velocity dispersion curves for a steel pipe with an outer diameter of 141.3mm and inner diameter of 116.3mm. It was generated using the Global Matrix Method [68] implemented in the software Disperse [86]. The dispersion curves presented in Figure 4.1 are the same as those presented in Figure 2.6 but instead of highlighting axisymmetric modes, the $T(0,1)$ mode as well as the flexural $F(1,2)$, $F(2,2)$ $\ldots F(n,2)$ modes are highlighted, in the frequency regime used for practical guided wave inspections. In the previous chapter only the reflection amplitude of the torsional mode was measured, by summing the contributions from all of the transducers with no phase shifts. If the mode converted reflected waves are also considered it can increase the reflection amplitude from non-axisymmetric defects, making the technique more sensitive to axial cracks.

In general, when considering a plate, focusing can be achieved with a single guided wave mode. The single mode can propagate in different directions from the defect and be monitored by multiple receivers. However, when the equivalent situation arises in a pipe, the different directions of the plate mode become higher order pipe modes, so focusing becomes a sum of higher order pipe modes.

4.2.1 Synthetic focusing algorithms

The type of focusing used in this study is not conventional phased array focusing as described in [53, 66, 96], but rather a form of synthetic focusing [30–32, 54]. With conventional focusing in a pipe, delay laws are applied to the transmitting transducers in order to get as much energy as possible at the target focusing location. Delay laws are then also applied to the receiving transducers after the signal has been scattered

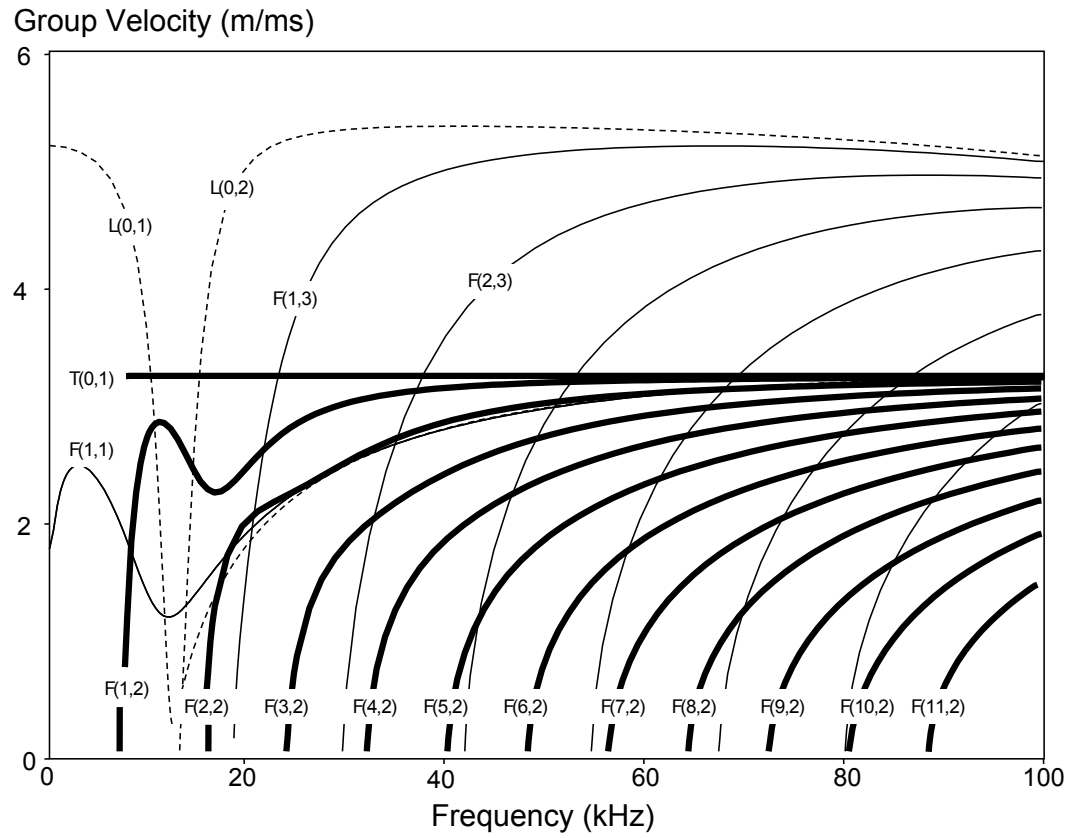

Figure 4.1: Group velocity dispersion curves for a nominal 5" schedule 120 steel pipe with an outer diameter of 141mm and a wall thickness of 12.5mm. Important modes are highlighted in bold. The figure was generated using the software Disperse [86].

off a defect. This process can be time consuming because each location in the target sample has to be interrogated separately in order to form an image. By contrast, in this study the time traces are collected and focusing algorithms are applied to the data in post-processing.

There are several methods available to synthetically focus guided waves. A review of the relative merits of three methods is presented in [32]. These methods for guided wave application are the Synthetic Aperture Focusing Technique (SAFT), Common Source Method (CSM) and Total Focusing Method (TFM). SAFT has existed in some form for many years, with early references to synthetic aperture focusing for ultrasonic non-destructive evaluation apearing in the 1980's [80, 102]. TFM was developed much more recently by Holmes et al. [57] and made possible by advances in desktop computing. Davies et al. [32] first introduced the CSM algorithm in his review of focusing algorithms.

When using the SAFT method each transducer in an array is fired in turn and a pulse-echo time trace is collected on the transducer that produced the signal [59]. For CSM all of the transducers are fired simultaneously and a time trace of the back-scattered signal is recorded at each individual transducer [31]. Both of these methods require N time traces where N is the number of transducers. In contrast the TFM algorithm requires the firing of each transducer in turn, and the recording of time traces on all other transducers for each firing [57]. This requires $N(N-1)$ time traces, but can be reduced to $N(N-1)/2$ time traces due to reciprocity.

For a circular array of transducers surrounding a pipe CSM was found to be the most appropriate technique [32]. CSM does not suffer from noise caused by waves propagating circumferentially around the pipe at the transducer location. CSM was also favoured in this work because it was possible to apply the focusing algorithm to data that had been collected from experiments measuring the reflection of the $T(0,1)$ mode, described in the previous chapter.

4.3 Focusing Using Common Source Method

The CSM algorithm, in this application, requires the excitation of an axisymmetric mode, and has been demonstrated to work with both longitudinal wave modes [67] and torsional wave modes [31]. Only the excitation of a torsional wave mode is being considered here, and further description of the algorithm will reference the $T(0,1)$ mode and its associated flexural $F(n,2)$ modes. The algorithm itself, described in detail by Davies and Cawley [31], first involves firing every transducer simultaneously in order to excite the axisymmetric $T(0,1)$ mode, which is then allowed to propagate along the pipe and scatter off any pipe discontinuities. Each transducer is monitored separately and the back-scattered field, $f(\theta, z=0, t)$ is recorded at the array location, $z=0$. When this process has finished there is a two dimensional data set over time, t, and circumferential position, θ. The data set can be decomposed into orthogonal modal components over a range of frequencies using a 2D Fourier transform;

$$F(n, z = 0, \omega) = \int_{-\infty}^{\infty} \int_{-\infty}^{\infty} f(\theta, z = 0, t) \exp(-in\theta) \exp(-i\omega t) \mathrm{d}\theta \mathrm{d}t \tag{4.1}$$

In Equation 4.1 the n represents the modal order where $n = 0$ for the $T(0,1)$ mode. Each mode in the $T(0,1)$, $F(n,2)$ mode family must then be individually backpropagated along the pipe at each frequency. The backpropagation of the nth order mode at frequency ω to axial position $z = \zeta$ is calculated using;

$$F(n, \zeta, \omega) = F(n, z = 0, \omega) \exp(-ik_0\zeta) \exp(-ik_n\zeta) \tag{4.2}$$

where k_0 is the axial wavenumber of the $T(0,1)$ mode and k_n is the axial wavenumber of the higher order modes. When determining the values of k_n it is assumed that the back-scattered torsional and flexural $F(n,2)$ wave modes can be considered to be fundamental shear horizontal (SH0) modes travelling in different helical directions along the pipe [31]. A similar simplification has been used by Li and Rose [67].

To generate a pipe image at axial position $z = \zeta$ the inverse Fourier transform of the backpropagated field for each mode is taken over the 6dB frequency bandwidth of the incident toneburst, $\omega \in \Omega$. The 6dB bandwidth is used rather than the full frequency spectrum to minimise computation time.

$$I(\theta, \zeta) = \int_{-\infty}^{\infty} \int_{\omega \in \Omega} F(n, z = \zeta, \omega) \exp(i\omega t) \exp(in\omega) \mathrm{d}\omega \mathrm{d}n \tag{4.3}$$

Figure 4.2 shows an unrolled pipe display image of a defect examined in this study, with a comparison between a finite element model and results obtained experimentally. The grey scale is linear with the images normalised to the peak amplitude of the defect signal. The defect is a through thickness axial crack with a length of $\lambda/2$, where λ is the wavelength (64mm) at the centre frequency (50 kHz) of the incident toneburst. The images are of results produced in this study.

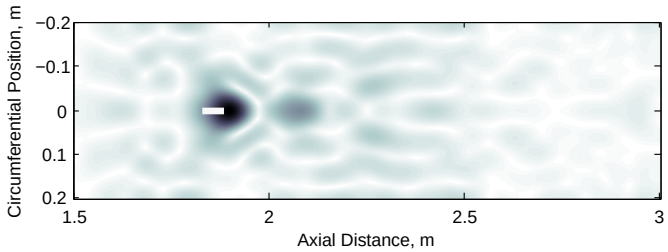

(a) FE model

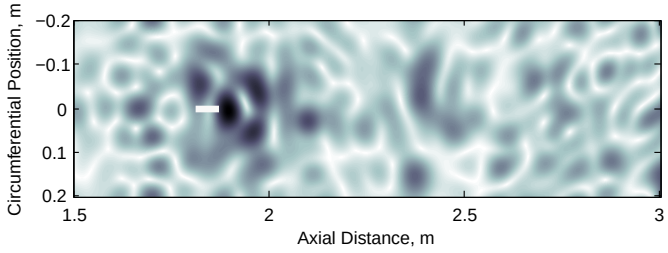

(b) Experimental measurement

Figure 4.2: Unrolled pipe display images produced using CSM algorithm. Images are of a through-wall crack with an axial extent of 32mm with both (a) FE data , and (b) experimental data shown . The grey scale is linear with the images normalised to the peak amplitude of the defect signal. Crack location is indicated by white line with width exaggerated. The centre frequency of the incident toneburst was 50kHz.

The distance of a defect from the transducer array should not greatly affect the reflection amplitude for either focused or unfocused guided waves. When unfocused guided waves are being used only the amplitude of the torsional $T(0,1)$ mode is measured. When guided wave focusing is used the amplitude of the flexural $F(n,2)$ modes are also measured. The attenuation of all of these modes is very low, sufficiently so that it can be neglected. Another point is that a sufficiently long time window is used when taking data that higher order modes are included in the summation. Therefore the reflection amplitude can be considered not to be significantly dependent on the distance between the defect and the transducer array.

4.4 Modelling and experimental procedure

The common source method synthetic focusing algorithm was applied to data gathered in the previous chapter. This was possible because the CSM algorithm requires the incident toneburst to be a pure $T(0,1)$ mode, as used previously. The difference between the previous measurements made in Chapter 3 and those presented in this chapter lie in the post-processing of the results. Rather than simply summing the contributions from each transducer, the individual transducer time traces were processed using the CSM algorithm. Because new data did not need to be collected, the same modelling procedure (see Section 3.3) and experimental procedure (see Section 3.4) were used as in the previous chapter.

An important point to note is that, as stated in Section 3.4, the transducers on the experimental equipment are arranged in adjacent pairs, with a single channel for each pair of transducers. Thus on reception the signal measured at each channel represents the sum of the contributions from two adjacent transducers. When only the $T(0,1)$ mode is being considered this is unimportant because the measured signals from all transducers are summed in order to eliminate the contribution from higher order flexural modes. Therefore, in guided wave applications measuring only the $T(0,1)$ mode the transducer ring can be considered to have the full 16 transducers. However, the CSM algorithm is reliant on the ability to individually address each transducer. Due to the transducers being arranged in pairs this is not strictly possible with the equipment used in this study. Instead there are the equivalent of eight transducers in the transducer ring, and this places limits on the toneburst frequencies that are available.

The highest order mode that can be controlled by a ring of transducers is $N-1$, where N is the number of transducers in the ring [16]. With a transducer ring consisting of the equivalent of eight transducers the highest order mode that can be controlled is of order seven. For the $F(n,2)$ mode family, the lowest order mode that can not be controlled is the eighth order mode, $F(8,2)$. From Figure 4.1 it is evident that the cut-off frequency for the $F(8,2)$ mode is approximately 65 kHz, so if the full frequency content of the incident toneburst is below the cut-off frequency then full mode control

can be maintained. This limits mode-controlled testing to frequencies below 65 kHz.

4.5 Results and Discussion

4.5.1 Reflection Amplitude as a Function of Crack Length

A plot of the reflection coefficient as a function of crack length can be seen for a through-thickness crack in Figure 4.3, and a crack of 80% through-thickness extent in Figure 4.4. The x-axis is scaled as a ratio of the crack length to wavelength of the incident $T(0,1)$ wave and the incident toneburst centre frequency is 50 kHz in both cases. To produce each data point for the focused results the CSM algorithm was applied to the data collected in [90], and the amplitude of the crack reflection was divided by the amplitude of the end wall reflection, obtained prior to cutting the defects. For the unfocused results the same process was performed, except that only the reflected $T(0,1)$ signal was used. The amplitude of each signal was identified as the peak of the Hilbert transform of the time domain signal. Note that as the end wall is an axisymmetric reflector, only the $T(0,1)$ mode is reflected and there is no contribution from the $F(n,2)$ modes, so the reference signal is the same for both the focused and the unfocused cases. The figure shows both FE and experimental data; both were processed in the same way.

For both the focused and unfocused guided waves the agreement between FE simulations and experiment is reasonable. Experimental results for the 80% depth crack are, in the majority of cases, higher than the FE predictions. This could be caused by a systematic error such as weak coupling when measurements were made of the endwall reflection amplitude before any machining took place; this is thought most likely to be due to noise in the signal. The finite element and experimental results are more closely matched with unfocused guided waves, and this applies both to the through-thickness and 80% depth notches. Even though the synthetic focusing algorithm has been shown to be very robust against coupling and phase errors [30], meaning non-uniform coupling and phase due to experimental set-up, the errors still have a measurable effect. Any coupling or phase errors are therefore likely to have a greater effect on focused guided wave results

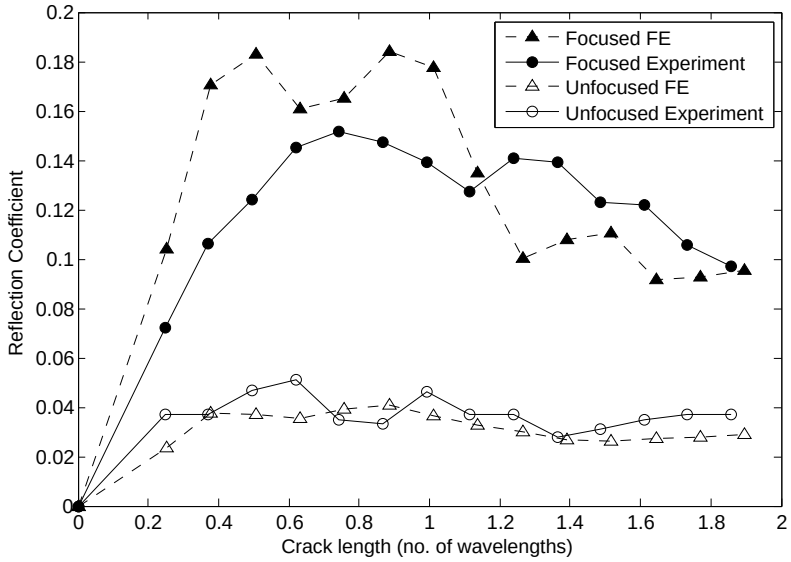

Figure 4.3: Comparison of FE data and experimental measurements showing how reflection coefficient depends on crack length. Focused and unfocused results are shown for a through-thickness crack. FE data is shown as a dashed line and experimental data is shown as a solid line.

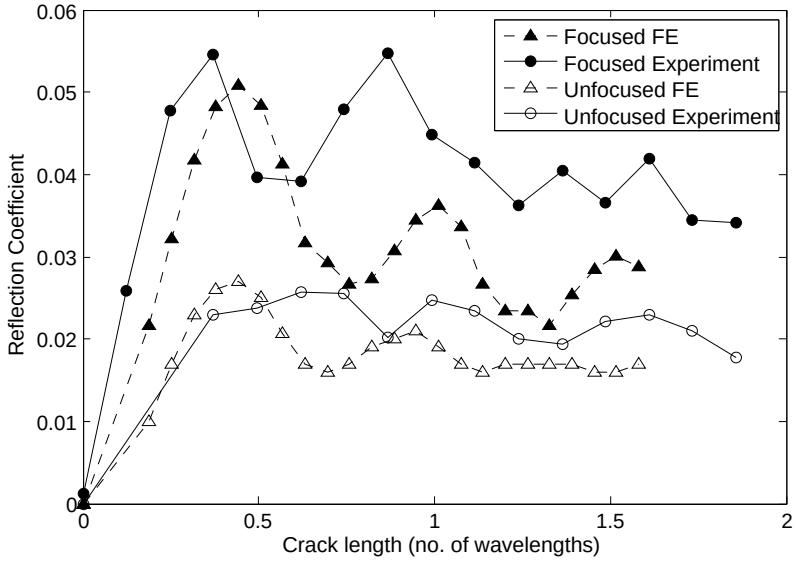

Figure 4.4: Comparison of FE data and experimental measurements showing how reflection coefficient depends on crack length. Focused and unfocused results are shown for an 80% deep crack. FE data is shown as a dashed line and experimental data is shown as a solid line.

than unfocused where only the T(0,1) mode is measured. It is also worth noting, and very significant, that the agreement between finite element and experimental data was achieved with very low amplitude signals.

It is clear from a comparison of the focused and non-focused results that employing focusing has led to an increased reflection amplitude. The reflection amplitude for focused guided waves has roughly doubled compared to non-focused guided waves at all crack lengths in the case of a part-depth crack, and increased by a factor of 3-4 in the case of a through-thickness crack. There remains a similar dependence on the crack length to the non-focused results with the reflection coefficient oscillating as crack length increases. There is a peak at a crack length of $\lambda/2$ followed by a trough at $3\lambda/4$ and a second peak at a crack length of λ. The pattern is due to interference of waves propagating along the surface of the crack; the origin of this pattern is described in detail in [90] and Chapter 3 of this thesis.

Despite the improvement in reflection amplitude it is still likely to be insufficient to locate axial cracks in the practical case which motivated this work. The results show that a through crack will produce a reflection with amplitude of approximately 10% of the amplitude of an end wall reflection, but for part depth cracks this value will be lower. The relationship between crack depth and reflection amplitude is not linear [36], as discussed in Chapter 3, so if the through wall extent of a crack is 20%, the reflection amplitude is lower than 20% of the reflection amplitude of a through thickness crack. The reliable detection limit on an in-service pipe depends on a number of factors but is typically 5% [73] so it is very unlikely that a crack of 20% through-thickness extent will be detected.

4.5.2 Frequency Dependence

Figure 4.5 shows how the reflection amplitude depends on the centre frequency of the incident toneburst. The data was simulated using FE software and focused results are again compared with non-focused results. The defect is a through thickness crack with a length of $\lambda/2$. For this part of the study the incident toneburst had 10 cycles in order

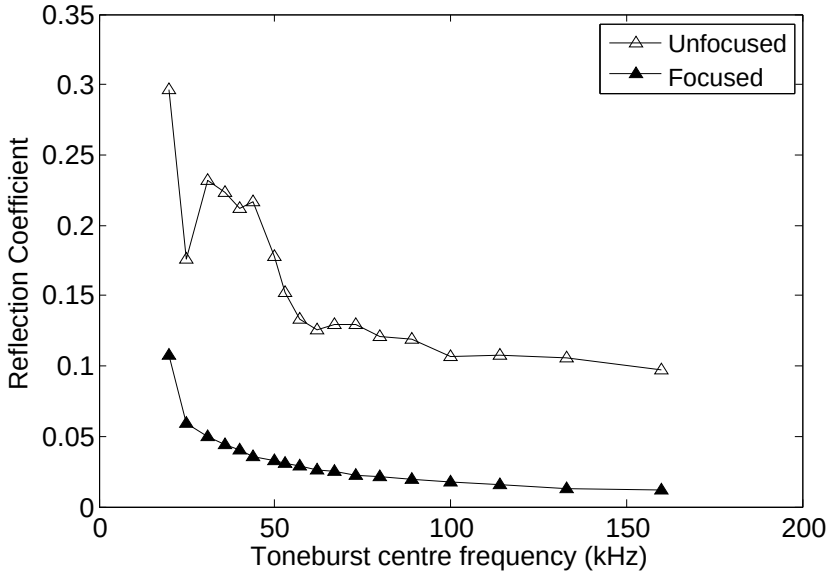

Figure 4.5: Results of FE models indicating how incident toneburst frequency affects reflection coefficient for both focused and unfocused guided waves. In all cases the crack length was equal to half the wavelength of the incident toneburst.

to narrow the bandwidth and allow greater separation of results on the frequency axis.

As seen previously in this paper the focused results have higher reflection amplitudes than the non-focused results. The non-focused results display a smooth reduction in the reflection coefficient as frequency is increased, as described in [90]. The focused results comprise a similar trend to lower amplitude at higher frequencies but the change in amplitude is not smooth. Instead there is a series of spikes and troughs as frequency is increased. The reason for this is that the CSM algorithm sums the contributions from not only the T(0,1) mode, but the numerous F(n,2) modes as well. However, the flexural modes have cut-off frequencies, as shown in Figure 4.1, and as the frequency is increased more flexural modes are available to contribute to the signal reflected from the crack. This results in a complicated relationship between reflection coefficient and toneburst centre frequency that would be affected by variables such as pipe dimensions and toneburst bandwidth.

Thus it can be seen that an important factor in the behaviour is that there is mode conversion taking place at the crack; a portion of the incident T(0,1) mode is being converted to various flexural modes upon reflection. This is expected as an axial defect

is not axially symmetric. In fact it has been shown that using a synthetic focusing algorithm for guided waves in pipes does not increase reflection amplitude in the case of an axisymmetric pipe feature [31]. If a defect is axisymmetric no mode conversion takes place to the F(n,2) modes and the only mode that is reflected is the incident T(0,1), which therefore carries all of the reflected energy. The CSM synthetic focusing algorithm sums all reflected modes and will only increase the reflection amplitude (relative to the amplitude of the T(0,1) mode) if flexural modes are present. An axisymmetric defect in a pipe is equivalent to an infinitely long defect in a plate perpendicular to the direction of wave propagation. This type of defect in a plate would only scatter a wave in the opposite direction to the incident wave, with no waves propagating in other directions to allow synthetic focusing. As described previously the waves propagating in direction other than in the opposite direction to the incident wave in a plate, become higher order modes in the case of a pipe.

4.5.3 Crack Depth

The effect that crack depth has on the reflection of guided waves has been studied, with results presented for both unfocused guided waves, measuring the reflection coefficient of the T(0,1) mode, and focused guided waves, using the CSM algorithm. Only FE analysis of the pipes was used to generate the data because with shallow cracks the amplitude of the reflected signal would be too small to measure, even in a laboratory environment. As discussed previously, FE models with through-thickness cracks and cracks with an 80% through-wall extent have been validated with experimental data, giving high confidence in the modelled results for more shallow cracks.

Cracks with a through-wall extent as low as 20% have been modelled, as this is considered a critical defect size in the practical application which motivated this work. Figure 4.6 shows the reflection coefficient as a function of crack depth for both focused and unfocused guided waves. In all cases the crack length is 32mm and the centre-frequency of the incident toneburst is 50 kHz. A crack length of 32mm was chosen because it produces the highest reflection coefficient at this frequency for part-depth

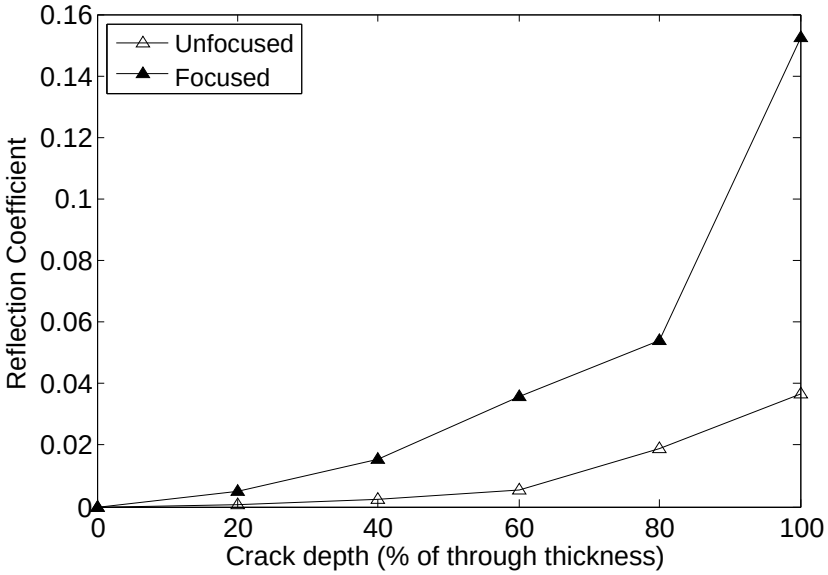

Figure 4.6: Results of FE models indicating how crack depth affects reflection coefficient for both focused and unfocused guided waves with a centre frequency of 50kHz. The crack length is equal to half the wavelength of the incident toneburst.

finite element models, with these results consequently being a 'best-case' scenario. It was possible to determine the optimum crack length by examining Figure 4.3 where it is shown that the highest reflection amplitude in the FE data is at $\lambda/2$. The results show that at a given crack depth the reflection amplitude from the focused results is two to three times higher than when the T(0,1) mode is measured, which is consistent with the earlier results. A 20% deep crack is shown to produce a reflection amplitude of 0.0048 when focusing is employed. In good conditions on site a reflection coefficient of 0.05 would typically be considered the limit of detectability, whereas in a laboratory it is likely a reflection coefficient of 0.01 can be measured. Thus even with a crack length that has been demonstrated as producing the largest reflection coefficient, the signal amplitude is approximately an order of magnitude too low to be detectable.

4.6 Conclusions

A study has been made of the potential to use focused guided waves to locate axially aligned defects in pipes. The need for focusing arises because standard guided wave

techniques are insufficiently sensitive to find realistic axial defects in pipes. In particular cracks with low through wall extent produce very small reflected signals. Focusing the guided waves using the common source method was employed on data from both finite element models and laboratory experiments. It was discovered that focusing does improve the reflection amplitude from an axial defect by roughly a factor of two to four, with the effect being greatest for through-thickness defects. However, although this is a significant improvement, and may be sufficient for some applications, the sensitivity to axial cracks is still rather weak.

The increase in reflection amplitude has been attributed to taking into account all of the flexural modes propagating in the pipe. At a non-axially symmetric defect a portion of an incident torsional wave will be mode converted to flexural modes. Non-focused guided wave measurements do not take this into account and only measure the amplitude of the reflected torsional mode. By taking into account the flexural modes as well the reflection coefficient has been increased.

Chapter 5

Circumferential guided waves

5.1 Introduction

It has been shown in previous chapters that long-range guided waves are not sensitive enough to detect axial cracks in pipes that are of critical size in the application of interest in the power industry. Synthetic processing improved the sensitivity to axial defects but did not provide the increase in sensitivity required to detect a critically sized axial crack. The reason that axial cracks do not produce a strong reflection is that the change in cross-section of the pipe is very small, and guided waves in a pipe are mostly sensitive to changes in cross-section.

An alternative approach is to use circumferential guided waves, propagating in the circumferential direction around a pipe, rather than axially along it. In this configuration the crack would be perpendicular to the direction of wave propagation so the technique is likely to be more sensitive to axial cracks than long-range guided waves would be. Obviously the primary advantage of long-range guided waves is that long lengths of pipe-work can be inspected from one location, and it is possible to inspect inaccessible locations. This advantage is lost when circumferential guided waves are used as only a single circumferential 'slice' of pipe-work is interrogated during each inspection.

The proposed method does however offer an advantage over current manual ultrasonic

techniques. A whole slice of pipe-work can be inspected at one time, compared to a single point with manual ultrasonics. The requirement for surface preparation is also greatly reduced with no need to grind and polish the pipe surface. Currently the cost of performing a standard ultrasonic inspection of an entire bend is approximately £200 plus an additional £70-£100 for surface preparation, taking approximately 90 minutes to complete [58, 79]. A circumferential guided wave inspection could conceivably reduce the inspection time to less than half an hour, reducing the inspection costs accordingly, and would eliminate preparation costs.

Although circumferential guided wave inspections have already been investigated and put to use in industrial applications, such as helicopter rotor hubs [103, 104] or even pipe-work [92], work still needs to be done investigating the suitability of this inspection technique for the application being discussed in this project.

Many pipes used in power stations are relatively thick-walled, in order to survive the high temperatures and pressures that they are exposed to. Typical five inch or six inch schedule 120 pipework that is used in power stations has an outer-diameter to wall-thickness ratio of approximately 11, compared to a nominal schedule 40 pipe, such as may be used to construct an oil or gas pipeline, having an outer-diameter to wall-thickness ratio in the range of 25-27. The CHIME system [92] is a current commercial technology that uses circumferential guided waves to detect corrosion and cracking in pipelines, but is ineffective if the circumferential curvature is too high, i.e. if the outer-diameter to wall-thickness ratio is too low. At high curvatures the head wave that propagates around the circumference of the pipe is incident on the outer wall above the critical angle, and does not therefore mode convert to a surface wave. A fuller description of this process can be found in Section 2.7. The power station pipes being investigated for this study are outside of the limits of CHIME, and therefore the method used by CHIME is not suitable for this application.

The system developed by Valle et al. [103], used to inspect helicopter rotor hubs, is capable of inspecting components with high circumferential curvature, such as the pipes used in power stations. A high frequency signal is excited and extensive digital signal processing is used to compensate for mode conversions, as no effort is made towards

mode control. For the application being studied here it is desirable to use a less complicated system that does not require too much signal processing in order to improve clarity of the physics and reduce computational effort. Furthermore, due to the use of high frequency signals, it is likely that surface preparation and an ultrasonic coupling agent would be required to perform an inspection, negating the advantage of using circumferential guided waves over manual ultrasonics.

For a circumferential guided wave inspection trying to detect axial cracks in pipes in a power station, crack characterisation is not necessarily the most important consideration. Instead it is necessary to discover whether a simple low-frequency circumferential guided wave inspection is capable of detecting a critically sized defect. This involves considering both the radial and axial extent of a crack and combining these two factors to determine whether this is a viable inspection technique. The technique would therefore be used to screen pipework for axial defects, moving quickly along the pipe and highlighting any areas of concern for further investigation using manual ultrasonics. It is not intended to use circumferential guided waves to sentence pipework.

5.2 Principles of circumferential guided wave inspection

To conduct a circumferential guided wave inspection a transducer is placed on a pipe at the axial location that needs to be inspected. When the transducer is fired a circumferential guided wave propagates in both directions around the circumference of the pipe and is monitored at the same location that it is excited from. If a defect is present in the pipe it will reflect the guided wave and this can be measured by the receiver. A schematic layout of a circumferential guided wave inspection is presented in Figure 5.1 showing the transducer location relative to a defect. The circumferential position is measured in degrees relative to the defect and z represents the axial position along the pipe. The arrows emanating from the transducer location represent the incident wave generated by the transducer, and the arrow pointing from the defect towards the transducer location

represents the reflection of the guided wave off a defect.

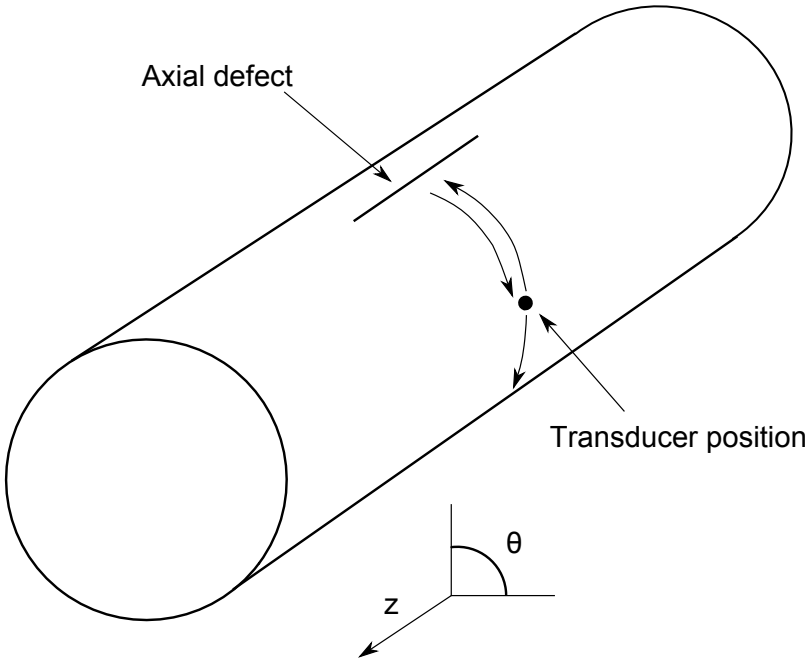

Figure 5.1: Schematic diagram illustrating a circumferential guided wave inspection.

Several methods are available to excite guided ultrasonic waves, as discussed in Section 2.6. Currently the two most popular methods used to excite circumferential guided waves are piezoelectric transducers (PZTs) and electromagnetic acoustic transducers (EMATs). PZTs were used by Valle et. al. [103, 104] as described in Section 2.7, and EMATs are studied in laboratory conditions [49, 56], and as commercial systems [82, 92] also discussed in Section 2.7. The two commercial systems just mentioned (CHIME and the IZFP system), along with limitations that have already been mentioned, are primarily designed to detect corrosion type defects, whereas here small cracks need to be detected which would have a smaller profile in most cases.

In this study it is more desirable to use PZTs than EMATs, because it is expected that critical sized defects will have small reflections, and the SNR for PZTs is superior to that of EMATs. If the method appears viable with PZTs then further work examining the use of EMATs could be conducted. EMATs do not require direct contact with a component so could be easily scanned along a pipe surface, unlike dry-coupled PZTs

that require a point-by-point inspection. Scanning would further improve inspection time and increase the ability to automate the inspection. However, EMAT coupling is weak so their use may be not as advantageous as hoped, and previous work by E.ON with EMATs has shown that they are not particularly effective in power station applications unless an oxide layer is present on the surface of a component [101]. The oxide layer produces a magnetostrictive effect that greatly increases transduction efficiency making an EMAT inspection possible. In a power station an oxide layer only forms on metal with a service temperature above 400℃, and whilst this is sufficient for some applications, many pipes that require inspecting do not reach this temperature. For this reason the only transduction method considered in this study is by PZT.

In order to monitor how the reflection amplitude is affected by altering the test parameters it is necessary to determine a consistent way to measure it. This is achieved by measuring the reflection amplitude relative to the amplitude of a wave that has propagated around the full circumference of an undamaged pipe. Measuring the reflection coefficient in this way is similar to measuring the reflection coefficient of the $T(0,1)$ guided wave mode, where the reflection amplitude is measured relative to the signal strength of an end-wall reflection. A key difference between the two measuring systems is that here it is possible to measure a reflection coefficient of greater than 1. A reflection coefficient higher than 1 may occur if a strong reflector located a short circumferential distance from the transducer reflector has a low circumferential displacement from the transducer. Beam spreading reduces the amplitude of a signal as it propagates and the circumferentially propagating wave has propagated the full distance of the circumference of the pipe when it is measured. The beam path for a guided wave reflecting from a discontinuity back to the transducer may be much shorter than the beam path of the circumferentially propagating wave, hence less beam spreading occurs and therefore the measured signal amplitude can be higher.

Theoretically it is possible to use either a single transducer to both transmit and receive the ultrasonic signal, or separate transmitting and receiving transducers located adjacent to each other. In practical situations it has been found that ring-down in the transmitter makes it less useful as a receiver, because the time taken to recover can affect the ability

to measure the signal reflected from a defect. When separate transducers are used for transmission and reception it is most convenient to position then at slightly offset axial positions and the same circumferential position. Trials demonstrated that there was no significant effect on the measured signal with the receiver up to 40mm away from the transmitter, which with a five inch pipe represents approximately 24% of the outer circumference.

To increase the volume of pipe that can be inspected at once it would be possible to use a three transducer system, with all three transducers aligned axially along the pipe at 40mm intervals. The central transducer would be a transmitter and the other two transducers would be receivers. Employing the system in this way would reduce the number of individual inspections that it would be necessary to carry out, and therefore increase the quantity of pipe that could be inspected during a set time period.

Alternatively, a full transducer array could be used to inspect longer sections of pipe during a single inspection. Furthermore, if necessary, focusing could be employed using the transducer array to enhance the sensitivity of the technique. Active phased array focusing could be used to focus energy at a particular pipe location [53, 66, 96], or a synthetic focusing algorithm such as those described in Chapter 4 could be used. The synthetic focusing algorithms are applicable to plates as well as pipes [32].

A phase velocity dispersion curve over the frequency range of interest is presented in Figure 5.2, scaled with frequency-thickness product. The subscript distinguishes the modes from the similar modes that can propagate in a plate. Although particle motion is similar, plate modes and circumferential modes are not identical, with the difference particularly marked for high curvature cases. Representing the frequency-thickness product for circumferential guided waves is only valid if the ratio of outer diameter to inner diameter remains constant. Two pipe sizes that are commonly used in power station are investigated in this project, nominal five inch schedule 120 pipe and nominal six inch schedule 120 pipe. The five inch pipe has a design outer diameter of 141.3mm and inner diameter of 115.9mm, with corresponding wall thickness of 12.7mm. A six inch schedule 120 pipe has an outer diameter of 84mm and inner diameter of 69mm, with a corresponding wall thickness of 15mm. For both pipe sizes the ratio of inner diameter

to outer diameter is 1.22, so the dispersion curves in Figure 5.2 are valid for both pipe sizes.

In Figure 5.2 the cut-off frequency for the $A1_C$ and $SH1_C$ modes is indicated with a dashed line at 1.63 MHz-mm, and in order to produce simple signals during inspections it is desirable to test below this frequency to minimise mode conversions. For the two pipe sizes investigated as part of this study, a five inch pipe with wall thickness of 12.5mm, and a six inch pipe with wall thickness of 15mm. This line represents cut-off frequencies of 130 kHz and 109 kHz respectively.

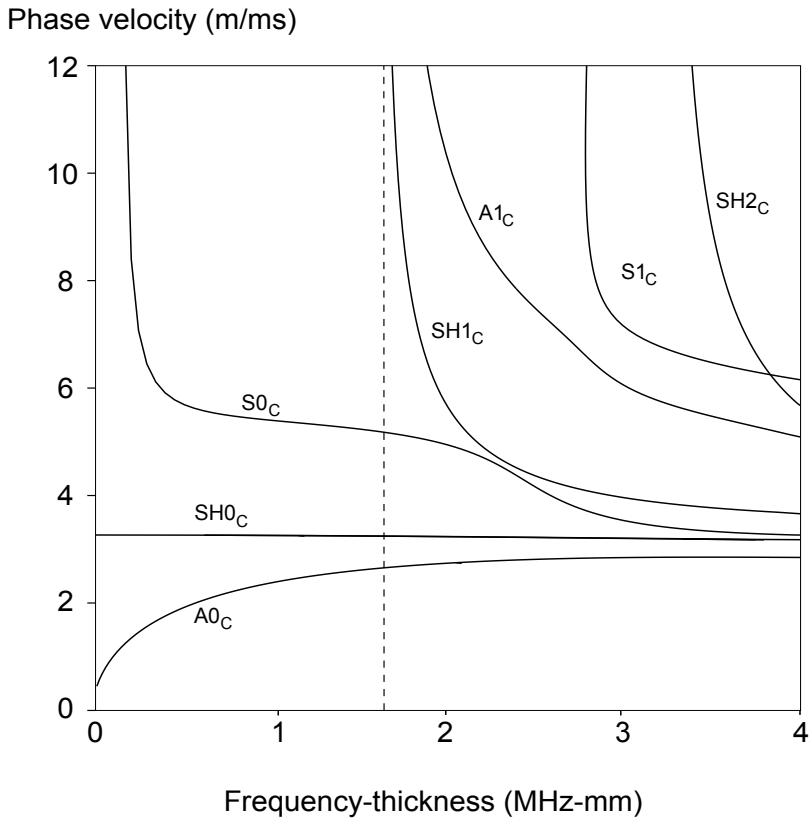

Figure 5.2: Phase velocity dispersion curves for circumferential guided waves in a steel pipe scaled with frequency-thickness product. The ratio of outer diameter to inner diameter is 1.22. The dashed vertical line indicates the cut-off frequency of the $A1_C$ and $SH1_C$ modes at 1.63 MHz-mm.

The maximum available toneburst centre frequency that ensures none of the frequency content of the incident toneburst is above the $A1_C$/$SH1_C$ mode cut-off frequency, is

approximately 70 kHz for the six inch schedule 120 pipes (with 15mm wall thickness), and 90 kHz for the five inch schedule 120 pipes (with 12.7mm wall thickness). If the frequency is increased noise appears in the signal at the frequency of the $A1_C$/$SH1_C$ cut-off frequency, making it difficult to identify a signal reflected from a defect. It is possible to eliminate the noise by ensuring pure-mode excitation, but this can only be achieved by creating an FE model and exciting every node through the thickness of the model. Using this procedure it is possible to excite the $SH0_C$ mode above the frequency of the $SH1_C$ cut-off frequency, but this obviously can not be achieved in a practical situation.

Although using low frequencies would provide a quick and simple – and therefore attractive – inspection, it does present other problems. Even if separate transmitting and receiving transducers are used there is a dead-zone that occurs whilst the receiver is measuring the signal emitted directly from the transmitter, and it would be impossible to measure a defect signal whilst at this time. The spatial length, l, of a toneburst containing n cycles is:

$$l = \lambda \times n, \tag{5.1}$$

or, in terms of phase velocity and wavelength:

$$l = \frac{V_{phase}}{f} \times n. \tag{5.2}$$

At the cut-off frequency of the $SH1_C$ and $A1_C$ modes in a five inch schedule 120 steel pipe, and with a five cycle incident toneburst of the $SH0_C$ mode, the spatial length of the incident toneburst is 125mm. This is more than 28% of the total outer circumference of a five inch pipe which – when the total path length of a signal between the transducer and defect is accounted for – means that 14% of the circumferential extent of the pipe on either side of the transducers can not be inspected. The problem is exacerbated when it is considered that it is not the centre frequency of the toneburst that needs to be below the cut-off frequency, but the highest frequency contained within the toneburst. To ensure that the frequency content of the incident toneburst above the cut-off frequency is below an acceptable amplitude, in the previously described case of a five inch schedule 120 steel pipe, the toneburst centre frequency needs to be below approximately 90 kHz.

At this frequency and with a five-cycle incident toneburst it would be impossible to locate a defect in an area of 20% circumferential extent either side of the transducer location. The dead zones are presented as a schematic in Figure 5.3.

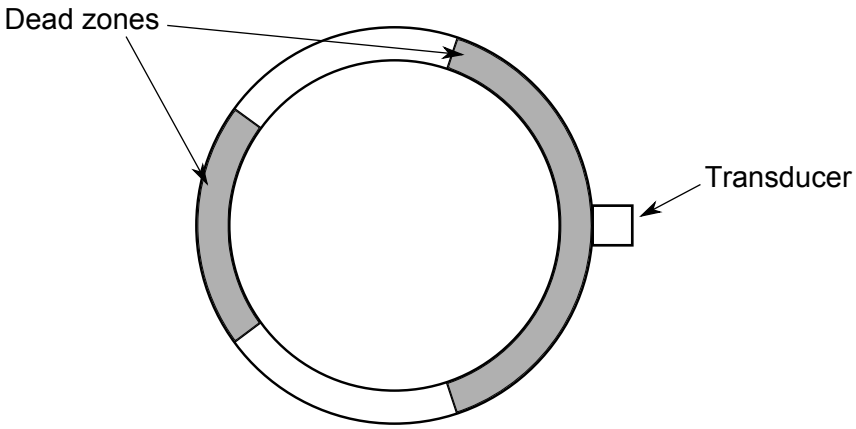

Figure 5.3: View of cross-section of pipe representing the dead-zones when conducting a circumferential guided wave inspection.

For a six inch schedule 120 pipe, with a wall thickness of 15mm, the maximum centre frequency for a five-cycle Hanning toneburst that can be used is approximately 75 kHz, to avoid mode conversion. The spatial length of a five cycle toneburst of the $SH0_C$ mode at this frequency is 213mm, which also equates to 20% of the outer circumference of the pipe. In fact both five inch and six inch schedule 120 pipework have a very similar ratio of outer diameter to wall-thickness so would be expected to have the equivalent size dead-zone.

In Figure 5.4 the length of the dead-zone is plotted as a function of frequency-thickness over the frequency range being studied. This can be used as a general tool that can quickly determine the spatial size of the dead-zone at any frequency. Because the dispersion curves of circumferential guided waves are dependent on the ratio of the outer diameter to pipe thickness Figure 5.4 only applies to pipework with a ratio of 11.2.

To generalise the calculation for the dead-zone to an arbitrary pipe size, the minimum size of the dead-zone must be plotted as a function of the ratio of outer diameter to wall thickness, and the results of this are presented in Figure 5.5. For reference the ranges of outer diameter to wall thickness ratios are presented for a number of pipe schedules. It is

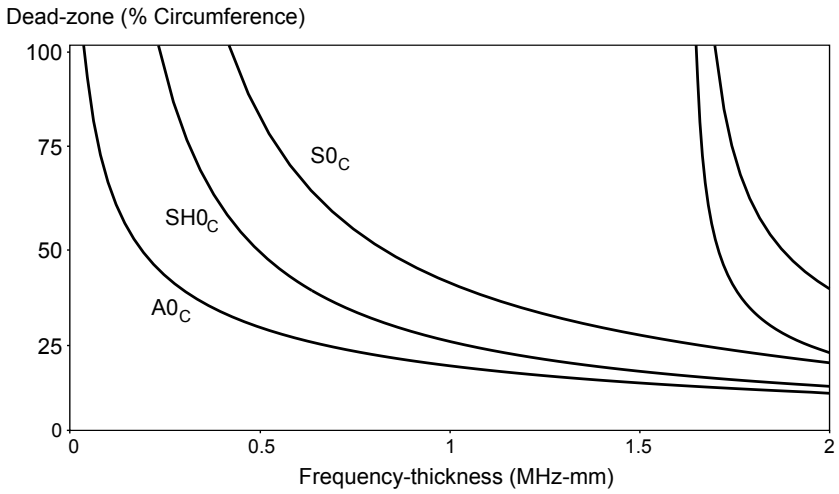

Figure 5.4: Length of dead zone in millimetres as a function of Frequency-thickness for the three fundamental circumferential guided wave modes. Dead-zone calculations in this figure are only valid for pipework with a ratio of outer diameter to pipe thickness of 11.2.

immediately apparent that there can be a very wide range of ratios for a given schedule, so knowledge of the pipe schedule is not sufficient to calculate the dead-zone. The outer diameter and wall thickness must be known.

There is a similar problem with defect detection on the opposite side of the pipe to where the transducers are located. If a defect were present at this location the path length for a signal reflecting from it would be the same as the path length for a wave propagating around the full circumference of the pipe. This signal would be expected to be of much higher amplitude than a reflection from a crack rendering the crack undetectable. The spatial size of the zone where defects can not be detected on the opposite side of the pipe to the transducers is equivalent to the spatial size of the dead zone in either direction from the transducer position.

Reducing the number of cycles in the incident toneburst in order to reduce the spatial length of the signal is not necessarily a solution to this problem, as reducing the number of cycles increases the bandwidth of the toneburst. With an increased bandwidth the centre frequency of the incident toneburst needs to be reduced, thereby increasing the spatial length and mitigating the reduction achieved by reducing the number of cycles. There are small gains to be made in reducing the spatial length of the incident signal

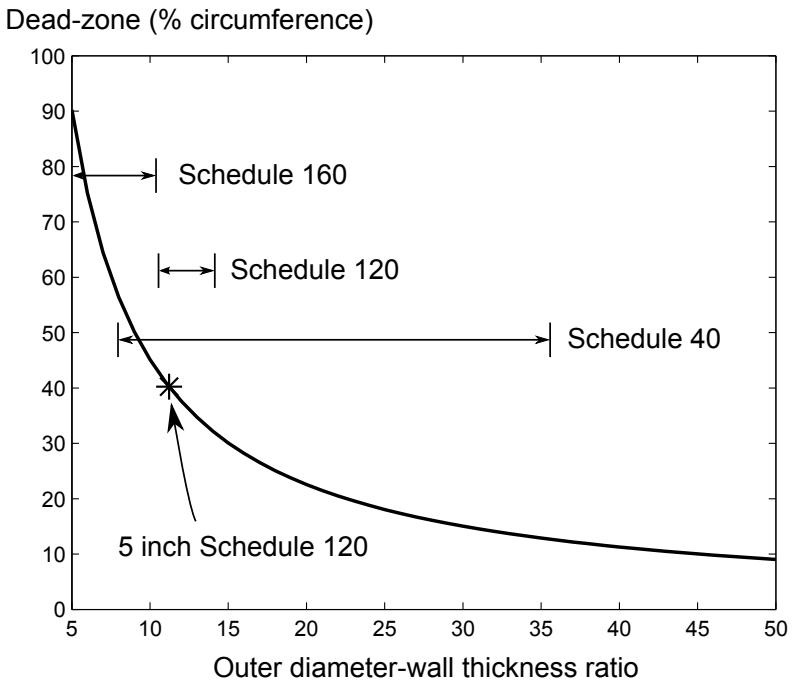

Figure 5.5: Minimum size of dead-zone for the $SH0_C$ mode as a function of ratio between outer diameter and wall thickness. The particular case of a five inch schedule 120 pipe is marked. The ranges of ratios for certain schedules are also displayed.

by reducing the number of cycles but practical considerations relating to some of the equipment used in this investigation (see Section 5.5) meant that this slight advantage was not worth pursuing.

As has been described previously, during a low-frequency circumferential guided wave inspection large portions of the circumference are rendered impossible to inspect due to the dead-zone of the transducers and the wave that propagates circumferentially around the pipe. However, for the application being examined in this study, it is known in which third of the circumference of the pipe that axial cracks are expected to form if they occur. Using this knowledge a full inspection of critical areas of the pipe can be performed from two inspection positions at each axial pipe location.

5.3 Mode selection

Selecting an appropriate wave mode is important when conducting a circumferential guided wave inspection. For this study the low frequency regime is being considered in order to limit mode conversion, and in this frequency regime three modes can exist, the $A0_C$, $S0_C$ and $SH0_C$ modes. Factors that need to be considered include ease of excitation; dispersion; response to defects; and the spatial length of the dead zone. The spatial length of the dead zone is related to the phase velocity of the mode and the frequency.

5.3.1 $S0_C$ Mode

In order to excite an S0 wave mode in a plate, Lowe and Diligent [72] placed a compression probe on the edge of a plate. This option is unavailable for circumferential guided waves in a pipe so the most appropriate method to excite the $S0_C$ mode is to use a shear transducer oriented in the circumferential direction. Use of the $S0_C$ mode has proved impractical for circumferential guided waves inspections. The primary reason that this is the case is that the dead-zone encompasses too much of the circumference to be useful in defect detection. The dispersion curves presented in Figure 5.2 indicate that the $S0_C$ mode has a significantly higher group velocity in the low frequency regime than the $A0_C$ and $SH0_C$ modes. A higher group velocity at a given frequency necessarily means a higher wavelength and a longer dead-zone. Increasing the frequency is not an option because the frequency constraints are the same as for the other modes, it being necessary to keep the amplitude of the highest frequency component in the incident toneburst at an acceptably low level, at the cut-off frequency of the $A1_C$ and $SH1_C$ modes.

5.3.2 $A0_C$ Mode

The $A0_C$ mode has a lower phase velocity than the $S0_C$ mode in the frequency range required for this inspection. This has the effect of reducing the spatial length of the dead-

zone to an acceptable level for performing an inspection. An efficient method of exciting the $A0_C$ mode is using an angled compression probe and the coincidence principle [8, 71]. Although it would be technically possible to achieve this in a practical situation using angled wedges, it may not be desirable because it would require surface preparation of the pipe surface, negating the main advantage of using low frequency circumferential guided waves. An alternative method would be to simply use a low frequency zero degree compression probe, because the $A0_C$ mode has particle displacements in the radial direction, which are very low amplitude for the $S0_C$ mode, and zero for the $SH0_C$ mode. The effectiveness of this approach is discussed in Section 5.6.

Figure 5.2 demonstrates that the $A0_C$ mode is dispersive at low frequencies, becoming significant below a frequency-thickness value of approximately 0.8 MHz-mm. This value is below the desired frequency for an inspection and therefore dispersion should have negligible impact on the propagation of the $A0_C$ mode. The propagation distances are also very short, further minimising the effect of dispersion.

Any fluid present in a pipe during inspection will cause attenuation of the $A0_C$ mode. For the application being studied here it is likely that any pipe being inspected would be free of fluids, although small amounts of standing water can accumulate at certain locations.

5.3.3 $SH0_C$ Mode

Similar to the $S0_C$ mode, excitation of the $SH0_C$ mode can be achieved with a shear transducer, but orientated in the axial direction. The phase velocity is slightly higher than the $A0_C$ mode but the dead-zone is short enough to perform an inspection, and the $SH0_C$ mode is non-dispersive at all frequencies. The $SH0_C$ mode is also unaffected by any fluids that may be present in the pipe, unlike the $A0_C$ mode. This makes it more suitable for applications where pipes may be filled with fluid. Because the $SH0_C$ mode has a sufficiently short dead-zone and is relatively simple to excite it would appear to be the most suitable mode to perform a circumferential guided wave inspection.

5.4 Finite element modelling

As for previous parts of this study, finite element modelling was conducted using ABAQUS Explicit software [5] and its time marching procedure. Full 3D models were created using 8-node 'brick' elements of pipes of two sizes. A five inch pipe section 1m long with an outer diameter of 141.3mm and inner diameter of 115.9mm has been modelled with 1000 elements along the axis, 360 elements around the circumference and 10 elements through the thickness of the pipe. Therefore the model consisted of elements with an axial extent of 1mm, a radial extent of 1.27mm and a circumferential extent that varied from 1.24mm on the outer surface to 1.01mm on the inner surface. Using the criteria of eight elements per wavelength [69] this mesh allows for a maximum toneburst frequency of 190 kHz, well above the frequencies investigated for this study.

The six inch pipe model has an outer diameter of 168mm, an inner diameter of 138mm and a length of 1m. Similar to the model of the five inch pipe there are 1000 elements along the axis, 360 elements around the circumference and 10 elements through the thickness. The elements therefore have an axial extent of 1mm, a radial extent of 1.5mm and a circumferential extent that varies from 1.47mm on the outer surface to 1.20mm on the inner surface. Again using the criteria of eight elements per wavelength the mesh allows for a maximum frequency of 160kHz, suitable for this study.

For the purpose of experimental validation the outputs of certain finite element models have been compared to experimental results. Although the pipes used in the laboratory experiments were nominally six inch schedule 120, there are small differences in the actual pipe dimensions that had to be accounted for in the models. Therefore two other pipe sizes were modelled to reflect the differences, with one having an outer diameter of 170mm and wall thickness of 16mm, and the other having an outer diameter of 168mm and a wall thickness of 14.5mm. These models shared the same element configuration as the six inch model described previously.

The models need to have an axial extent of 1m to ensure that the circumferential wave that propagates around the circumference and back to the transducer location is separated from the end wall reflection from the pipe. When a node is excited to generate

a circumferential wave it will also excite a wave that propagates axially in both directions along the pipe. The mode that propagates axially along the pipe depends on the mode that is intentionally excited to propagate circumferentially. If a shear transducer is orientated along the axis of the pipe in order to generate a circumferential $SH0_C$ wave, then an $S0_C$ wave mode will also be generated and will propagate axially along the pipe. The greatest length of pipe required to achieve separation of the signals occurs with the largest pipe diameter, and when the $SH0_C$ mode is propagating circumferentially and the $S0_C$ mode is propagating axially. In this case the pipe model must have an axial extent of at least 824mm.

An image of an FE model used in this study to investigate circumferential guided waves is presented in Figure 5.6. The nodes representing the crack and the nodes representing the receivers are both highlighted, with the excitation node being a single node at the centre of the array of receiving nodes.

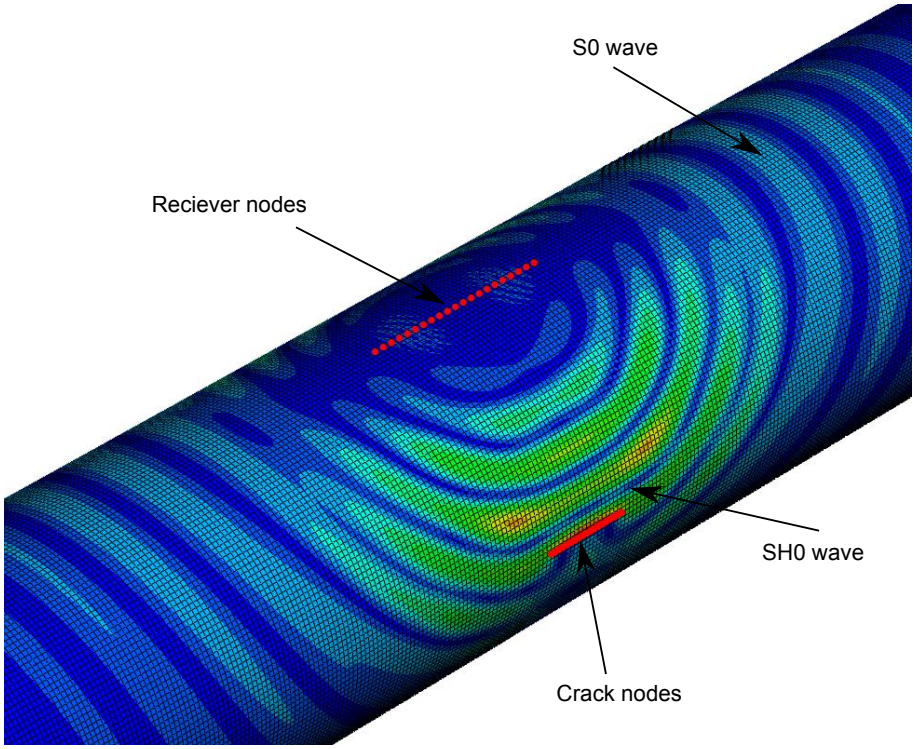

Figure 5.6: Image of finite element model used to study circumferential guided waves. Crack nodes and monitoring nodes are highlighted. The excitation node is at the centre of the array of receiver nodes. The $SH0_C$ wave propagating circumferentially and the $S0_C$ mode propagating axially are also labelled.

Defects are modelled in the same manner as described in Chapter 3, with a 'V' notch shaped profile. In all cases the mid-point of the crack is at the same axial position as the mid-point of the pipe. It is necessary to model cases of cracks emanating from both the inner surface and outer surface of the pipe, with cracks originating at the inner surface to predict the behaviour of real-life defects, and cracks originating at the outer surface to compare to laboratory validation experiments. It is expected that due to the differing curvature of the inner and outer surfaces of the pipe, the sensitivity of a mode will not be the same for a crack originating on the outer surface and a crack originating from the inner surface of a pipe. Cracks with depths ranging from 10% of the through-thickness extent of the pipe up to through-thickness cracks are modelled, originating, in separate analyses, from both the inner and outer surfaces.

Wave mode excitation is achieved by prescribing a five cycle sinusoidal oscillation modulated by a Hanning window to a single node on the outer surface of the pipe. The excitation node is at the same axial location as the centre of the crack, and is circumferentially offset from the crack by 90 degrees. Reception nodes are arranged in a linear array along the axis of the pipe, at the same circumferential position as the excitation node. The length of the array of reception nodes was initially long enough to determine the maximum practical axial separation of the transmitting and receiving transducers. After this the monitoring node representing the same transducer separation as the laboratory experiments, or the monitoring node that is co-located with the excitation node, were used to monitor ultrasonic wave propagation.

The ultrasonic mode generated by the excitation transducer is determined by the axis of excitation. If the node displacements are in the axial direction, to generate a circumferential $SH0_C$ wave, then the wave pattern will look similar to that presented in Figure 5.6. In the image the $SH0_C$ wave can be seen propagating circumferentially and reflecting and diffracting from a crack. It is also possible to see an $S0_C$ wave propagating axially along the pipe. An $S0_C$ circumferential wave was excited by orientating the node displacements in the circumferential direction. This would also have the effect of generating an $SH0_C$ wave that propagated axially along the pipe. Radial displacement of the excitation node would generate an $A0_C$ wave in all directions. All three modes

were simulated in this study to examine the reflection characteristics from axial cracks in pipes.

5.5 Experimental procedure

Laboratory experiments were performed on two sections of nominal six inch pipe. Each section was 1m long to ensure the separation of the circumferentially propagating wave and the end-wall reflection. Two pipe sections were used thereby making it possible to examine the effect of defect length and the effect of defect depth. Defects were machined into the two pipes using a milling machine with a 5mm drill-bit. The defects are therefore notches with a width of 5mm, and all part-depth notches have a flat profile on the sides and bottom. A picture of one of the sections of pipe mounted on the milling machine is presented in Figure 5.7. The pipe is resting on 'v' blocks and an aluminium bar that is used to hold the transducers in position is visible attached to the pipe. The bar and transducers were kept in position during machining in order to improve coupling consistency between the transducers and the pipe.

Experimental results were collected for the $SH0_C$ mode. To generate an $SH0_C$ wave in the circumferential direction low-frequency piezoelectric shear transducers produced by Guided Ultrasonics Ltd.[1], orientated in the axial direction, were used. The transducers have an area measuring 14mm by 14mm, including a contact patch measuring 14mm by 2mm. They do not require an ultrasonic coupling agent to transmit ultrasonic energy into a component, but a sufficient force must be applied to the transducer against a component to achieve coupling. In this experiment the transducers are held in place by an aluminium bar measuring 20mm in height, 50mm in width and 1m in length. A picture of the bar is presented in Figure 5.8a. There is a slot in the centre of the bar to allow cables to be attached to the transducers, which can be seen protruding from the bar in Figure 5.8a.

Also visible in both Figure 5.7 and Figure 5.8a are jubilee clips attached to either end of the aluminium bar. The jubilee clips serve to hold the bar and transducers in place

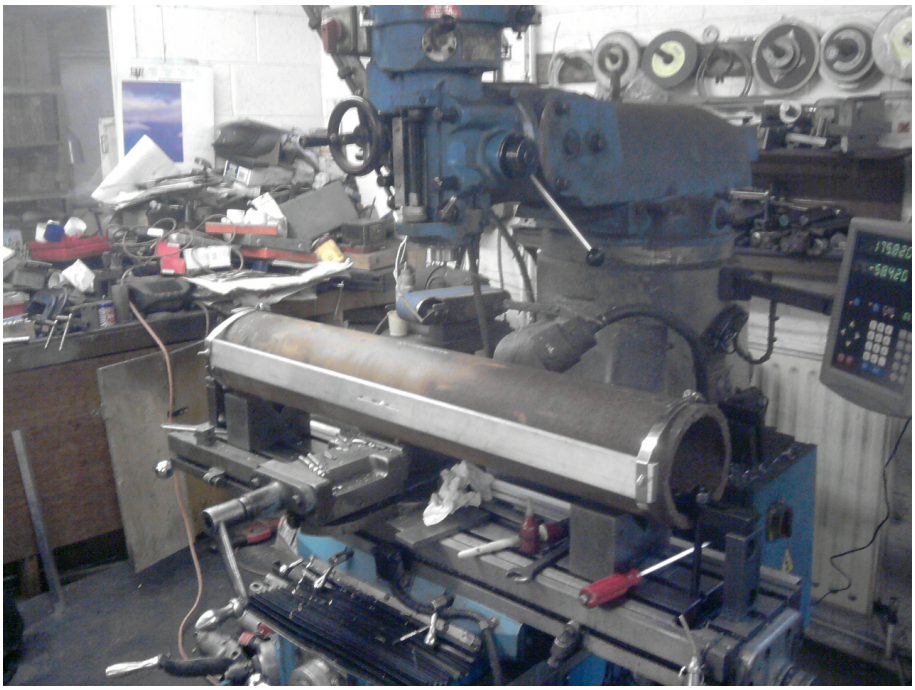

Figure 5.7: Experimental set-up for circumferential guided wave experiments. A 1m section of six inch pipe is mounted on a milling machine to cut axial slots. An aluminium bar used to hold the transducer in place is visible in front of the pipe.

and to apply the necessary pressure to the transducers to achieve ultrasonic coupling. The aluminium bar needs to be as long as the pipe sections to ensure that there are no reflections of ultrasonic waves from the jubilee clips that may affect the results. A picture of two transducers being held against a pipe section by the aluminium bar is presented in Figure 5.8b. There is an element spacing of approximately 1mm and therefore the transducer pitch is 15mm. The transducers had approximately a 15mm pitch in all experiments.

The transmitting transducer is excited with a five-cycle Hanning-windowed toneburst with a centre frequency in the range of 50 kHz to 85 kHz, at increments of 5 kHz. The excitation was generated by a Wavemaker Duet STR 1-3a function generator. The Wavemaker Duet has a number of pre-defined output functions, one being the five-cycle Hanning toneburst, and for this reason a five cycle excitation was preferred over a four-cycle excitation. The reception transducer was monitored with a Lecroy Waverunner 6030A oscilloscope, after the signal had passed through a pre-amplifier, with gain set to 50dB, built into the Wavemaker Duet. An image of the function generator and

(a) Transducer holder **(b)** Transducers

Figure 5.8: Image of equipment used to attach transducers to pipe. a) shows the aluminium bar holding transducers in place with transducer cables protruding from the centre of the bar. b) is a side view of the bar with both transducers shown held against the pipe.

oscilloscope is presented in Figure 5.9, with the function generator on the bottom and oscilloscope, displaying a time trace from an experiment, on top.

All signals were passed through a band-pass filter to remove high frequency and low frequency noise. Signals also consisted of 100 averages to remove random noise from the signal.

Although nominally both sections of pipe were six inch schedule 120 pipe-work, there were variations in pipe dimensions. The pipe used to measure the effect of crack length has an outer diameter of 170mm and a wall thickness of 16mm, and the pipe used to measure the effect of crack depth has an outer diameter of 168mm and a wall thickness of 14.5mm. Both the wall thickness and outer diameter of the pipes were measured at multiple locations with minimal variation found in the measurements.

To measure the effect of defect length a notch with a depth of 8mm was machined into the pipe, a wall loss of 50% of the through-thickness extent of the pipe. The notch had an initial length of 10mm and this was increased in increments of 10mm up to 120mm. An ultrasonic measurement was taken at each length increment. The length of the notch was extended equally from the centre of the notch for each increment, maintaining the position of the mid-point of the notch so the transducers did not have to be moved after each cut.

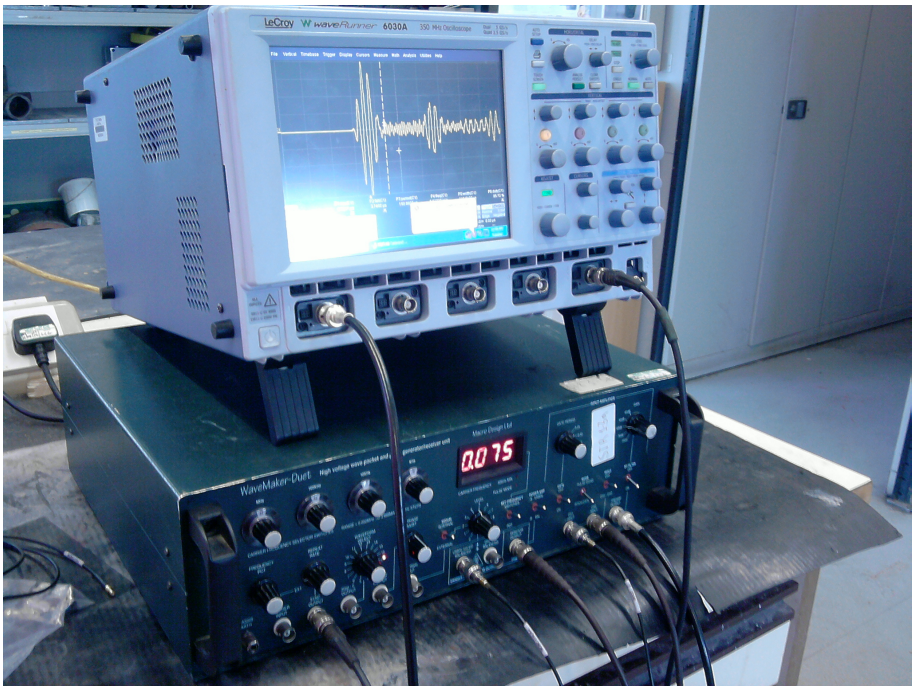

Figure 5.9: Function generator and oscilloscope used to generate and monitor circumferential guided wave signals. The function generator is on the bottom and the oscilloscope on the top.

To measure the effect of defect depth a notch was cut with an axial extent of 120mm in the pipe with a wall thickness of 14.5mm. The initial depth of the notch was 1.45mm, 10% of the through-thickness extent of the pipe, and was increased by increments of 1.45mm until a through-thickness notch was achieved.

5.6 Results and discussion

Results are presented showing how various parameters affect the reflection coefficient of circumferential guided waves from an axial crack in a pipe. In Figure 5.10 typical time traces are presented for both finite element and experimental data displaying the expected response from an axially aligned defect with an axial extent of 60mm and a through-thickness extent of 50%. The incident toneburst in both example time traces has a centre frequency of 65 kHz and the $SH0_C$ circumferential guided wave mode is being excited. It is possible to identify both the defect signal and the wave that has

propagated around the full circumference of the pipe. The signal beyond the propagating wave signal is the end-wall reflection from the $S0_C$ mode propagating axially along the pipe.

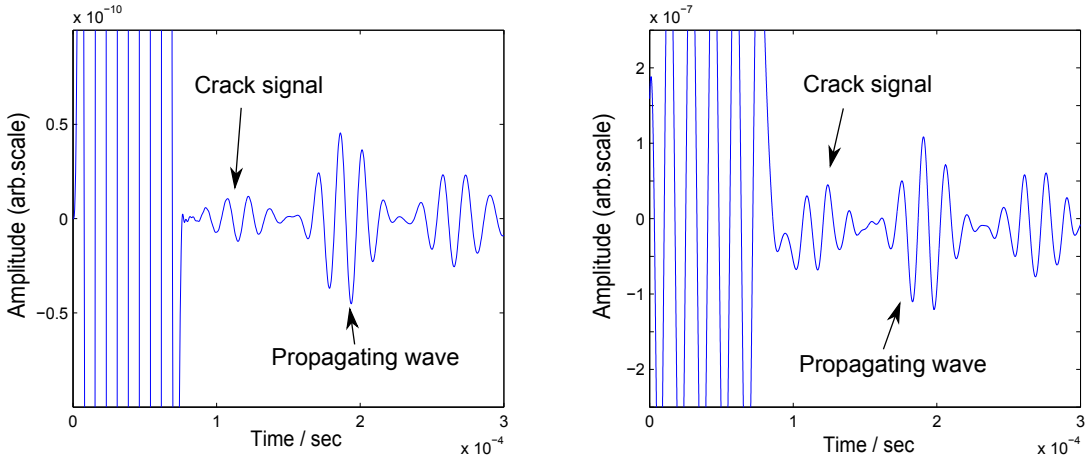

(a) Finite element **(b)** Experiment

Figure 5.10: Typical time trace data from both a finite element model and a laboratory experiment. Defect signal is from an axial notch with 60mm axial extant and 50% through-thickness extent. Toneburst centre frequency is 65 kHz.

Time traces for the $A0_C$ and $S0_C$ modes, generated with FE modelling, are presented in Figure 5.11. From the figure it can be seen that the $A0_C$ mode is a promising mode for performing a circumferential guided wave inspection. The dead-zone is suitably small that the crack signal can be clearly identified, and because the propagation distances are very short there is little evidence of dispersion.

In contrast the $SH0_C$ mode does not appear suitable for circumferential guided wave inspections for this application. Because the wavelength is high there is an unacceptably large dead-zone which makes separating the signal reflected from the crack and the signal of the propagating wave impossible. In Figure 5.11b the crack is positioned for optimal detection, with an angular displacement of 90° from the transducer location. At this position it is possible to measure a meaningful reflection coefficient because the peak of the Hilbert transform of the crack reflection is between the signals from the incident toneburst and the propagating wave. However, only a small change in the circumferential position of the crack is required before sensitivity is adversely affected.

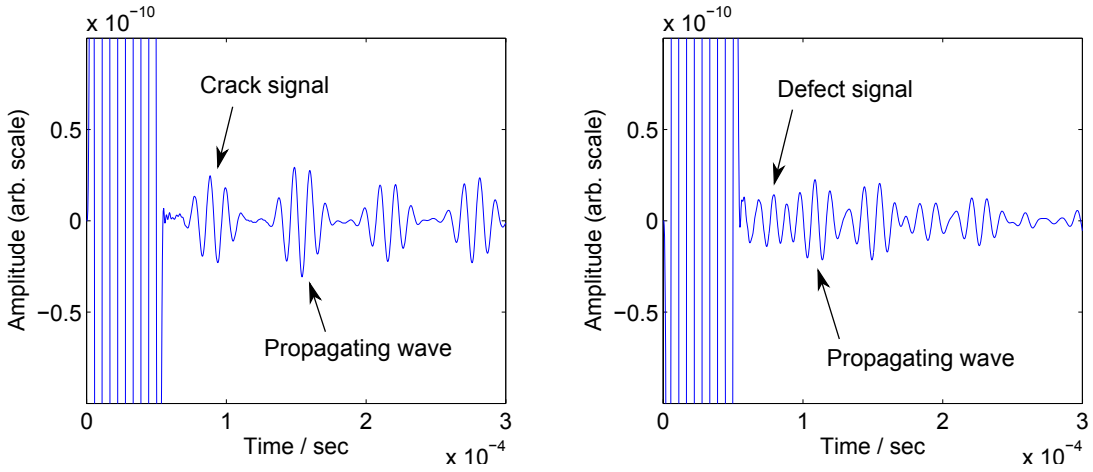

(a) $A0_C$ mode **(b)** $S0_C$

Figure 5.11: Typical time trace data from finite element modelling for $A0_C$ and $S0_C$ modes. Defect signal is from an axial crack infinite axial extant and 50% through-thickness extent. Toneburst centre frequency in both cases is 90 kHz.

5.6.1 Crack Length

A chart plotting the reflection coefficient of the $SH0_C$ circumferential guided wave mode as a function of crack length is presented in Figure 5.12, with a comparison between experimental and finite element data. The centre frequency of the incident toneburst is 65 kHz and the maximum length of the crack is 120mm, equating to a crack length of just under 2.5 wavelengths of the incident toneburst (λ). The crack depth is held constant at 50% of the through-thickness extent of the pipe wall.

The experimental data points and FE data points show the same pattern, with the reflection coefficient increasing with crack length until the crack length is twice the wavelength of the incident toneburst, at which point the reflection coefficient begins to decline with increasing crack length. However, the reflection coefficients measured experimentally is of a consistently higher amplitude than the equivalent FE data points. A possible reason for this discrepancy is variable contact conditions between the transducers and the pipe section. Although the transducers remained attached to the pipe throughout the machining process, the milling causes the pipe to vibrate which could cause the transducers to move. If this happened on the first cut and caused the transducers

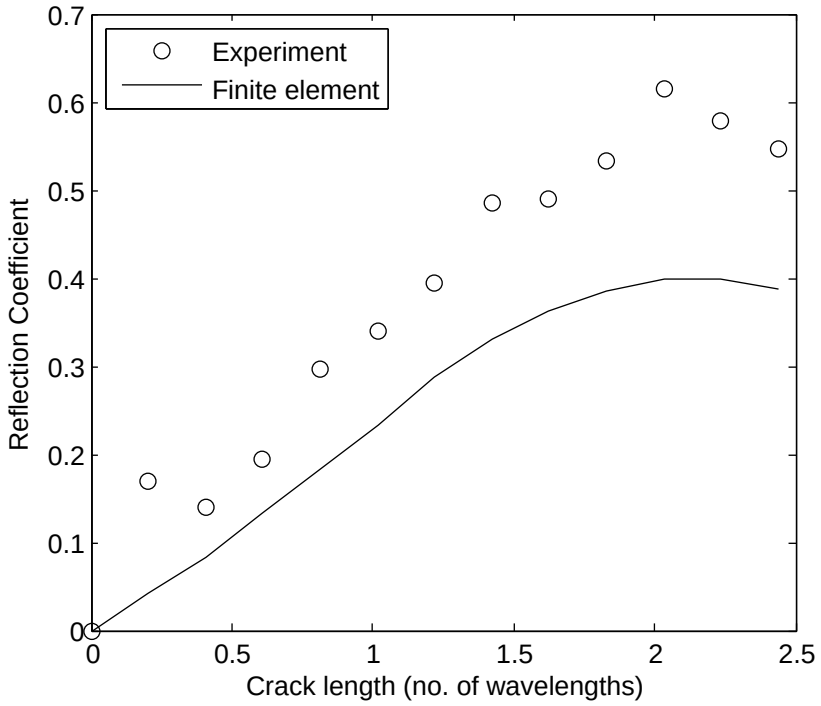

Figure 5.12: Comparison between FE and experimental data showing the reflection coefficient of the $SH0_C$ mode from an axial crack in a pipe as a function of crack length. The crack has a through-thickness extent of 50% and the incident toneburst centre frequency is 65 kHz.

to move into a position with better contact conditions, where they remained for the duration of the machining, this could explain the difference between the finite element and experimental data. The reflection coefficients were all measured relative to the amplitude of the propagating wave in the clean pipe and a change in contact conditions during the first cut could cause the results in Figure 5.12.

From Figure 5.12 it is seen that as the crack length extends beyond two wavelengths of the incident toneburst then the reflection coefficient starts decreasing. In Figure 5.13 the reflection coefficient of the $A0_C$, $SH0_C$ and $S0_C$ modes is plotted as a function of crack length for longer cracks.

For a through-thickness crack all three modes have a similar sensitivity to each other, and the reflection coefficient follows a similar pattern as crack length is increased for all three modes. There is a clear peak in reflection coefficient when the crack length is 2λ,

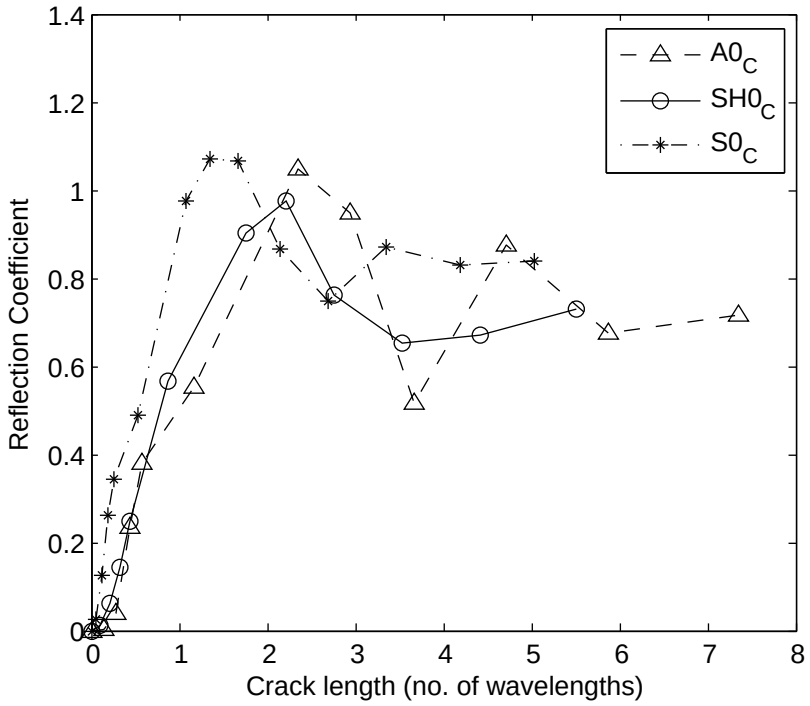

Figure 5.13: Finite element data for reflection coefficient as a function of crack length extending to full length of pipe section. Cracks are through-thickness and toneburst centre frequency is 75 kHz.

followed be a trough at a crack length of between 3λ and 4λ At crack lengths beyond this point the $SH0_C$ and $S0_C$ modes reach a plateau where the reflection coefficient no longer varies as crack length is increased, whereas the reflection coefficient of the $A0_C$ mode continues oscillating until the crack length reaches 6λ. A very similar pattern has been observed in plates for the reflection coefficient of an SH0 wave from a perpendicular crack by Rajagapol and Lowe [87], and it is caused by crack-tip diffractions constructively and destructively interfering with the reflected signal.

5.6.2 Crack Depth

Figure 5.14 plots the reflection coefficient of the $SH0_C$ mode from an axial crack in a pipe, as a function of crack depth, with a comparison between FE and experimental data. The data show reasonable agreement, with the FE data showing the reflection coefficient increasing monotonically with crack depth. The experimental data points for

crack depths between 30% and 60% of through-thickness extent display a noticeably higher reflection amplitude than the equivalent FE data points. The other experimental data points are in very close agreement with the FE data points.

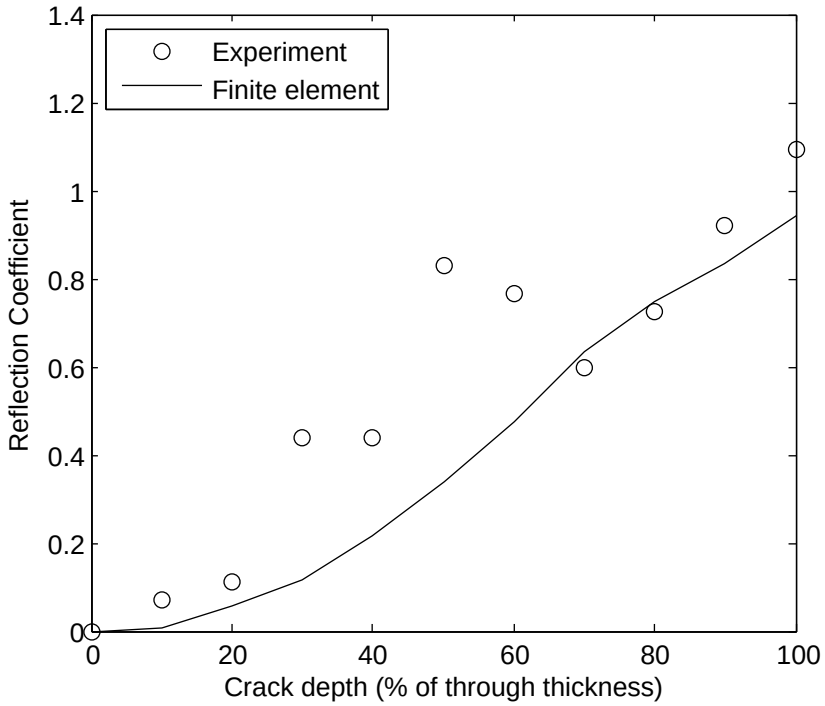

Figure 5.14: Comparison between FE and experimental data showing the reflection coefficient of the $SH0_C$ mode from an axial crack in a pipe as a function of crack depth. The crack has an axial length of 120mm and the incident toneburst centre frequency is 65 kHz.

The reason for the high differences is likely to be variable coupling between the transducers and the pipe section caused by vibration during the milling process. The vibrations from the milling machine were discussed previously for the experiment into the effect of crack length on reflection coefficient, but only appeared to have an effect during the first cut. The milling process for increasing the depth of a notch causes more violent vibrations in the pipe than the milling process for increasing notch length, so a higher variability is evident in the results. Measurements were taken with several centre frequencies at each crack depth, and the pattern demonstrated for experimental data in Figure 5.14 is present at all frequencies.

A finite element study was conducted to examine any possible difference in reflection

coefficient between a crack emanating from the inner surface and a crack emanating from the outer surface of a pipe. It is important to understand the difference because the laboratory experiments, out of necessity, featured a crack emanating from the outer surface. In a real pipe a crack would emanate from the inner surface. There is essentially zero difference in the reflection coefficient for a crack of given depth whether it is emanating from the inner or outer surface, when the reflection of the $SH0_C$ mode is being considered. This indicates that the stress and displacement fields are symmetric about the mid-point of the pipe wall for the $SH0_C$ mode circumferential guided wave.

However, the reflection coefficient of the $A0_C$ mode does appear to depend on whether the crack is emanating from the inner or outer surface. In Figure 5.15 the reflection coefficient of the $A0_C$ mode is plotted as a function of crack depth for cracks emanating from both the inner and outer surfaces. There is a difference between the two which is most pronounced with crack depths ranging from 20% to 50% of through-wall extent. The results indicate that the differing curvatures of the inner and outer surface affect the propagation of the $A0_C$ mode in the circumferential direction. If the $A0_C$ mode were to be used in a practical inspection then this is promising because the reflection amplitude of the $A0_C$ mode from a crack emanating from the inner surface is higher than for a crack emanating from the outer surface at the critical crack depth.

Another interesting feature of the results presented in Figure 5.15 is that the reflection coefficient does not increase monotonically with crack depth. Somewhat counter-intuitively, between 40% and 60% crack depth the reflection coefficient reduces as the crack depth increases. This phenomenon has been observed in the plate case by Lowe et al. [71] who provide a detailed explanation. The pattern is attributed to axial and shear crack opening displacements and their relative importance for different crack depths according to mode shape. The work here demonstrates that the same theory applies to circumferential guided waves, with the added complication that the reflection coefficient is also dependent on whether the crack is emanating from the inner surface or outer surface of the pipe.

In Figure 5.16 the reflection coefficient is plotted as a function of crack depth for an incident S0 mode, for the separate cases of a crack emanating from the inner surface and

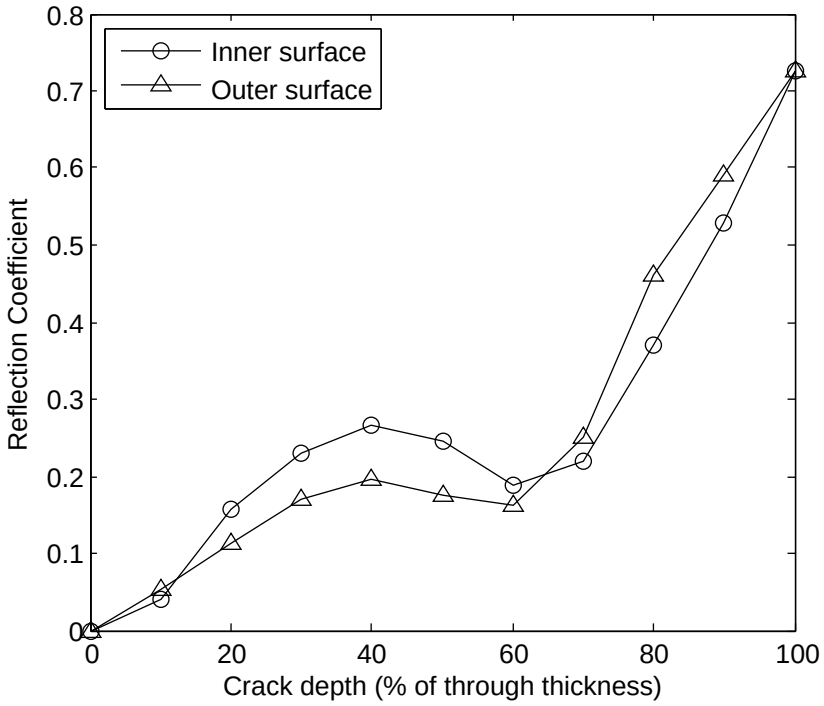

Figure 5.15: FE results plotting reflection coefficient as a function of crack depth with incident $A0_C$ mode. Results are presented for separate cases of cracks emanating from the inner surface and outer surface.

a crack emanating from the outer surface. There is a stark difference between the two cases with the crack emanating from the outer surface having a much higher reflection coefficient for any part-depth crack. For a crack emanating from the outer surface the reflection coefficient increase rapidly with crack depth and reaches its maximum value at a crack depth of approximately 70%. In contrast, for a crack emanating from the inner surface of the pipe, the reflection coefficient increases slowly as crack depth increases.

The results in Figure 5.16 suggest that the particle displacements on the outer surface of the pipe are much larger than the particle displacements on the inner surface of the pipe. Evidence of this is presented in Figure 5.17 where the values of circumferential stress and displacement are presented as a function of radial position for the $S0_C$ mode at the inspection frequency. Both values are clearly lower at the inner surface than at the outer surface. A much larger proportion of the incident energy is then reflected by a crack emanating from the outer surface of the pipe, where the particle displacements are larger.

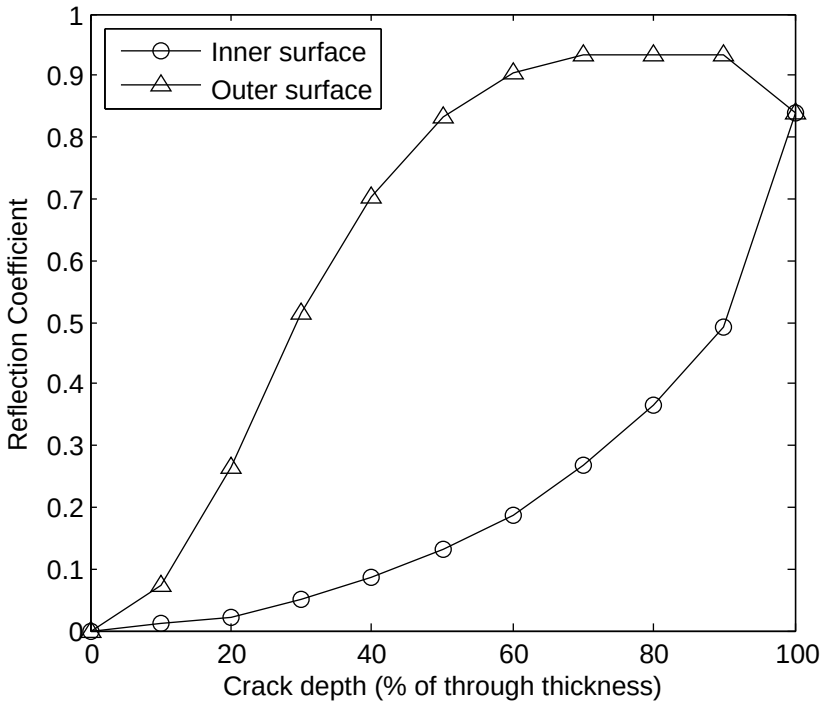

Figure 5.16: FE results plotting reflection coefficient as a function of crack depth with incident $S0_C$ mode. Results are presented for separate cases of cracks emanating from the inner surface and outer surface.

The reflection coefficient from a through-thickness crack appear to be of lower amplitude than the reflection coefficient from a part-depth crack originating at the outer surface of a pipe with a through-thickness extent of greater than 50%. This could be caused by constructive interference from a tip diffraction at the bottom of the crack, which would not be present for a through-thickness crack. This could be tested by varying the angular position of the crack relative to the transducer, or varying the input toneburst frequency. Unfortunately, the size of the dead-zone when using the $S0_C$ mode provides little scope for varying either of these parameters.

A high variation in reflection coefficient between cracks emanating from the inner or outer pipe surface has implications for a practical inspection. If cracks are known to originate at the outer surface of a pipe the $S0_C$ mode may be particularly desirable due to its high sensitivity to this type of crack. However, in this study the focus is on cracks originating at the inner surface of the pipe, and the $S0_C$ mode is insensitive to this type of crack. In combination with the issue of size of dead-zone discussed previously, this

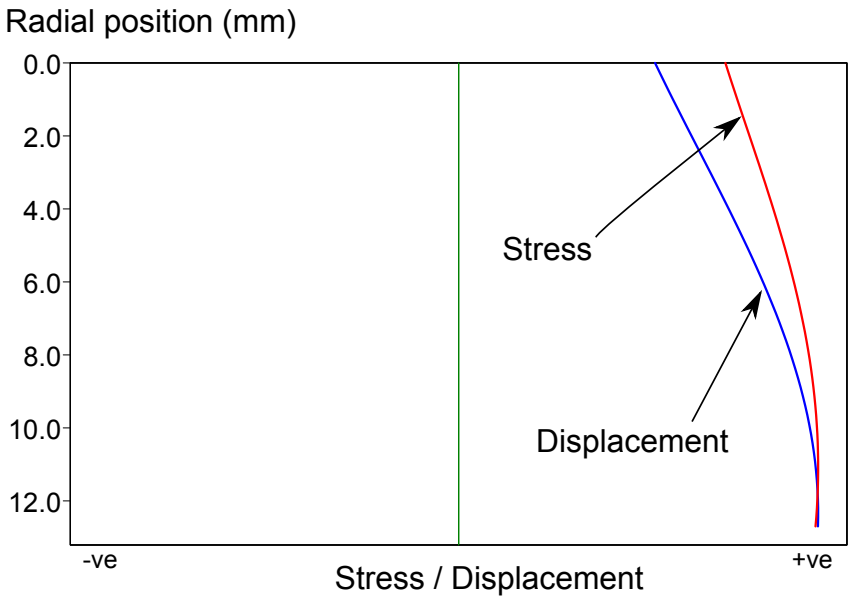

Figure 5.17: Values of circumferential stress and displacement for $S0_C$ mode as a function of position in pipe wall. Radial position of 0mm represents inner surface and radial position of 12.7mm represents outer surface. Displacement is displayed in blue and stress in red.

makes the SO_C mode undesirable for an inspection for the application being studied.

5.6.3 Smallest detectable critical defect

It is important to provide a reasonable estimate for the smallest crack that can be detected in a practical situation, as this will have great bearing on whether circumferential guided waves can provide a viable inspection technique. The critical depth of a crack has been calculated as 20% of the thickness of the pipe but this doesn't take into account the axial extent of a crack. The axial extent of a crack has little effect on the safety case, but short cracks can exist and from Figure 5.12 and Figure 5.13 it can be seen that cracks with a small axial extent have low reflection coefficients.

Results presented in the previous section suggest that, although the sensitivity of all three fundamental circumferential guided wave modes is similar for a through-thickness defect, there may be differences in sensitivity when detecting a shallow part-depth crack. A comparison of how the reflection coefficient of the different modes varies with crack depth for shallow part-depth cracks (see results in Figure 5.14, Figure 5.15 and Figure 5.16)

suggests that certain modes may be more sensitive to shallow cracks than others. At the critical crack depth of 20% the reflection coefficient of the $A0_C$ mode is higher than the reflection coefficient of the $SH0_C$, and the reflection coefficient of the $S0_C$ mode is either higher or lower depending on whether the crack originates at the inner surface or outer surface.

In Figure 5.18 the reflection coefficient of the $SH0_C$ and $A0_C$ modes is plotted as a function of crack length for a crack with a through-wall extent of 20%. At this stage the $S0_C$ mode was not considered, having been deemed unsuitable for this application.

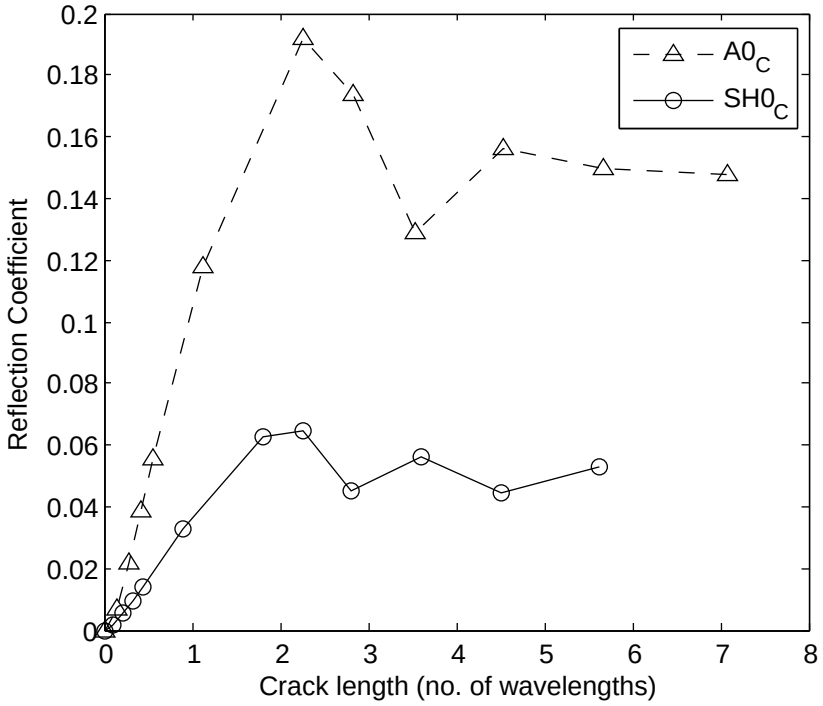

Figure 5.18: FE data showing reflection coefficient of the $SH0_C$ and $A0_C$ modes as a function of crack length for a crack with a through-wall extent of 20%. The centre frequency of the incident toneburst is 90 kHz.

For an axial crack with a through-wall extent of 20% the $A0_C$ mode is significantly more sensitive than the $SH0_C$ mode, with a peak reflection coefficient 9.5dB higher. The models suggest that when using the $SH0_C$ mode, a crack with an axial extent less than 30-40mm will be very difficult to find in a practical situation. This is concerning because a crack may form from the bottom of a small number of pits, with a total axial extent of 8-10mm. However, with the $A0_C$ mode it should be possible to reliably detect an

axial crack with a through-wall extent of 20% and axial extent of 15mm. Whilst this is not quite acceptable, it is close to being a viable inspection method for this application. With some further work circumferential guided waves may become suitable to detect small axial cracks in pipes that are of concern to the power industry.

5.7 Conclusions

In this chapter the use of circumferential guided waves to detect axial cracks in pipes has been investigated. Finite element modelling has been conducted to investigate various experimental parameters with validation using laboratory experiments. Although there are some discrepancies between the FE data and experimental data the trends agree very well and the differences have been explained by small problems in the experimental procedure.

The principles and practicalities of a circumferential guided wave experiment have been explained including transducer layout, frequency selection and mode selection. It has been shown how the reflection coefficient varies with the crack length and depth for both the $SH0_C$ and $A0_C$ modes.

The $A0_C$ mode has been deemed most suitable for a circumferential guided wave inspection. Of the three modes available in the low frequency range investigated during this study it had the highest sensitivity to cracks emanating from the inner surface of the pipe, and it is therefore possible to detect cracks of low axial extent using this mode. Of the three modes investigated over the frequency range used in this study, the $A0_C$ mode has the shortest wavelength, and therefore the smallest dead-zone, making it more desirable than the other two modes. Although the $A0_C$ mode is slightly dispersive in the frequency range being proposed for this inspection, the dispersion effect is negligible because of short propagation distances.

Although circumferential waves lack some of the advantages of long-range guided waves, they have proved much more sensitive to axially aligned defects in pipes, in principle because the defect is perpendicular to the direction of wave propagation. Using the

$A0_C$ mode it should be possible to detect a crack of critical depth with an axial extent of 15mm, although ideally it should be possible to detect a crack with an axial extent of 8-10mm for this application. Circumferential guided waves in pipes would provide a very good screening tool where the requirements are slightly less stringent than here. It could be a very quick and simple technique with a high enough sensitivity to complement manual ultrasonics, being used for screening in many applications.

During the study both finite element models and the pipe sections used for the laboratory experiments were 1m long, so that end-wall reflections did not interfere with the results. It is possible to infer from this that a circumferential guided wave inspection would be impossible within 0.5m of a feature, such as a weld, that would produce a similar reflection. This problem can be largely mitigated by ignoring the need to separate the end-wall reflections with the signal produced by the propagating wave. It is only necessary to ensure that the time window where a defect is expected is free from end-wall or feature reflections.

A high priority for any future work would be to use a suitable zero degree compression probe to provide experimental validation of the FE work studying the $A0_C$ mode. It would then be prudent to investigate whether the sensitivity of the circumferential guided wave technique to axial cracks could be improved. For instance, using an array of transmitting transducers, focusing could be used to increase the sensitivity to cracks of small axial extent. Even a small increase of sensitivity would be enough to detect a critical defect. A study could be done to compare the reflection amplitude from an axial crack from a plane wave, with the reflection amplitude of a focused wave. It would be necessary to determine whether active phased array focusing was superior, or synthetic focusing as described in Chapter 4. Synthetic focusing is applicable to plates along with pipes [32]. If a similar increase of sensitivity is achieved as when using synthetically focused long-range guided waves, around 6-10dB, it would be sufficient to detect a critical defect. Care must be taken to ensure the process is no more time or labour intensive than current manual ultrasonic inspections.

Other transduction technologies, in particular EMATs, could be investigated to determine whether they are more suitable than piezoelectric transducers, by improving coupling

consistency and facilitating more rapid scanning. EMATs are already used in other circumferential guided wave pipeline inspections [82, 92] because they offer advantages over piezoelectric transducers. In a power station, however, the use of EMATs is limited to components that operate above 400℃ so their use would not be universal. It would only be worth pursuing EMATs as a transduction device if enough pipework within a power station was suitable for inspection.

Chapter 6

Guided wave inspection of sootblower pipework

6.1 Introduction

In this chapter a secondary application for guided waves in power stations has been investigated – the guided wave inspection of sootblower supply pipework. The work is applicable to many power stations that have large quantities of sootblower pipework. Although commercially available guided wave equipment and software exists for the inspections, there is a degree of novelty in the interpretation of the results. Instead of identifying specific areas of concern that might indicate a localised defect, it is intended to use the guided wave results to assess the general condition of the pipework, for the purpose of deciding whether it needs to be replaced. An assessment of the general condition of sootblower pipework is suitable because usually an entire sootblower pipework system is replaced at once, rather than repairing or replacing small damaged sections. A guided wave inspection could offer a very quick and effective tool that can determine if and when the pipework should be replaced.

All coal and oil fired boilers require a sootblower system. It is designed to remove carbon deposits and other combustion products from the inside of boilers, as these deposits can build up over time and reduce heat transfer efficiency. To remove these deposits steam

is diverted from the main steam line and distributed along a large network of pipes to the sootblowers. The sootblowers blast the inside of the boiler wall with the steam thus removing any deposits. There are many sootblowers for each boiler spread over different levels, so a large supply network is required to feed them all.

The primary degradation mechanism for sootblower pipework is internal wall loss by erosion and corrosion, and currently sootblower pipework is inspected using ultrasonic thickness measurements. Based on the results of the thickness measurements an assessment is made regarding the condition of the pipework. If the condition is deemed to be unacceptable the pipework is replaced. Rather than replacing small sections of sootblower pipework, usually all of the pipework for a given unit is replaced at the same time.

Ultrasonic thickness measurements are often unreliable as an indicator of general pipe condition because the sampling density is often too low to capture enough data for a full assessment. For instance, a localised area of thinning could be missed if it fell between two inspection locations. Performing thickness measurements also requires the removal of lagging from the pipework, a costly and time consuming activity. It would be advantageous to use guided waves instead of thickness measurements, as complete coverage is provided and only minimal removal of lagging is required.

Wall thinning in sootblower pipework is usually reasonably uniform and therefore it is not necessarily the case that any obvious defect signals would be present during a guided wave inspection. Instead, it is intended that an estimation of the condition of a pipe section can be determined by examining the amplitude of coherent noise at that section. Based on the noise level the pipework can be classified as 'good', 'medium', or 'poor' and appropriate action can be taken based on that assessment.

The work presented here was conducted at Kingsnorth power station, a 2000MW coal-fired power station in Kent, consisting of four boiler units. Although the specific configuration of a sootblower system is possibly unique to a single location, the principles can be applied to any sootblower system.

6.2 Wavemaker G3

All guided wave inspections described in this chapter and Chapter 7 were performed using the Wavemaker G3 instrument produced by Guided Ultrasonics Ltd. [1]. In some of the previous chapters the Wavemaker G3 instrument was used but not with the commercial WaveProG3 software provided with the equipment. For the applications described in this chapter the commercial software was used, and the use of equipment and associated software is described here. The use of guided waves for non-destructive testing is covered in British Standards [3].

A transducer ring is required for an inspection and is attached to a pipe in order to transmit and receive ultrasonic signals. A large range of pipe sizes can be inspected by connecting an appropriately sized transducer ring housing to the G3 instrument. Transducer ring housings for larger pipe diameters contain more transducers to ensure control of higher order flexural modes [16].

Commercially available transducer ring housings contain two rings of transducers allowing for directional control of the generated waves [27]. The transducers are dry-coupled piezoelectric shear transducers [12] and can be oriented in either the circumferential or axial direction. If they are oriented in the circumferential direction a torsional mode is excited [16], whereas if they are oriented in the axial direction it is possible to excite longitudinal modes [13]. In all inspections described in this study the fundamental torsional $T(0,1)$ mode was excited by orienting the transducers in the circumferential direction.

Depending on the specific application, transducer ring housings are available in a range of styles, including solid, inflatable and low profile. A solid ring has two halves that are placed around the pipe being inspected and clamped together. The transducers are all spring-loaded to ensure that coupling is as consistent as possible. The sootblower pipework inspected during this procedure was a mixture of 2 inch and 2.5 inch outer diameter pipework, necessitating the use of two different solid transducer rings. A specific 2.5 inch transducer ring was not available for the inspections, however it was possible to use a three inch transducer ring with 'extended transducers'. Extended transducers are

longer than standard transducers and therefore allow smaller diameter pipework to be inspected than the transducer ring is designed for. The 2 inch pipework was inspected using a 2 inch transducer ring. A solid transducer ring also was used at Fiddler's Ferry power station as described in Section 7.2.

An inflatable ring is a collar with the transducers attached to it. It is wrapped around a pipe and then inflated to ensure good contact for the transducers. An inflatable transducer ring was used at Port of Liverpool power station, described in Section 7.1. Solid rings are used for smaller pipe diameters, below eight inches, and inflatable rings are used for larger pipe diameters, above six inches [73]. In certain applications, for instance when two or more pipes are in close proximity, it is necessary to use a low profile transducer ring. A low profile ring requires less clearance around the pipe than other types of transducer ring so is suited to applications where a solid or inflatable ring cannot be fitted around a pipe.

After selecting an appropriate transducer ring and attaching it to a pipe a guided wave inspection can take place. A typical inspection would involve exciting the transducers over a range of frequencies, in the frequency range of 20 kHz - 50 kHz [73]. The data is averaged to minimise incoherent noise – with standard options of 2, 4, 8, 16, 32 and 64 averages – but averaging more than 16 times does not usually confer a worthwhile benefit [73].

The results of a guided wave scan can be presented in multiple ways, but in this study the results are presented as an A-scan with a plot of reflection amplitude as a function of axial position on a pipe. The Wavemaker G3 has multiple channels so transducers can be addressed, not necessarily individually, but in small groups. This allows for mode control of the incident signal and the measurement of flexural modes that exist due to mode conversion when the incident axisymmetric mode is reflected from a non-axisymmetric discontinuity [16]. The reflection amplitude of both the $T(0,1)$ mode and mode converted flexural mode are plotted on the same A-scan. On the A-scan plots produced by the Wavemaker G3 and associated software the axisymmetric mode is presented in black and the non-axisymmetric mode is presented in red. Plotting the reflection amplitude of both the axisymmetric and non-axisymmetric mode allows for the

identification of non-axisymmetric discontinuities, as an incident wave will mode-convert upon reflection from a non-axisymmetric discontinuity [69].

The A-scan results produced by the Wavemaker G3 software feature distance-amplitude-correction (DAC) curves that allow the data to be calibrated. Correct calibration of the DAC curves allows for the accurate measurement of the change of pipe cross-section. Four DAC curves are available when using the Wavemaker G3 software, a flange DAC, a weld DAC, a call-line DAC and a noise DAC. The flange DAC represents a reflection of 100% of the incident energy, as produced by a flange or pipe end. The weld DAC has a default amplitude of 22% of the flange DAC, representing the typical weld signal amplitude in pipes in the size range of 3-12 inches. The call-line DAC has a default amplitude of 5% of the flange DAC amplitude and represents the typical signal amplitude at which an indication would be considered for follow-up inspection. The noise level DAC is typically user defined according to the noise level of the guided wave signal.

The DAC curves can be calibrated using a series of reflectors of known amplitude, usually welds [73]. Welds are useful for calibrating DAC curves because they are easily identifiable; have a relatively consistent amplitude; have a reflection amplitude that is not frequency dependent; and appear regularly along most sections of pipework.

6.3 Sootblower system description

A sootblower supply system is a large array of pipework designed to distribute steam to the inside surface of a boiler, for the purpose of cleaning the boiler wall to improve heat transfer. The sootblowers themselves are the devices that enter the boiler and they can move in and out to provide full surface coverage of the inside of the boiler. Each boiler has many sootblowers and they are supplied with steam from the cold reheat, the steam conditions being 42.5bar and 348°C. There is a complicated network of pipework called the sootblower supply system, and further use of the term 'sootblower pipework' refers to the sootblower supply system, rather than the sootblowers themselves.

Figure 6.1 is an isometric diagram of the sootblower pipework on the 'A-side' of a unit

at Kingsnorth power station. A mirror image of this pipework is present on the 'B-side' of the unit, with an isometric diagram of the 'B-side' presented in Figure 6.2. On the section of the pipe where steam enters the system from the cold reheat there is an isolation valve. The valves are represented by a 'zig-zag' pattern, located next to position 3 in Figure 6.1 and next to position 1 in Figure 6.2, and immediately prior to the vertical section of pipework on either side of the boiler. In both Figures 6.1 and 6.2 there are black dots and associated designations, representing where the steam exits the supply system and enters an individual sootblower. There are also red dots indicating guided wave inspection locations of the system.

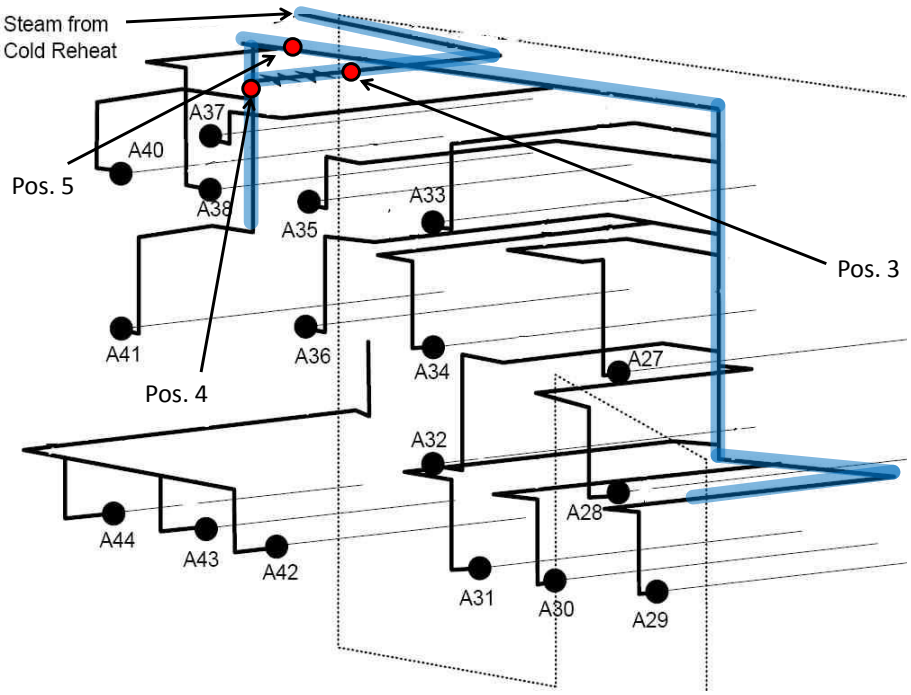

Figure 6.1: Schematic of sootblower supply pipework on A side of a boiler at Kingsnorth power station. The primary distribution line is highlighted in blue and inspection locations are indicated with red circles. The black dots represent where the sootblower supply system is attached to individual sootblowers, with the associated numbers being the sootblower designations.

The lines highlighted in blue in Figures 6.1 and 6.2 form the primary distribution system, with lines to each individual sootblower branching from this main line. The pipe size of the pipework in the main line is nominally 2.5 inches, with an outer diameter of 75mm

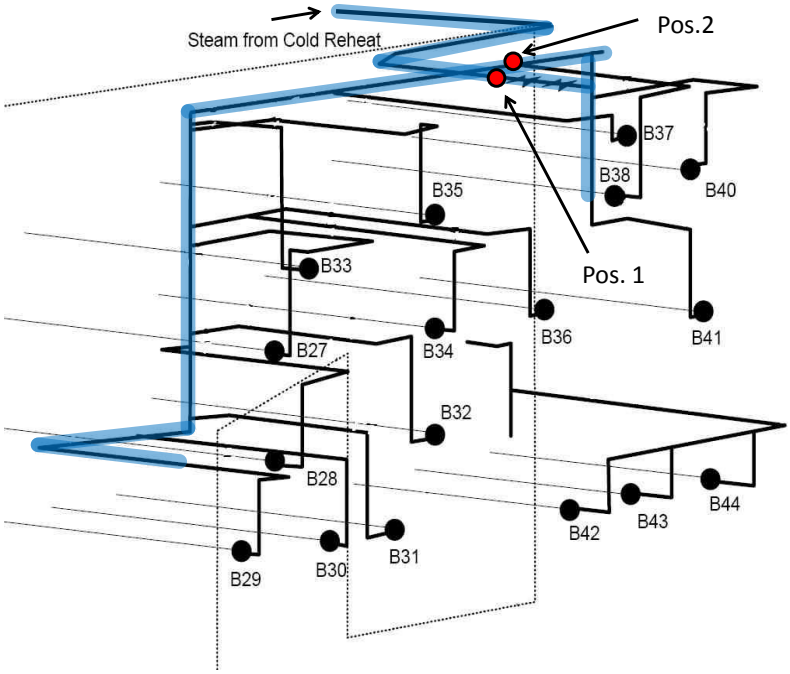

Figure 6.2: Schematic of sootblower supply pipework on B side of a boiler at Kingsnorth power station. The primary distribution line is highlighted in blue and inspection locations are indicated with red circles. The black dots represent where the sootblower supply system is attached to individual sootblowers, with the associated numbers being the sootblower designations.

and a wall thickness of 5.5mm. The size of the branched pipework is nominally 2 inches, with an outer diameter of 60mm and a wall thickness of 4.5mm. The majority of the branches are welded onto the primary distribution line to form T-pieces, and the lines supplying the two sootblowers that are not on branches, but at the ends of lines – B29 and B41 – have a reducer (see Figure 6.3) that reduces the pipe size from 2.5 inches to 2 inches.

A sootblower system is not required to run continuously and therefore it is turned on and off regularly, usually at least three times per day. Running the system in this way creates pressure waves that can cause erosion on the inside surface of the pipes. When the system is turned off standing water can accumulate causing internal corrosion of the pipework, and together erosion and corrosion can cause wall thinning throughout

Figure 6.3: Photograph showing reducer connecting 2 inch supply to sootblower B29 with 2.5 inch main supply pipework

the system. The problem is generally worse at the top of the system where the steam pressure is higher.

6.4 Proposed pipework classification system

The primary concern with sootblower pipes is general wall thinning, rather than specific areas of corrosion or cracking. Therefore the aim is to use guided waves to monitor the general condition of the pipe, rather than attempt to locate specific defects. Currently this is achieved using a spot thickness meter, but to provide good coverage this involves removing large amounts of insulation and can only monitor the pipe thickness directly underneath the probe, which restricts how comprehensive a survey can be.

An alternative approach to measuring the general condition of a pipe would be to use guided waves to measure the level of coherent noise generated during a guided wave inspection. Coherent noise is created by pits and other small discontinuities in pipes that individually would be of no concern. However, when combined with each other they can be cause for concern. The advantage in using guided waves is that they allow for full coverage of a pipe system, unlike spot-thickness checking. Furthermore, this is achieved with only minimal removal of lagging. Thus, the purpose of the proposal to look at the general condition of a pipe, rather than for specific defects, is that there may be an accumulation of small defects that would not produce a large enough guided wave signal to be identified as a defect. It may however be apparent from the results that

the condition of the pipework requires that it is replaced. For this proposal to be viable it is necessary that the condition of pipework can be ascertained from the guided wave signal, using the noise level and attenuation to make a judgement. The classification system therefore needs to be calibrated by comparing guided wave results to the actual condition of pipework in order to set criteria for 'good', 'medium' and 'poor' condition.

A potential problem with the classification system is that guided waves are sensitive to change in cross-sectional area, so if there was uniform wall loss along the whole pipe this would not necessarily be discovered. However, uniform wall-loss is unlikely and a small number of spot-thickness measurements in the vicinity of the transducer ring location, where lagging has already been removed, would address this concern.

6.5 Experimental procedure

The experimental procedure for developing a pipe classification system was conducted in two stages. Initially, guided wave measurements were made *in situ* using standard commercial equipment produced by Guided Ultrasonics Ltd [1]. Secondly, some of the pipework that was removed to be replaced has been surface scanned to quantify the condition of the inner surface. The results of the two tests were compared to determine whether the noise level in the guided wave signal correlates with the actual condition of the pipework.

6.5.1 Guided wave procedure

Guided wave inspections were carried out at Kingsnorth power station on units 2 and 4. As well as inspections on in-service pipes, it was also possible to inspect a brand new section of pipe that was due to replace the existing pipework. The clean pipe provided an excellent calibration piece because the noise level measured in a clean pipe would obviously be at the lowest possible level.

Five guided wave inspections were carried out on the 2.5 inch primary distribution line

at the top of the sootblower supply system on unit 2 at Kingsnorth power station. The locations of these inspections are labelled in Figures 6.1 and 6.2. Figure 6.4 shows an expanded view of the 'A-side' sootblower pipework from Figure 6.1, centred on the inspection locations. Position 1 and position 3 are located immediately up-stream of the isolation valve on the 'B-side' and 'A-side' of the boiler respectively. Using guided waves at these locations allowed the section of pipework from the cold reheat to be inspected. The pipe sections are approximately 17m long with two bends on each side.

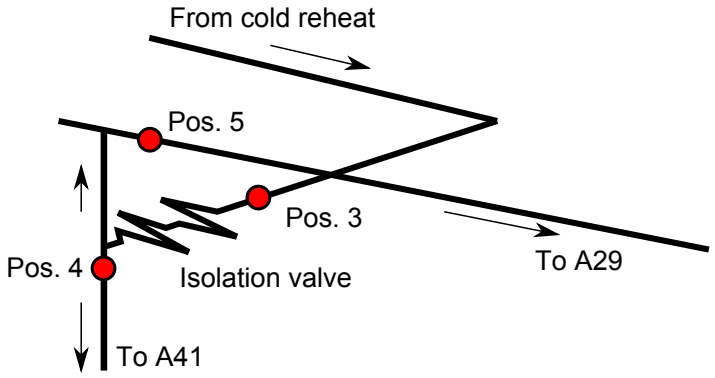

Figure 6.4: Expanded view of sootblower pipework on 'A-side' of boiler centred on inspection locations. Arrows indicate direction of steam flow. Red circles indicate inspection positions.

Two further inspections were carried out on the horizontal sections of the primary distribution pipework. These are positions 2 and 5 in Figures 6.1 and 6.2. From these two inspection locations it was possible to inspect the horizontal sections as well as a large part of the vertical sections providing steam to sootblowers A29 and B29. The horizontal section is approximately 15m in length and the vertical section on the far side of the bend is approximately 10m in length.

The vertical section of pipework supplying sootblower A41 was also inspected, with the transducer ring located immediately below where the pipe from the cold reheat is connected, at position 4 on Figure 6.1. This inspection was only possible on the 'A-side' of the boiler because there was an axial weld at the equivalent location on the 'B-side' of the boiler. The inspection range extended from the top of the vertical section, where the vertical pipework is connected to the horizontal pipe section with a T-piece, to an

area close to sootblower A41, where a reducer is located to reduce the nominal pipe size from 2.5 inches to 2 inches. The total inspected length is approximately 12m.

The 2 inch pipework connecting to sootblowers 29B, 30B and 31B on unit 4 was also inspected with the inspection locations presented in Figure 6.5. The three sections of pipework were between five and eight metres long and all attached to the main 2.5 inch main supply line with either a reducer (for 29B) or a T-piece. It is these sections of 2 inch pipework that it was possible to section in order to examine the inner surface.

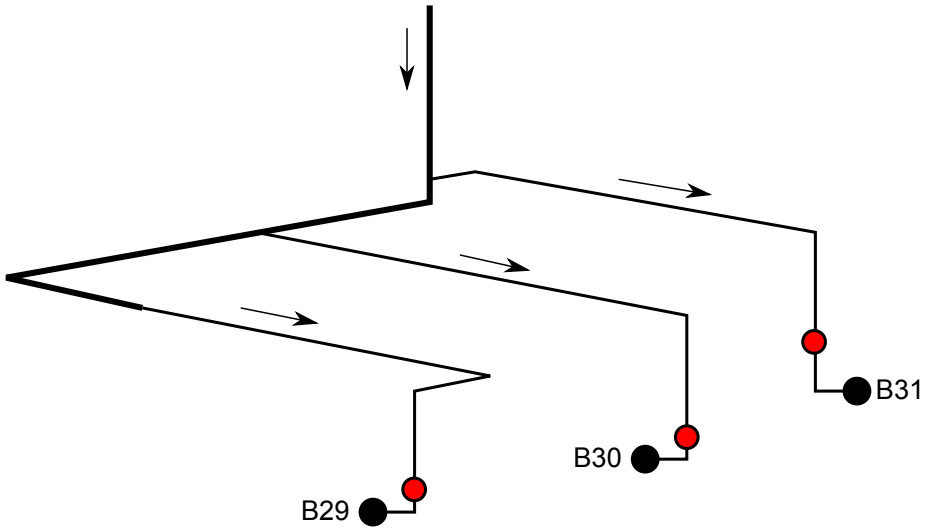

Figure 6.5: Schematic diagram of sootblower pipework where inspections were performed on 'B-side' of unit 4. Red and black circles indicate inspection locations and black circles indicate where pipework enters individual sootblowers. Arrows indicate direction of steam flow.

As described in Section 6.2, all guided wave inspections were carried out using the Guided Ultrasonics Wavemaker G3 equipment. The 2.5 inch pipework was inspected using a 3 inch solid transducer ring with extended transducers, and the 2 inch pipework was inspected with a 2 inch solid ring with standard transducers. In all cases the $T(0,1)$ mode was deployed.

In order to accurately quantify the level of noise in a guided wave signal the distance-amplitude-correction (DAC) curves have to be set carefully. A DAC curve is used to correct for attenuation in the signal, which increases with distance from the transducer

ring. The reflection of the incident wave off a discontinuity that is close to the transducer ring will appear to have a higher reflection coefficient than the reflection coefficient from a discontinuity that is further from the transducer ring, despite the same proportion of energy reflecting from both discontinuities. The DAC curve corrects for this so that reflected signals can be treated in the same way regardless of the distance from the transducer.

The level of the noise DAC curve can be adjusted by the user and set to the noise level in the guided wave signal. The amplitude of the noise DAC is then directly measured relative to the amplitude of another DAC curve, either the end-wall DAC curve or the weld DAC curve, thus quantifying the noise level in a guided wave signal. Examples of DAC curves are presented in Figures 6.8 and 6.9, in Section 6.6.

The DAC curve can be calibrated by monitoring the reflection coefficient of a discontinuity with a uniform reflection, such as a weld. Welds in small-bore pipework are known to have a relatively uniform reflection coefficient of 20-25% [73], and a DAC curve can therefore be produced using this knowledge. Comparing the noise amplitude in the guided wave signal to the DAC curve, calibrated using the weld reflections, will lead to a quantified noise amplitude at any point along the pipe. Because it is the general condition of the pipe that is of interest it will be the noise amplitude over a length of pipe that will be measured.

In addition to the amplitude of noise in the guided wave signal the level of attenuation also gives an indication of the general condition of the pipe. Attenuation is caused by many small signal reflections from minor discontinuities and is higher if there are more discontinuities, or if the discontinuities are larger. Attenuation can be quantified using the DAC curve. The correct calibration of DAC curves is covered in British Standards [4].

6.5.2 Surface scanning procedure

The purpose of the research described in this chapter is to determine whether it is possible to learn of the general condition of pipework based on only guided wave results.

In order to achieve this it is necessary to examine the inner surface of the pipe as this is the area that suffers from corrosion. To gain knowledge about the inside surfaces of the pipework several sections were removed from the station and cut in half along the length. This allowed the inner surface to be scanned with a white-light scanner to provide a quantitative assessment of the condition of the pipe.

The white light scanner used for this project, pictured in Figure 6.6, is the advanced topometric sensor (ATOS) industrial 3D scanner produced by GOM GmbH [2]. It relies on the interferometry of white light to measure the position of points on the surface of a component in three dimensional space. The information about the internal surface of the pipe section can be used to calculate the wall-thickness, with the assumption made that the outer surface is in good enough condition that it can be considered to be smooth.

Figure 6.6: White light scanner used to scan the inner surface of a pipe section and provide quantitative data about the condition of it.

Pipe sections with lengths in the range of 0.5m to 1m were acquired when parts of the sootblower supply pipework on unit 4 of Kingsnorth power station were removed. The pipe sections all have a nominal diameter of 2 inches, with an outer diameter of 60mm and a wall thickness of 4.5mm, and are the sections used to supply sootblowers 29B, 30B and 31B as seen in Figure 6.2.

The output data acquired from the scanner is an irregular array of positions on the inner surface of the pipe. The average point separation can be controlled but the output clusters data points in areas where there is high variation in wall thickness. For all scans used in this study the average point separation was set to 0.025mm. To produce a regular array of data suitable for analysis the 'triscatteredinterp' function in Matlab [75] was used to interpolate the data. This function takes a non-uniform spread of data points – as produced by the scanning equipment – and produces an array of uniformly spaced interpolated data points. The grid size of the interpolated data was 1mm both axially and circumferentially.

The average wall thickness at each axial position was measured so that the cross-sectional area could be plotted as a function of axial position along the pipe, because the $T(0,1)$ guided wave mode is sensitive to changes in cross-sectional area. From the cross-section data, both the root-mean-square (RMS) of the cross-section and the maximum cross-section change can be acquired and used to quantify the roughness of the inner surface of the pipe.

6.6 Results and discussion

Comparisons between guided wave data and measurements of the actual condition of pipework have been made for the 2 inch pipework supplying sootblowers 29B, 30B and 31B of unit 4 at Kingsnorth power station (see Figure 6.5). Additional guided wave measurements were taken of the 2.5 inch pipework at the top of the sootblower supply system on unit 2 at Kingsnorth power station (see Figure 6.1, Figure 6.2 and Figure 6.4). There was no opportunity to scan the internal surface of the pipework from unit 2 but the guided wave results from this unit provide very good indications about the differences in noise levels that can exist.

To obtain a reference level for the noise and attenuation a guided wave test was performed on a clean 6m length of 2 inch pipe, giving the results presented in Figure 6.7. For this test the transducer ring was placed at the end of the pipe. The pipe was due to replace

existing sootblower pipework and should therefore be defect free and have a good surface condition. Because there are no welds in the pipe section the DAC was calibrated using multiple end-wall reflections. The amplitude of noise in the pipe was 48dB below the amplitude of the end-wall reflection, and 32dB below the nominal weld DAC, for the section of results between 0m and the first end-wall reflection. An indication is located immediately prior to the first end-wall reflection, labelled in Figure 6.7, and is caused by another pipe resting on the pipe being tested at this location. This appears to cause an increase of the noise level after the first end-wall reflection, although no guided wave assessments would be made beyond the first end-wall reflection.

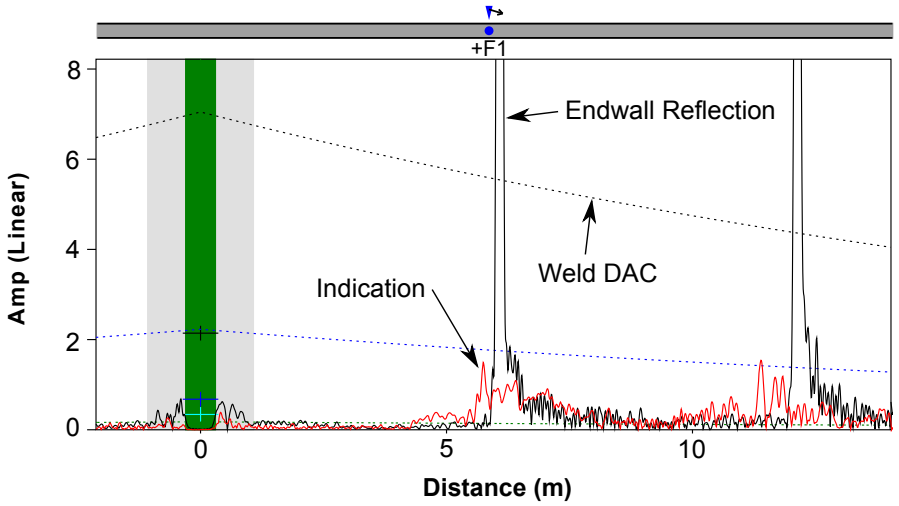

Figure 6.7: Guided Wave results for a brand new section of 2 inch pipe intended to replace existing sootblower pipework. Because there are no welds the end-wall reflections are used to calibrate the DAC curves. The noise level is 32 dB below the weld DAC, in the section between 0m and the first end-wall reflection

.

The guided wave results for sootblower 29B are presented in Figure 6.8. Sections that were also scanned are shaded and labelled as 'Section 29B-2' and 'Section 29B-3'. In Section 29B-2 the noise level is low, measured using the DAC curves to be 37 dB below the amplitude of an end-wall reflection. The noise level in Section 29B-3 is higher, being at or slightly above the amplitude of the call-line DAC, which is 26dB below the amplitude of an end-wall reflection. The DAC curves are displayed more clearly in Figure 6.9, which

shows the same guided wave results as Figure 6.8 but with an expanded y-axis. The noise DAC curve is also included on Figure 6.9 calibrated to the noise level in section 29B-2. Once the noise DAC curve has been calibrated in this manner, it is possible to directly read its amplitude relative to the weld or end-wall DAC curves, and thus quantify the noise level.

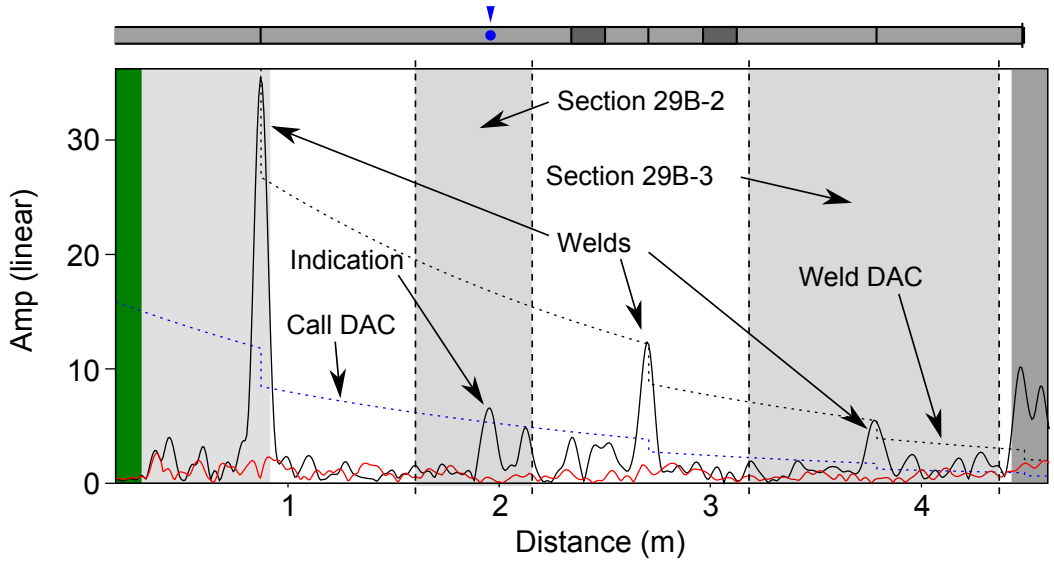

Figure 6.8: Guided Wave results for supply line to sootblower 29B.

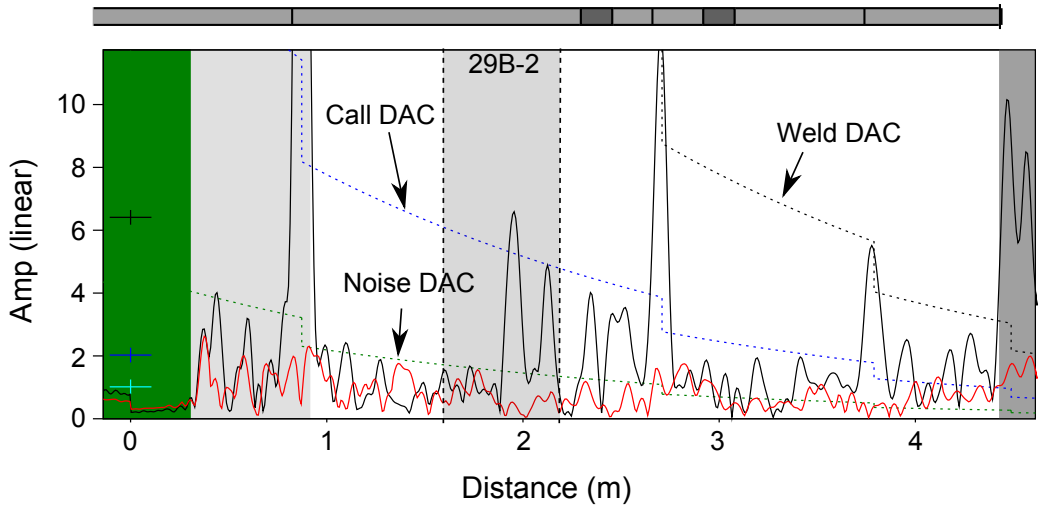

Figure 6.9: Guided wave results for sootblower 29B with expanded y-axis.

It may not be appropriate to use the noise level as an indicator in this instance however, as it is generally flat with respect to distance, suggesting that it is primarily electronic

noise. Coherent noise, as produced by imperfections in the pipe material, would be expected to reduce in amplitude as the distance from the transducer ring is increased. By contrast electronic noise would be expected to have a constant amplitude that is not dependent on the distance from the transducer ring. The difference between coherent noise and electronic noise is illustrated in Figure 6.10 where the coherent noise can be seen decreasing in amplitude with increasing distance from the transducer location. At a distance of approximately 7.5m from the transducer location there is a transition from coherent noise to electronic noise, where the noise level becomes constant with respect to distance, indicating that it is electronic noise.

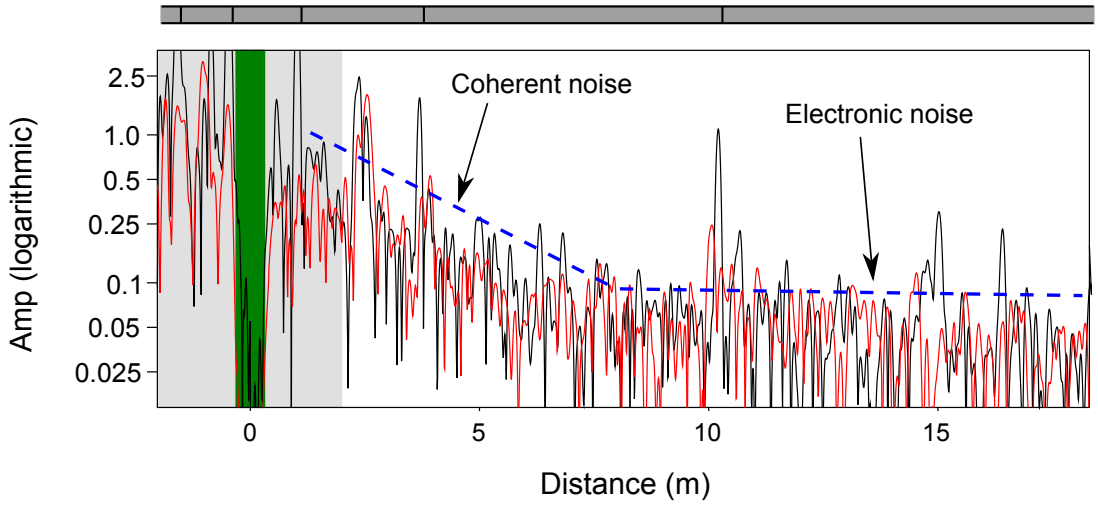

Figure 6.10: Logarithmic plot of guided wave results from sootblower pipework illustrating the difference between coherent noise and electronic noise. The blue dashed line indicates the noise level.

A very important point to note regarding the guided wave results presented in Figure 6.10 is that the amplitude is presented on a logarithmic scale. The advantage of using a logarithmic scale is that an exponential decrease in amplitude with respect to distance is represented as a straight line, making it much easier to identify the distance at which coherent noise transitions to primarily electronic noise. It also aids in the partially subjective assessment of where the DAC curves should be placed, because it is a simpler task to ensure that a straight DAC curve is parallel to the top of the noise than a curved DAC line.

Instead of using noise to assess the condition of sootblower 29B, it would be more appropriate to use attenuation to assess the condition of the pipe. Attenuation is easier to measure in this case because it does not necessarily rely on being able to measure the noise level. It is possible to use consistent reflectors over a range of distances, for example welds. With the DAC curves set using welds and an attenuation measurement then being made, the noise level is no longer necessary to perform an assessment of the state of the pipework.

All of the guided wave results presented so far have used DAC curves to compensate for the reduction in signal amplitude as the distance from the transducer ring is increased. An alternative approach is to use Time Corrected Gain (TCG) on the results, whereby a variable level of gain is applied to the signal dependent on the distance from the transducer ring. The intended effect of TCG is to level out the signal so that a series of reflectors that produce the same amplitude reflection will have the same amplitude in the guided wave results. The advantage of TCG in this application is that it would make it easier to directly compare noise levels in different parts of the signal. The disadvantage would be that it is more difficult to implement than DAC curves, in terms of having to balance the signal to ensure that it is correct. TCG has not been used in this study because the software used does not support this feature.

The scanned data for Section 29B-2 is presented in Figure 6.11, with both an unrolled pipe image and a surface profile of the pipe shown. For the unrolled pipe image a circumferential position of 0mm is equivalent to the 9'o'clock position looking along the pipe, with negative position values representing the lower half of the pipe and positive position values representing the upper half of the pipe.

Areas that appear red in the unrolled pipe image are where the surface is further from the centre of the pipe, and therefore show thinner sections of pipework. In localised areas 1mm of material has been lost from the pipe wall, approximately 20% of the wall thickness. In particular there is a clear channel of thinned material at the bottom-dead-centre position, although because it appears largely consistent along the length of the pipe, it would not necessarily cause large guided wave reflections. Pipework with wall loss on this scale in this application would not be considered dangerous. Very small areas

in blue that appear to be show gains in wall thickness are most likely small deposits that can form on the inside of pipework.

The surface profile was generated by calculating the average position of the inner surface at each axial position, so the surface profile is in effect showing the relative cross-section of the pipe at each axial location. For a sense of perspective of the amount of cross-sectional change, a line representing the outer surface of the pipe is presented in Figure 6.11b, located at a pipe surface position of 4.5mm (the nominal thickness of the pipe is 4.5mm).

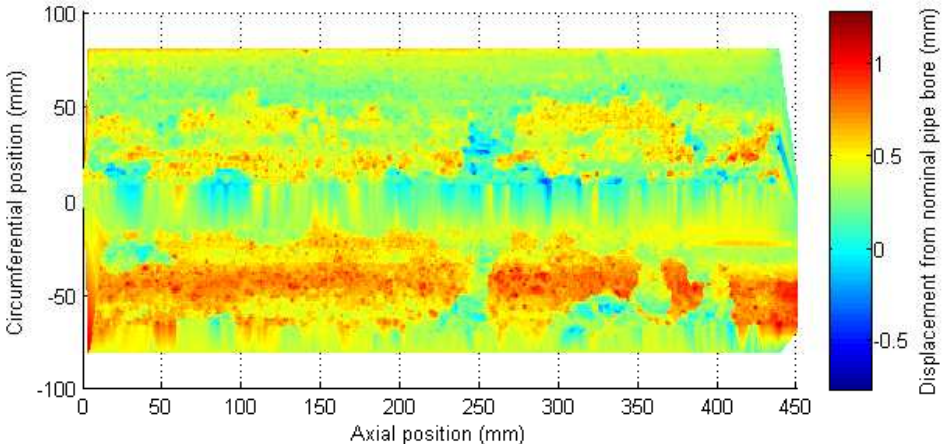

(a) Surface Image

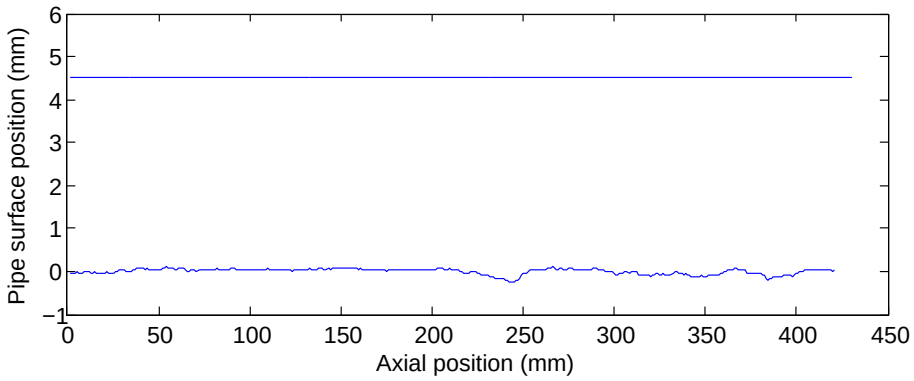

(b) Surface Profile

Figure 6.11: Unrolled pipe image (a) and inner surface profile (b) of sootblower section 29-2. The colour scale in the pipe image indicates displacement from nominal pipe bore with red being further from the centre of the pipe. The surface profile diagram also displays the nominal position of the outer surface of the pipe, at 4.5mm, to provide a sense of scale.

An increase of wall thickness is evident from Figure 6.11b at an axial position of 240mm, where the average wall thickness increases by 0.3mm, or 6.7%. The axial position of the increase coincides with the indication labelled in Figure 6.8, and the amplitude of the indication is approximately 6.5% of the end-wall reflection amplitude. The wall thickness increase and reflection amplitude of the indication are of very similar magnitude and it is therefore very likely the indication is caused by this change in wall thickness.

To produce an estimate of the physical roughness of the pipe surface the root-mean-square (RMS) of the average cross-section was calculated from the scan data. This was compared to the noise level and attenuation measured from the guided wave results. The results are presented in Table 6.1 for all of the pipe sections that were scanned, along with the results for a clean section of pipework that was tested using guided waves, but not scanned with the white light scanner.

Pipe section	RMS (mm)	Noise level (dB)	Attenuation (dB/m)
29-2	0.0690	-37	3.73
29-3	0.0470	-22	3.73
30-1	0.0447	-40	2.25
30-4	0.0953	-35	2.25
31-2	0.1061	-36	2.87
Clean pipe	(0)	-48	0.37

Table 6.1: Table displaying the RMS, noise level and ultrasonic attenuation for sections of sootblower pipework. The RMS was measured using a white light scanning device and the noise level and attenuation were measured using guided wave results. The RMS value for the clean pipe has not been measured, but is assumed to be very small as the pipe has not been in service.

It is difficult to produce a meaningful comparison using the data in Table 6.1 because the majority of the values for both the RMS and noise level are low. The single exception is the much higher noise level in Section 29B-3, but this is due to electronic noise being dominant in this part of the guided wave signal. The values for RMS, noise and attenuation are all reasonably consistent. Compared to the clean pipe all of the sootblower pipes showed a higher level of noise in areas remote from pipe features,

between 35dB and 40dB below the end-wall reflection amplitude, however this level of noise is still not excessive. All of the pipework scanned with the white light scanner was in reasonably good condition, and this was obvious from a visual inspection. Values for the RMS were all at 0.1061 mm or below, small compared to the wall thickness of 4.5mm.

The attenuation in the ex-service sootblower pipework is high compared to the clean section of pipe, in the range 2-4dB/m in contrast to 0.37dB/m in the clean pipe. It is unlikely that this large difference is due to material properties because the clean section of pipe should be the same material as the ex-service pipework. This suggests that attenuation is strongly affected by even a modest deterioration in pipe surface condition.

In fact measuring the attenuation may be much more suitable for determining the condition of pipework in certain circumstances than measuring the noise level. In particular, if the noise is dominated by electronic noise, as is the case with the results presented in Figure 6.8, then attenuation may be the only metric available to determine the pipe condition. For lightly corroded pipework with low noise, attenuation is likely to be the most reliable metric for determining pipe condition, but as the pipe condition deteriorates further it may be that noise is a superior metric. Further work is required on poor condition pipework to establish the most suitable metric. Ideally a combination of noise information and attenuation information would be used to assess the condition of the pipe.

In addition to attenuation caused by the state of the pipework, additional attenuation is caused as a result of pipe features such as welds, supports, bends and coatings. Localised features such as welds, supports and bends would be expected to produce a sudden decrease in signal amplitude, and not greatly affect the measured attenuation for other sections of pipework. Coatings however would increase the measured attenuation over the full pipe length, generally to an unknown degree. Therefore, if a coating were present, it would not be suitable to use a measurement of attenuation as an indication of the general state of pipework.

6.7 Conclusions

Initial work towards a pipe classification system based on the general condition of pipework has been developed. The methodology has been described, comparing guided wave results to scanned images of the inside surface of the pipe, and data has been collected for a small number of ex-service pipe sections. It has been possible to compare the results from the ex-service sections to a brand new section of pipework.

Developing a full classification system has been difficult because all of the pipes tested were in a reasonably good condition, with very similar levels of surface roughness, noise and attenuation. Compared to a clean pipe the noise in the ex-service pipe was slightly higher, but the attenuation increased significantly. This suggests that the attenuation is more sensitive to the condition of the pipe surface than the noise level, and may be a better indicator of pipe condition in future inspections.

A more useful comparison could have been made if some of the pipework had been in significantly worse condition. This would have allowed for the RMS, noise and attenuation to be measured over a much larger range, and from this it would be possible to determine if any correlation existed between the results.

To advance this project a larger data set of guided wave results and associated surface scans would be required, including pipework with high levels of corrosion. It should not be too difficult to achieve this as there is a large quantity of old sootblower pipework in UK power stations, with substantial amounts due to be replaced. It is intended to gather more samples as maintenance schedules allow in order to improve this work. With a larger data set more conclusive statements regarding the effectiveness of this inspection technique could be made, and in the future it is expected that guided wave techniques will provide the primary assessment of the condition of sootblower pipework.

An inspection used to establish the general condition of pipework would be conducted in exactly the same manner as a standard guided wave inspection, in terms of practical application. Differences would occur in interpretation of the results. Although the evidence is currently not entirely conclusive, due to limited data, assessing the general

condition of pipework using guided waves appears to be a viable type of inspection, and would have applications in certain areas.

Chapter 7

Other applications

A key role of this research project was to assess the potential of using guided waves in a power station environment. There are areas of power stations that are very different to those found in the petrochemical industry and this provides unique challenges and applications that may not have been considered previously. The vast majority of guided wave development has been for the petrochemical industry where there are long lengths of pipe with a low feature density. The feature density of pipework in a power station is typically higher than for a pipeline or at a refinery, with features including hangers, supports, drains, vents etc, and it is recognised that the guided wave method is more difficult if the feature density is high [70]. Pipes in power stations also have a particularly large number of bends, and together with the high feature density this makes a guided wave inspection difficult. Pipe features and bends cause attenuation of a guided wave signal limiting inspection range, and many of the features produce similar signals to defects, making genuine defects more difficult to identify.

However, there is a large variety of pipework in the power industry, and it is likely that some will be suited to a guided wave inspection. The aim is therefore to identify suitable pipework by using guided waves in a number of applications. Consideration will have to be given to the nature of the pipework and the potential benefits of using guided waves.

Two applications are described in this chapter. The first is the inspection of a process steam line at Port of Liverpool power station, and the second is an oil transfer line at

Fiddler's Ferry power station.

7.1 Port of Liverpool steam line

7.1.1 Introduction

Port of Liverpool power station is a gas-fired combined heat and power (CHP) station that provides electricity to the national grid and process steam to two industries located nearby. The process steam is delivered to the industries by two 12 inch pipelines, that are each over half a mile in length. For contractual reasons, it is important that the pipelines are operational for as much time as possible, because the businesses that receive the steam cannot operate without it. If steam is not available to the businesses for too long it can lead to large financial penalties for E.ON, so there is a commercial motivation for investigating improved NDT methods.

The need to inspect the steam lines at Port of Liverpool power station arose when chemical overdosing led to stress corrosion cracking at the welds. Stress corrosion cracking takes the form of circumferential cracks within the welds. Currently the welds are inspected using standard ultrasonic testing which is time consuming. Minimising the time required for an inspection is therefore very important, a key area where guided waves have an advantage over manual ultrasonic testing. The intention was to use guided waves to screen welds for circumferential cracking, with follow up inspections using manual ultrasonics where required. As additional added value it would also be possible to identify any areas of suspected corrosion within the pipeline from the same inspection.

7.1.2 Pipeline description

Two 12 inch steel steam lines exit the power station to carry process steam at 200℃ to nearby businesses. The northern line is approximately 0.5 miles (800m) in length and the southern line is approximately 0.7 miles (1100m) in length. All work described

here took place on the southern 'Brocklebank' line. Approximately half of the southern line is at ground level, with the other half at high level, with vertical sections of pipe to connect the two levels. To allow for thermal expansion of the line whilst it is in operation, approximately every 100m along the pipeline there is an expansion loop going from either low to high level or high to low level. Similar loops exist to allow roads and a railway to cross the pipeline. In total eight expansion loops and road/rail crossings exist on the line. A schematic diagram of the lines as they leave the power station is presented in Figure 7.1. The vertical leg on the southern line represents a typical vertical leg, with a single weld, indicated by a circled number, at the top and another at the bottom. Figure 7.2 is a picture of the steam lines that are represented in the diagram in Figure 7.1. On the northern line a loop used to cross a road is visible.

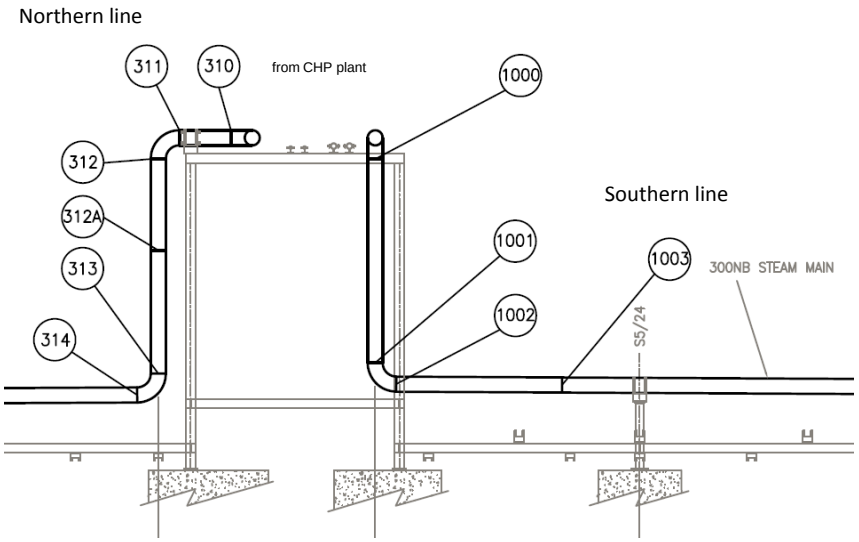

Figure 7.1: Schematic diagram of process steam lines where they leave Port of Liverpool power station. The northern line is to the left of the diagram and the southern line to the right. Welds are indicated with circled numbers.

The pipelines are held in place using clamped supports, one of which is pictured in Figure 7.3. The clamps are quite large and are fixed very securely to the pipe. They feature regularly on both the vertical and horizontal sections of pipework. As well as being used to hold the pipe in place, similar devices are used to hold the lagging in place,

Figure 7.2: Picture of steam lines leaving Port of Liverpool power station with northern and southern lines labelled. A road crossing can be seen on the northern line.

particularly on the vertical legs of the pipeline.

Figure 7.3: Picture of clamp used to hold steam line in place at Port of Liverpool power station.

The main cause of concern within the line is circumferential cracking within the welds

on the vertical legs of the expansion loops, and on the vertical sections of pipe where the pipeline changes level. By examining the mode converted signals it should be possible to identify non-axisymmetric circumferential defects within welds [69]. In the same inspection that is used to monitor the welds, it would also be possible to screen the pipe for corrosion defects. CHP power stations usually have very short outages – often only two or three days – so it is not possible to de-lag and visually inspect the steam lines. Performing weld and corrosion inspections at the same time would be of enormous benefit to the site owners.

Because the pipeline is outdoors and carries steam there is the possibility for corrosion to occur on either the inside or outside of the pipe. It is not a high risk however as the temperature of the contents quickly boils off any water that comes into contact with the pipe.

7.1.3 Inspection procedure

The pipeline was inspected using commercial guided wave equipment produced by Guided Ultrasonics Ltd. [1]. The instrument was a Wavemaker G3 and a 12 inch inflatable transducer ring (pictured Figure 7.4), containing 24 pairs of transducers, was used to excite the guided waves. The transducers were configured to excite the $T(0,1)$ guided wave mode. A clamp used to hold lagging in place can be seen above the transducer ring in the Figure.

It is the welds on the vertical pipe legs, for example those labelled '1000' and '1001' on Figure 7.1, that are of most concern. They can develop circumferential cracking due to the forces involved when the pipeline expands or contracts. Circumferential cracking in a weld would be detected by measuring the non-axisymmetric component of the reflected signal. A weld without a circumferential crack would be expected to have a very low amplitude non-axisymmetric component because minimal mode conversion takes place at a defect-free weld.

Areas of the pipeline that are potentially corroded are identified using the DAC call-line.

Figure 7.4: Picture of inflatable transducer ring used to perform guided wave inspections at Port of Liverpool power station.

After calibrating the DAC curves using welds in the pipeline, a DAC curve representing a change in cross-sectional area of 5% of the pipe cross section can be used to locate areas of concern. Any indication with an amplitude above the call-line with no clear source, such as a support or weld, would be subject to further inspection. Using the call-line set to 5% of the pipe cross-section is standard practise when attempting to detect corrosion using guided waves [73]. Any areas that are called would require additional inspections, including external visual inspections and ultrasonic thickness checks.

Inspections were performed at multiple locations along the pipeline. At every vertical section of pipe in the first five expansion loops, as measured from the power station, as well as a single vertical section where the pipe level changes, two inspections were made. These inspections were necessary to get full coverage of all the welds in the vertical sections. One inspection was performed with the ring at the top of a vertical section, to monitor the weld at the bottom, and vice-versa. It would have been possible to inspect both welds from a single inspection location at the mid-point between the two welds, but lagging had already been removed in order to conduct manual ultrasonic inspection of the welds so the method of two inspection locations per vertical leg was more convenient.

A small number of inspections were also performed on the ground level horizontal pipe sections. These inspections also had the aim of inspecting welds, although the risk

of cracked welds was deemed substantially lower in the horizontal sections than in the vertical pipe sections.

7.1.4 Results

In total 28 'shots' were made, with four on horizontal pipe sections and the rest on vertical pipe sections. An interesting feature of the results was the reflection amplitude of pipe clamps that are used to hold the pipework in place. The amplitude of the signal reflected from these clamps is very high, much higher than the reflection amplitude of a weld signal, which can be seen in Figure 7.5. Clamped supports are known to be difficult to characterise because the reflection amplitude varies greatly depending on the tightness of the clamp [70, 73]. The high amplitude signals observed in this study indicate that the clamps are tight and are therefore strongly ultrasonically coupled to the pipe. No comprehensive study about how large clamps affect guided waves could be found, only a study of the reflection of guided waves from simple supports [48]. However, it seems likely that if a clamp is strongly ultrasonically coupled to a pipe, it would effectively increase the cross-sectional area of the pipe, and thus have a high reflection coefficient. The signals reflected from the clamps also have a large non-axisymmetric component, indicating that the clamps are not axisymmetric. This can be seen in Figure 7.5 in the clamp indication located at -4m. The clamp signal has a high amplitude flexural component that is visible in red.

The amplitude of the signal reflected from one of the clamps is highly frequency dependent, with a much larger amplitude at lower frequencies than at higher frequencies. The frequency dependence of the clamped supports is demonstrated in Figure 7.6 where the guided wave results for a single section of pipe are presented for a range of frequencies. It is clear that while the welds maintain a consistent amplitude at all frequencies, the amplitude of the support signal increases greatly as the frequency is reduced. At the lowest frequency used during the Port of Liverpool inspections the amplitude of clamped support reflections was between 8 and 12 dB above the amplitude for a weld. However at the highest frequency used during the inspections the amplitude of the reflected signals

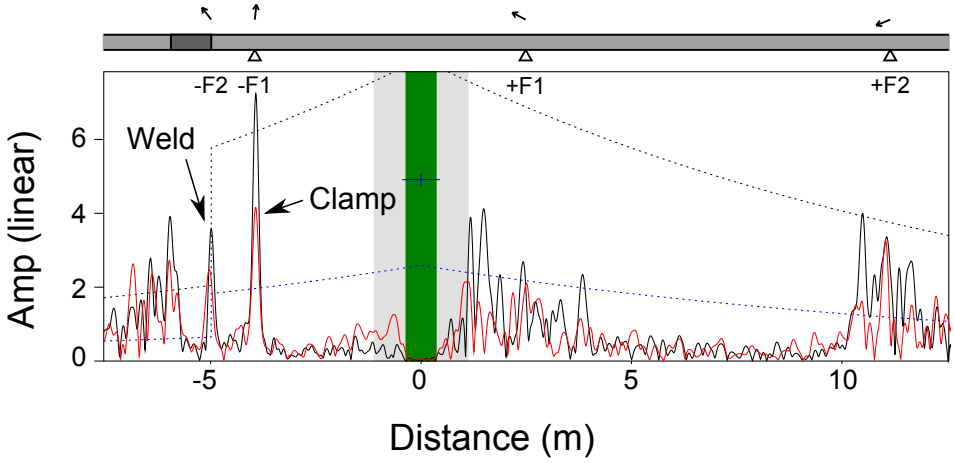

Figure 7.5: Guided wave results from Port of Liverpool power station demonstrating the reflection amplitude of clamped support.

from the supports was approximately the same as the amplitude of a weld signal.

Having large non-axisymmetric reflectors throughout the pipeline presents significant problems when conducting a guided wave inspection. The guided wave results for a shot taken from the top of a vertical pipe section, presented in Figure 7.5, illustrate the problem. At a distance of approximately -4m there is the large signal from a clamped support, with the non-axisymmetric component clearly visible in red. Beyond the support, at -5m, is the weld signal marking the beginning of a bend. This signal also appears to have a large non-axisymmetric component. A good weld would normally produce an axisymmetric reflection, and manual ultrasonic testing on this particular weld indicated that it contained no cracks.

The results suggest that a $T(0,1)$ wave that is transmitted beyond a clamped support undergoes strong mode conversion to flexural non-axisymmetric wave modes. When the flexural modes reflect off an axisymmetric feature, in this case a weld, it appears as if the feature is non-axisymmetric. The guided wave inspection of welds is therefore undermined somewhat because any weld located beyond a support relative to the transducer location will appear to contain a large non-axisymmetric defect, even if it doesn't.

Another issue with large reflections from the supports is that it causes high attenuation

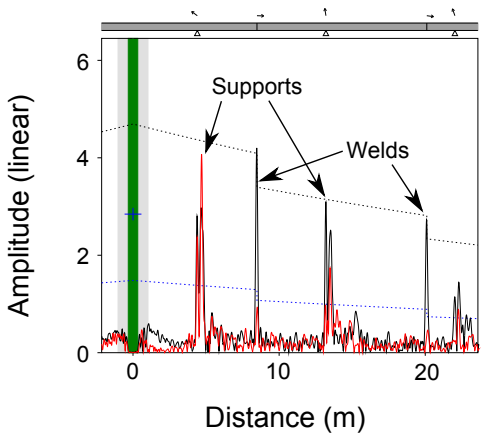

(a) High frequency (9.6)

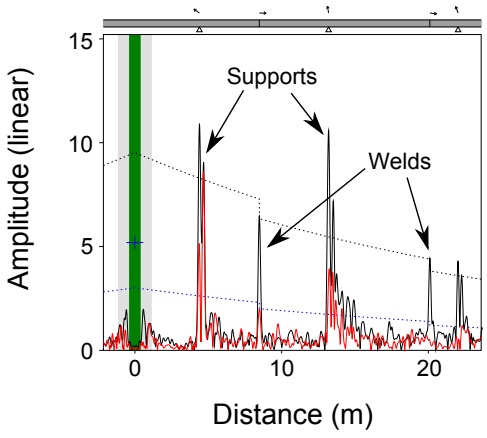

(b) Medium frequency (7.1)

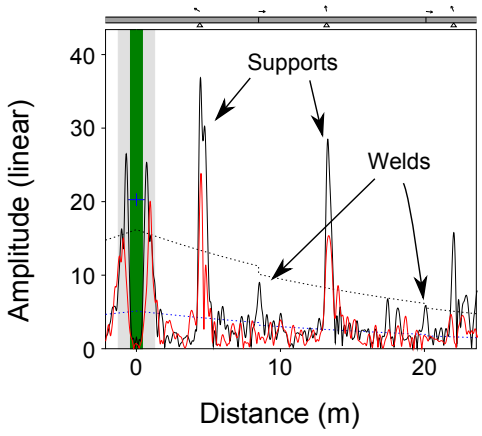

(c) Low frequency (4.6)

Figure 7.6: Guided wave time trace for a section of pipe on a Port of Liverpool steam line over a range of frequencies, with clamped supports and welds labelled. The number in parentheses in the sub-figure description is the frequency regime as stated when using the Wavemaker G3 system. Amplitude is scaled for clarity.

in the signal, limiting the range of the inspection. In a test conducted on a horizontal pipe section it became difficult to identify weld signals above the noise level at inspection ranges greater then 10m. If only short pipe sections can be inspected at once it limits the viability of a guided wave inspection for this application.

The signal-to-noise-ratio (SNR) increases as the frequency of the signal is increased, due to the reduced effect of the clamped supports at high frequency. The SNR is

measured by comparing the amplitude of noise in the signal to the call-line DAC, which as stated previously represents a 5% change in the cross-section of the pipe. The call-line is used to calculate SNR because this is the level that would normally be used when determining whether a signal represented an area of concern. At high frequency the SNR is approximately 6-10 dB, whereas at low frequency the noise level is typically above the amplitude of the call-line DAC. Guided wave results from a long straight section of pipe, between two expansion loops, are presented in Figure 7.7. Weld and clamped support signals are labelled on the figure and demonstrated the amplitude of the support signals at high frequency. It is also evident that a reasonable inspection range of approximately 40m is achieved.

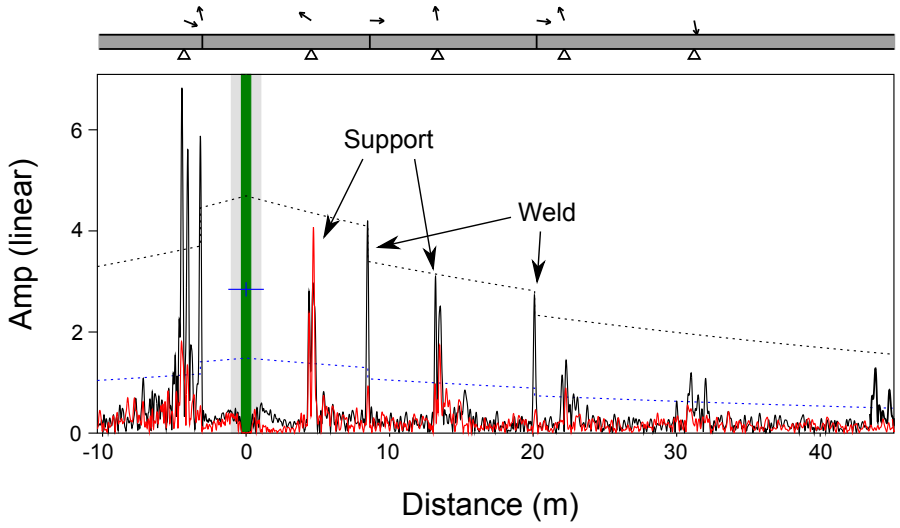

Figure 7.7: Guided wave results from a long straight section of main steam line at Port of Liverpool power station.

Even at high frequency SNR is poor where a guided wave has propagated beyond a bend, due to a combination of the bend and the presence of a large clamped support, with clamped supports located adjacent to most bends. At the highest frequency used in this study, the noise level of a signal beyond a bend is the same as the amplitude of the call-line DAC, with the SNR therefore 0 dB.

7.1.5 Conclusions

Guided waves have not proved to be a particularly effective NDT technique for inspecting the steam lines at Port of Liverpool power station. The technique was being used primarily to detect circumferential cracking in welds, with a secondary purpose of detecting corrosion. It has proven difficult to detect cracks in welds because of the presence of large clamped supports on the pipeline. The supports cause mode conversion of the $\mathrm{T}(0,1)$ wave and make it appear as if axisymmetric features are non-axisymmetric, rendering it impossible to determine whether there are cracks in a weld. A non-axisymmetric component is present in the weld signals beyond a clamped support over the full frequency range used for these inspections. The ability to detect corrosion over long lengths of pipework is also diminished by the high signal attenuation caused by the supports, although at high frequency it is possible to detect corrosion due to the reduced reflection amplitude from the clamped supports, and corresponding improvement in SNR.

Despite the limitations of the guided wave technique for this application, there may still be an area where it can be utilised. On the northern steam line part of the pipework is buried beneath a road. Being buried makes pipework more difficult to inspect and also increases the susceptibility of pipework to corrosion. The pipe is in a concrete culvert so would not require digging, but access would still be difficult, especially to the bottom of the pipe. Despite not requiring any digging, inspecting pipework that is beneath a road is expensive because of the disruption to traffic. As it is a relatively short section of pipework that is underneath the road it should be possible to inspect it using guided waves, even assuming the highly attenuating clamped supports are present.

The inspection of buried pipes has been discussed by several authors [16, 27, 65] including buried pipes with a bitumen (or similar) coating [61] or more generally surrounded by a fluid [18]. Tightly bonded bitumen coatings have a large detrimental effect on the range that can be achieved when using guided waves, because the guided waves leak into the coating. Fortunately at Port of Liverpool power station the steam line is merely placed in a concrete culvert and covered with gratings. Therefore the inspection range would be similar to the horizontal pipe sections, with results similar to those presented in

Figure 7.7. A high frequency inspection for this application could have a range of 40m, sufficient to inspect all of the underground pipework, and would be sensitive enough to detect critical corrosion under the road crossing.

7.2 Fiddler's Ferry oil line

7.2.1 Introduction

Fiddler's Ferry is a large coal-fired power station in North West England. At start-up and shut-down the boilers require bunker fuel oil (BUFO) and the oil is stored in a large tank on site. The oil is transported from the tank to the boilers using a six inch pipeline that is approximately 1/4 mile long. The station had some new pipework ready to replace what was already in place, but not enough to replace the whole line. To target the replacement sections most efficiently guided waves were used to determine the general condition of the pipe, an application of the system described in Chapter 6.

7.2.2 Pipeline description

The BUFO oil line has a nominal diameter of six inches and is approximately 1/4 mile (400m) long. The tank is located behind the cooling towers from the perspective of the station so the pipe circles around two cooling towers. Much of the pipework is at very low level, either resting on the ground or in a shallow ditch. For this reason external corrosion is a high concern, due to the contact of the pipe with potentially wet mud. From Figure 7.8 it can be seen that the pipeline runs close to a cooling tower, and spray from the cooling tower, along with rain, would ensure that the pipework comes into contact with a large amount of water.

To curve around the cooling towers as seen in Figure 7.8, many relatively short sections of straight pipe were welded together at slight angles. In proximity to one of the cooling towers several short sections of pipework had already been replaced and the new sections

Figure 7.8: Picture of section of Fiddler's Ferry BUFO oil line taking a curved path around a cooling tower.

were attached to the existing sections with flanges rather than welds. A high density of flanges was therefore present on this section of pipeline, with a flange every 5-10m.

Two parallel pipes are visible in Figure 7.8, and originally they both had the same function. One of the pipelines is no longer in use, so it was only necessary to inspect one of the pipelines – the one that has had the lagging removed in Figure 7.8.

7.2.3 Inspection procedure

The pipeline was inspected with a Wavemaker G3 instrument manufactured by Guided Ultrasonics Ltd. [1]. The transducers were housed in a six inch solid transducer ring pictured in Figure 7.9. The transducers were configured to excite the $T(0,1)$ mode.

A large number of inspection locations were required to complete the survey – 32 in total for 400m of pipework. Inspection ranges were limited by a high number of flanges where new sections of pipe had been inserted around a cooling tower. The effect of a slight angle at a weld is also unknown so each section of pipe on the curved pipe in Figure 7.8 was inspected individually.

Figure 7.9: Ring of transducers in use for guided wave inspection.

Each pipe section that was inspected was categorised according to its general condition as either 'good', 'medium' or 'poor'. The categories were determined by a combination of noise level in the signal; the level of attenuation; and the ability to identify pipe features such as welds and flanges. The noise level can be quantified using the same method described in Section 7.1, comparing the amplitude of the noise to the amplitude of the call-line DAC. Calibrating the DAC curves also allows for the attenuation in the signal to be measured in dB/m. Attenuation is generally dependent on frequency so the attenuation measurements provided by the Wavemaker G3 software, and stated here, are for a signal with a frequency of 30 kHz. Example results for each category are presented in Section 7.2.4. If the noise level is low and all pipe features are easily identifiable the pipe is clasified as 'good'. If there is modest noise present but it is still possible to identify large features such as welds and flanges the pipe was classified as 'medium'. If the noise and attenuation is very high and even features such as flanges cannot be identified then the pipe is classified as being in 'poor' condition.

7.2.4 Results

It was possible to inspect and classify the vast majority of the BUFO oil pipeline at Fiddler's Ferry power station. These were mapped out to allow the station to target the

replacement sections of pipework most appropriately. A map of the pipework is presented in Figure 7.10 with the pipework colour-coded according to the criteria of the guided wave inspection. Most of the pipework located close to the cooling towers was classified as being in 'poor' condition, except for a small number of sections that had recently been replaced. Most of the pipework classified as 'good' was closer to the station. Here the pipework was not lying on wet mud so the environmental conditions were not as detrimental to the condition of the pipe. Example guided wave results for each class of pipe are presented below.

An example of the guided wave results from a good piece of pipe can be seen in Figure 7.11. The signals representing welds and supports are labelled on the figure. Welds and supports are easily identifiable at the relatively long range of 15m. There is little noise in the signal and the attenuation is low. The SNR in this section of pipe has been calculated to be approximately 18 dB before the weld located at +6m and approximately 10 dB immediately before the weld located at +12m. The SNR is largely unaffected by frequency. The value of attenuation can also be calculated using the DAC curves. For the good section of pipe the measured attenuation, at 30 kHz, is 1.6 dB/m.

The guided wave results from a 'medium' condition section of pipe can be seen in Figure 7.12. Again the welds and supports are labelled. Unlike the good condition pipe section the SNR of a medium condition section of pipe is highly affected by frequency, with higher frequencies leading to a higher SNR. In this case the features are less obvious against the noise, especially as the distance from the transducers is increased, as attenuation is higher than in a 'good' piece of pipe. The measured attenuation for this section of pipework is not strongly dependent on frequency, and at 30 kHz is 5.4 dB/m. The SNR close to the transducer ring location is in fact quite good, at 9 dB. Beyond three meters from the transducer ring location however the SNR reduces to 0 dB. There is a non-axisymmetric signal present in the weld signals, and this is most likely due to the fact that there is a 10 degree bend at the weld location.

Figure 7.13 presents the results for a 'poor' section of pipe. A flange signal located 10m from the transducer ring is only just detectable. Welds that are known to exist from visual inspections are not detectable in the guided wave results, and this is true

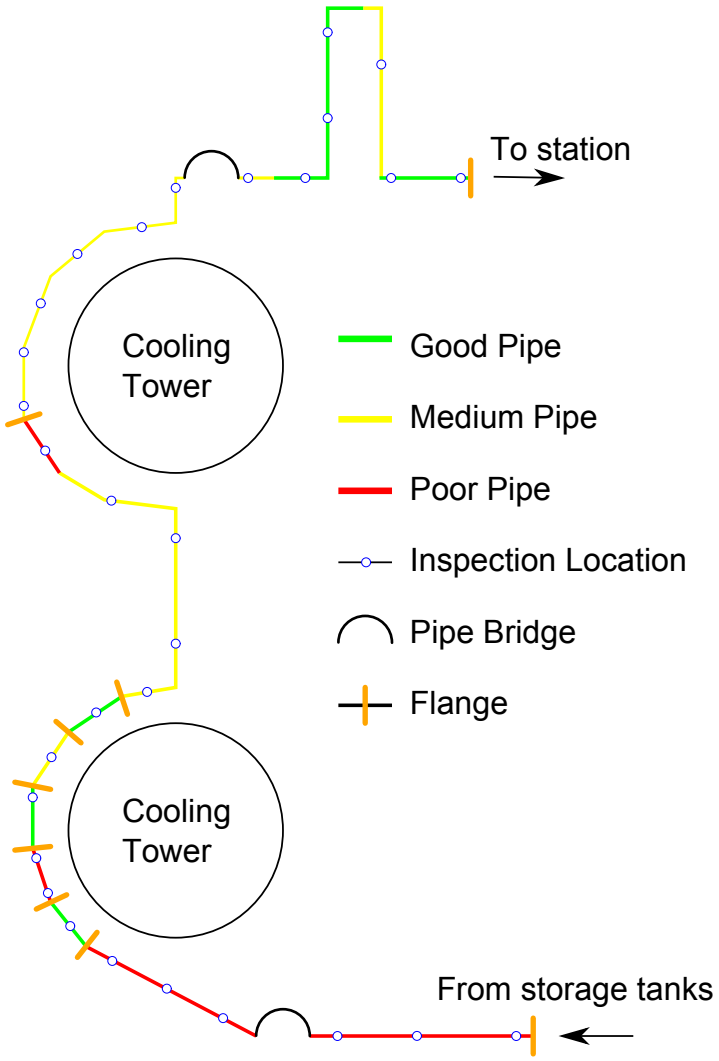

Figure 7.10: Pipe layout of fuel oil line at Fiddler's Ferry power station. Pipeline is colour coded according to condition of pipework based on guided wave inspections. (Not to scale).

over the full frequency range. Because no signals from known features besides a solitary flange are present, it is difficult to calibrate the DAC curves correctly. It is also reasonably meaningless to state a SNR in this case. It is however possible to measure the attenuation based on the noise level, and interestingly for the example provided in Figure 7.13 the attenuation is 4.9 dB/m at 30 kHz. This is a slightly lower attenuation than for the pipe classified as being 'medium' condition. When differentiating between 'medium' and 'poor' condition pipework it is therefore more important to examine SNR and the

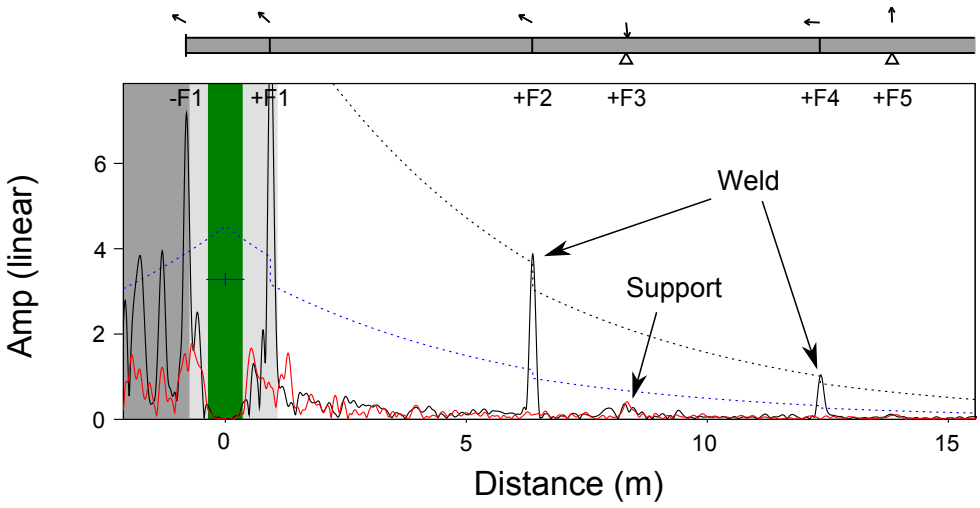

Figure 7.11: Sample guided wave result for a good piece of pipe.

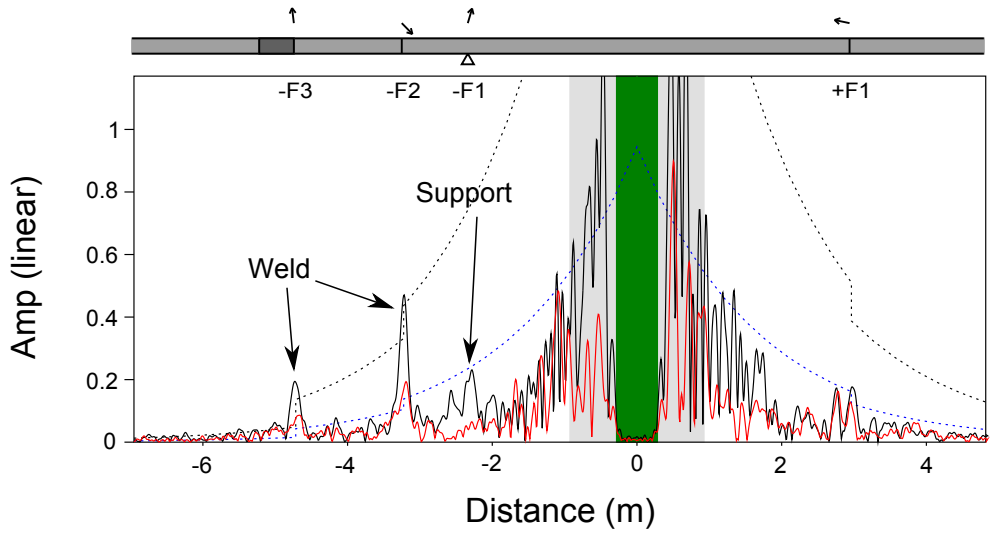

Figure 7.12: Sample guided wave result for a medium piece of pipe.

detectability of known features than compare the levels of attenuation.

7.2.5 Conclusions

The BUFO oil line at Fiddler's Ferry power station has been successfully inspected using guided waves. The aim was to classify each section of the pipeline according to the general condition of the pipework and use the information to target areas of pipework that should be replaced. This has been done with guided waves proving capable of

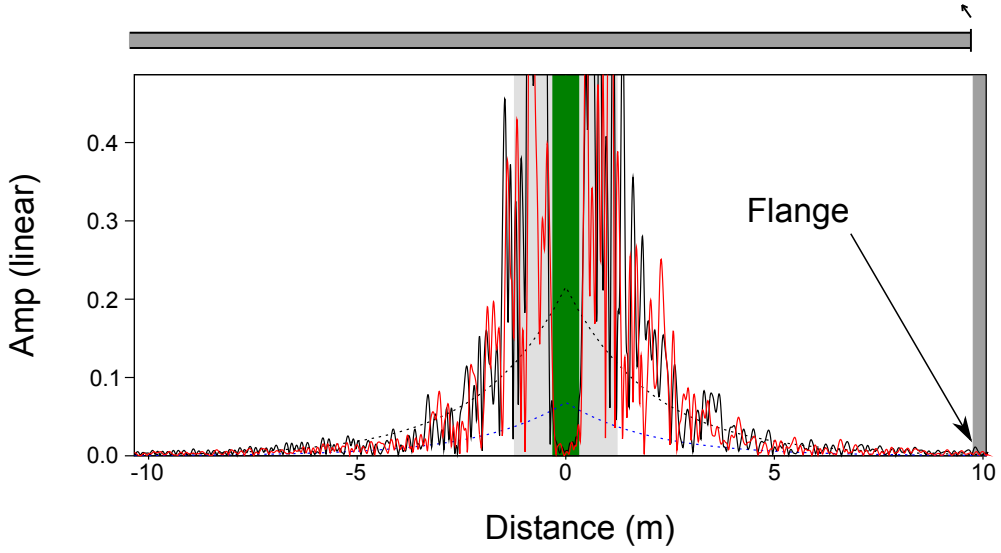

Figure 7.13: Sample guided wave result for a poor piece of pipe.

determining the general condition of pipework using a similar system to that described in Chapter 6.

Classification is achieved by examining factors including signal-noise-ratio, attenuation and detectability of known pipe features such as welds. A pipe in 'good' condition will have a high SNR and low attenuation. Pipes in a 'medium' of 'poor' condition will both have high attenuation but the SNR will be much higher for a 'medium' section of pipe than a 'poor' section of pipe, and features such as welds will be much easier to identify. Although the classification system has not been officially adopted by E.ON, it is hopeful that in the future it can be adopted as an official procedure for suitable pipework.

The success of this work is important because all coal-fired power stations in the UK have a similar oil transport system to Fiddler's Ferry. Many of these pipelines have not been inspected for many years and are susceptible to environmental damage, resulting in external corrosion. Therefore there is a widespread potential application for guided waves on these systems.

Chapter 8

Conclusions and future work

Guided waves have been investigated for potential power station applications. Although guided wave inspections are already commonplace in the petrochemical industry, they are not widely used in the power generation industry. Power stations provide a challenging environment for guided wave inspections due to much shorter pipes with a much higher feature density than in the petrochemical industry. Features such as welds, bends, supports and line branches all contribute to making a guided wave signal difficult to interpret and thus limit the inspection range.

The primary focus of this guided wave research for power station applications has been in attempting to detect axial cracks in pipes. Axial cracking is a serious problem currently requiring a high level of resources to detect. If guided waves could screen pipes for axial cracking it would greatly reduce the effort required for inspections. A secondary application that emerged during the research into power station applications for guided waves is a general pipe classification system. Rather than detecting specific defects, the general condition of pipework could be assessed in order to inform a decision on which sections of pipework need replacing.

8.1 Axial cracking in pipes

Research into the scattering of guided waves from axial defects in pipes has been conducted, for the purpose of detecting axial cracks in power station pipework. Detecting axial defects using guided waves is a particular challenge because the decrease in pipe cross-section is very small for an axial defect.

Initially the $T(0,1)$ guided wave mode was studied to assess its ability to detect axial cracks, using finite element models validated with laboratory experiments. The work showed that in a power station environment it would be difficult to detect any axial crack that was not a through-thickness defect. Therefore conventional guided waves using the $T(0,1)$ modes are considered unsuitable for screening pipework for axial defects.

In order to improve the sensitivity of guided waves to axial defects a form of synthetic focusing was applied to previously gathered guided wave results. The focusing algorithm, called the Common Source Method, was applied to guided wave results in post-processing so the data collected in the study of the $(T0,1)$ mode could be re-analysed using the algorithm.

By considering the contribution from mode-converted flexural modes a synthetic focusing algorithm improves the sensitivity of guided waves to defects. This was indeed found to be the case with an increase of reflection amplitude when using the algorithm by a factor of 2-3 compared to the reflection amplitude of the $T(0,1)$ wave mode. However, despite the increase of sensitivity it was still insufficient to detect a critical depth axial defect, a critical defect defined as having a depth of 20% of the thickness of the pipe wall or more. When using a synthetic focusing algorithm the sensitivity of guided waves to axial defects was still far short of what is required.

Because long-range guided waves offer an unrealistic prospect of detecting critical size axial defects in pipes circumferential guided waves were studied. An axial defect would be perpendicular to a circumferential guided wave propagating in the circumferential direction around the pipe and would therefore produce a much higher amplitude reflection than a long-range guided wave mode propagating parallel to the crack. One of the key

advantages of long-range guided waves is the ability to inspect long sections of pipework from a single location, and this advantage is lost when using circumferential guided waves. However, circumferential guided waves do offer a significant advantage over manual ultrasonics in terms of speed and pipe surface preparation.

Circumferential guided waves have been found to be much more sensitive to axial defects than long-range guided waves. Using the SH0 mode it is possible to detect a crack of a critical depth. However, to reliably detect a crack at the critical depth of 20% wall thickness the crack must have an axial extent of 30-40mm. Although many realistic cracks are longer than this, it is possible for cracks to form that are shorter than 30mm. However, FE modelling has suggested that the A0 mode would be more sensitive to axial cracks with a lower axial extent than the SH0 mode. With suitable low-frequency compression probes the FE modelling could be validated in a laboratory, and if successful applied in the field.

Using circumferential guided waves could significantly improve the efficiency of inspections of cold-form bends compared to a standard ultrasonic inspection. Currently a standard ultrasonic test of an entire cold-form bend costs approximately £250-£300 and takes approximately 90 minutes. It is estimated that a circumferential guided wave test of a bend could be performed in less than 30 minutes and cost less than £100. This is obviously of great benefit in terms of both inspection time and cost and could provide valuable savings during a station outage. It is recommended that circumferential guided wave inspections be pursued with the development of a prototype system that can be deployed on site.

8.2 Sootblower pipework

Initial work has been completed on the development of a pipe classification system designed to determine the general condition of a pipe using guided wave results. A pipe classification system could be used to target pipe replacements, which is very useful in certain applications.

The methodology has been described for comparing guided wave data to white light scan data that reveals the surface condition of a pipe, and a small number of samples have been tested. All of the samples tested so far have been in a reasonably good condition so do not provide a large enough spread of results to determine the level of correlation between pipe surface condition, noise and attenuation.

In order to fully develop the classification system more samples will have to be acquired that are in a worse condition than those that have already been tested. If a strong correlation was found it could lead to a powerful tool utilising guided waves in a power station environment. A pipe classification system also has potential uses on pipework other than sootblower systems, as demonstrated on the BUFO oil line at Fiddler's Ferry power station.

It is recommended that further development of the pipework classification system is undertaken, with more samples collected that are in worse condition than the current samples. If the attenuation and noise measurements from the guided wave are found to correlate with the level of degradation in a pipe section then a classification system could be a viable inspection technique. Only a limited quantity of further work would be required to achieve this and could lead to an efficient method used to decide whether systems such as sootblower pipework need to be replaced.

8.3 Discussion of use of guided wave testing for power plant applications

Power stations have been shown to be challenging environments for conducting guided wave inspections. Many power station components do not have advantageous attributes for such inspections, being too small or short for a guided wave inspection, or containing too many features to reliably identify defects. This is due to the nature of the pipes, and also the nature of defects that need to be found. Axial cracks in cold-form bends have proven to be particularly difficult to detect using long-range guided waves, due to their orientation being parallel to the direction of wave propagation.

Conversely, there are some areas within a power station where guided wave inspections could prove very useful, particularly for components that are large and have a low feature density. Power station components that have been identified with these features include fuel oil supply pipelines at coal power stations and process steam supply pipelines at CHP stations. In these components guided waves are an effective screening tool that can be used to identify areas of corrosion or even possible weld defects.

Additionally, long sections of pipework have been identified, for instance sootblower pipework, that suffers from pitting and corrosion type damage, rather than cracking. Guided waves are well suited to detecting this type of damage and could therefore prove useful for this application. A process of interpreting guided wave results to determine the general condition of pipework is also being developed and if successful could expand the range of uses for guided wave inspections in power stations.

8.4 Discussion of potential of guided wave testing for future power plant applications

A number of power station pipework systems have been investigated as possible applications for guided wave inspections. However, a power station is a complex machine with many pipe systems and potential guided wave applications that have yet to be studied.

Potential applications could include detecting wall-thinning in boiler tubes. There are thousands of boiler tubes in a typical coal fired power station, each several hundred feet in length, so it is almost impossible to achieve full inspection coverage. Guided Ultrasonics Ltd produce a system that can be used to inspect boiler tubes [1], but it has not yet been used by E.ON. It would be interesting to test the capabilities of the system in this application. The difficulty when inspecting boiler tubes is that many are webbed and the effect of webbing welded to the tubes will have to be taken into account.

Another possible application area would be inspecting low-temperature pipework (LTP). LTP has been viewed as having a low priority for inspection because it is subject to lower

temperatures and pressures than other parts of a power station boiler. It will over time, however, become more important to inspect such pipework. When inspecting LTP using guided waves it may only be necessary to achieve a simple task such as locating welds. Often original drawings of LTP can be lost or inaccurate, and a rapid method to locate numerous welds under insulation could be extremely useful. In many cases LTP still has asbestos insulation, and in these cases being able to perform an inspection with minimal contact with the asbestos is highly desirable.

In Chapter 7 the use of guided waves at Port of Liverpool combined heat and power (CHP) station was described. At Port of Liverpool high temperature process steam was delivered along two pipelines that are mostly above ground in an industrial area. Other types of CHP exist to provide hot water and cooling to residential and commercial buildings in an urban area, for example the Citigen CHP near to the Barbican Centre in London. These stations have a large network of district heating pipes that are extremely difficult and expensive to inspect with traditional methods, due to most of them being buried underneath public roads. Guided waves could provide a much faster and cheaper option to inspect the pipework than digging up large sections for visual and thickness inspections.

8.5 Key findings

- Long-range guided waves are not sensitive enough to detect axial cracks in pipes at the critical crack depth of 20% through-wall extent. Although the sensitivity can be improved with synthetic focusing it is not sufficient to detect a critical defect.
- Circumferential guided waves are much more sensitive to axial cracks than long-range guided waves, and results indicate that it should be possible to utilise them to detect such defects. The circumferential guided wave inspection offers significant improvements in both speed and cost of inspection compared to current ultrasonic testing.
- Long-range guided waves have found successful applications in other areas of power stations, for instance screening for corrosion in oil supply lines and cracking in the

welds of process steam lines.

- Initial work has been carried out on a pipe classification system intended to broadly classify the general condition of pipework using guided wave measurements of noise and attenuation. This work is ongoing and shows much promise.

8.6 Recommendations

- If the modelling results are validated then a system should be produced to conduct circumferential guided wave inspections on site, using the circumferential $A0$ mode. Experimental validation of the findings with real defect samples would be required. A site inspection would require an ultrasonic flaw detector that is capable of exciting signals in the 50 - 100 kHz range.

- To further develop the pipe classification technique more samples need to be inspected with guided waves and scanned with the white-light scanning system. The samples should be in a relatively poor condition to extend the range of samples that have already been collected.

- Additional applications for guided waves in power stations should be investigated. It is likely that other applications can be found due to the large variety of systems in a power station. Specific examples include monitoring wall thinning in webbed boiler tubes, and locating welds in low temperature pipework. Detecting welds in this manner is a high priority task because of undocumented weld repairs and pipework changes making existing drawings unreliable.

References

[1] *Guided Ultrasonics Ltd*. 17 Doverbeck Close, Nottingham, NG15 9ER, United Kingdom, 2010.

[2] *GOM GmbH*. Mittelwag 7-8, 38106 Braunschweig, Germany, 2011.

[3] BS 9690-1. Non-destructive testing - Guided wave testing - Part 1: General guidance and principles, 2011.

[4] BS 9690-2. Non-destructive testing - Guided wave testing - Part 2: Basic requirements for guided wave testing of pipes, pipelines and structural tubulars, 2011.

[5] Abaqus. *Abaqus Analysis User's Manual*. Simulia, Rising Sun Mills, 166 Valley Street, Providence, RI 02909-2499, 6.5 edition, 2004. www.simulia.com.

[6] J. D. Achenbach. *Wave Propagation in Elastic Solids*, volume 16 of *Applied Mathematics and Mechanics*. North-Holland, 1st edition, 1973.

[7] D. Alleyne and P. Cawley. A two-dimensional fourier transform method for the measurement of propagating multimode signals. *J. Acoust. Soc. Am.*, 89:1159–1168, 1991.

[8] D. N. Alleyne and P. Cawley. The interaction of Lamb waves with defects. *IEEE Trans. Ultrason. Ferroelectr. Freq. Control*, 29(3):381–397, 1992.

[9] D. N. Alleyne and P. Cawley. Optimisation of Lamb wave inspection techniques. *NDT & E International*, 25(1):11–22, 1992.

[10] D. N. Alleyne and P. Cawley. The long range detection of corrosion in pipes using Lamb waves. *IEE Colloquium*, 240(6):1–8, 1994.

[11] D. N. Alleyne and P. Cawley. The effect of discontinuities on the long-range propagation of Lamb waves in pipes. *J. Proc. Inst. Mech. Eng., Part E: J. Proc. Mech Eng.*, 210(3): 217–226, 1996.

[12] D. N. Alleyne and P. Cawley. The excitation of Lamb waves in pipes using dry-coupled piezoelectric transducers. *Journal of Nondestructive Evaluation*, 15(1):11–20, 1996.

[13] D. N. Alleyne and P. Cawley. Long range propagation of Lamb waves in chemical plant pipework. *Mat. Eval.*, 55:504–508, 1997.

[14] D. N. Alleyne, M. J. S. Lowe, and P. Cawley. The reflection of guided waves from circumferential notches in pipes. *J. Appl. Mech.*, 65(3):635–641, 1998.

[15] D. N. Alleyne, B. Pavlakovic, M. J. S. Lowe, and P. Cawley. Rapid, long range inspection of chemical plant pipework using guided waves. *Key Eng. Mater.*, 270-273:434–441, 2004.

[16] D. N. Alleyne, B. N. Pavlakovic, M. J. S. Lowe, and P. Cawley. Rapid long-range inspection of chemical plant pipework using guided waves. *Insight*, 43(2):93–96, 2001.

[17] David Alleyne. *The non-destructive testing of plates using ultrasonic Lamb waves*. PhD thesis, University of London, 1991.

[18] C. Aristégui, M. J. S. Lowe, and P. Cawley. Guided waves in fluid-filled pipes surrounded by different fluids. *Ultrasonics*, 39(5):367–375, 2001.

[19] B. A. Auld. *Acoustic fields and waves in solids*. R. E. Kreiger, Malabar, FL., 2 edition, 1990.

[20] H. Bai, A. H. Shah, N. Popplewell, and S. K. Datta. Scattering of guided waves by circumferential cracks in steel pipes. *J. Appl. Mech.*, 68:619–631, 2001.

[21] M. Beard, M. Lowe, and P. Cawley. Development of a guided wave inspection technique for rock bolts. *Insight*, 44:19–24, 2002.

[22] M. Beard, M. Lowe, and P. Cawley. Non-destructive testing of rock bolts using guided ultrasonic waves. *Int. J. Rock Mech. & Mining Sci.*, 40:527–536, 2003.

[23] M. Beard, M. J. L. Lowe, and P. Cawley. Ultrasonic guided waves for inspection of grouted tendons and bolts. *ASCE J. Materials in Civil Engineering*, 15:212–218, 2003.

[24] H. Bian and J. L. Rose. A physical interpretation of elastic guided-wave reflection from normal ends of a waveguide. *IEEE Trans. Ultrason. Ferroelectr. Freq. Control*, 51(7): 838–847, 2004.

[25] L. Brekhovskikh and V. Goncharov. *Mechanics of continua and wave dynamics*. Springer Verlag, Berlin, 1985.

[26] R. Carandante, J. Ma, and P. Cawley. The scattering of the fundamental torsional mode from axisymmetric defects with varying depth profiles in pipes. *J. Acoust. Soc. Am.*, 127(6):3440–3448, 2010.

[27] P. Cawley, M. J. S. Lowe, D. N. Alleyne, B. Pavlakovic, and P. Wilcox. Practical long range guided wave testing: Applications to pipes and rail. *Mat. Eval.*, 61(1):66–74, 2003.

[28] P. Cawley, M. J. S. Lowe, F. Simonetti, C. Chevalier, and A. G. Roosenbrand. The variation of the reflection coefficient of extensional guided waves in pipes from defects as a function of defect depth, axial extent, circumferential extent and frequency. *Proc. Inst. Mech. Eng.*, 219:1131–1143, 2002.

[29] Y-M. Cheong, D-H. Lee, and H-K. Jung. Ultrasonic guided wave parameters for detection of axial cracks in feeder pipes of phwr nuclear power plants. *Ultrasonics*, 42:883–888, 2004.

[30] J. Davies and P. Cawley. Synthetic focusing for high resolution guided wave pipe inspection: further results and robustness studies. In D. O. Thompson and D. E. Chimenti, editors, *Review of Progress in Quantitative NDE 27*, pages 142–149. AIP, 2008.

[31] J. Davies and P. Cawley. The application of synthetic focusing for imaging crack-like defects in pipelines using guided waves. *IEEE Trans. Ultrason. Ferroelectr. Freq. Control*, 56:759–771, 2009.

[32] J. Davies, F. Simonetti, M. J. S. Lowe, and P. Cawley. Review of synthetically focused guided wave imaging techniques with application to defect sizing. In D. O. Thompson and D. E. Chimenti, editors, *Review of Progress in Quantitative NDE 25*, pages 142–149. AIP, Plenum, New York, 2006.

[33] A. Demma, P. Cawley, M. Lowe, A. G. Roosenbrand, and B. Pavlakovic. The reflection of guided waves from notches in pipes: a guide for interpreting corrosion measurements. *NDT & E International*, 37:167–180, 2004.

[34] A. Demma, P. Cawley, and M. J. S. Lowe. Scattering of the fundamental shear horizontal mode from steps and notches in plates. *J. Acoust. Soc. Am.*, 113(4):1880–1891, 2003.

[35] A. Demma, P. Cawley, M. J. S. Lowe, and B. Pavlakovic. The effect of bends on the propagation of guided waves in pipes. *Journal of Pressure Vessel Technology*, 127: 328–355, 2005.

[36] A. Demma, P. Cawley, M. J. S. Lowe, and A. G. Roosenbrand. The reflection of the fundamental torsional mode from cracks and notches in pipes. *J. Acoust. Soc. Am.*, 114:611–625, 2003.

[37] Alessandro Demma. *The interaction of guided waves with discontinuities in structures*. PhD thesis, University of London, 2003.

[38] O. Diligent, T. Grahn, A. Bostrom, P. Cawley, and M. J. S. Lowe. The low frequency reflection and scattering of the S0 Lamb mode from a circular through-thickness hole in a plate: finite element, analytical and experimental studies. *J. Acoust. Soc. Am.*, 112 (6):2589–2601, 2002.

[39] O. Diligent and M. J. S. Lowe. Reflection of the S0 Lamb mode from a flat bottom circular hole. *J. Acoust. Soc. Am.*, 118(5):2869–2879, 2005.

[40] J. J. Ditri. Utilization of guided elastic waves for the characterization of circumferential cracks in hollow cylinders. *J. Acoust. Soc. Am.*, 96(6):3769–3775, 1994.

[41] J. J. Ditri. Some results on the scattering of guided elastic SH waves from material and geometric waveguide discontinuities. *J. Acoust. Soc. Am.*, 100(5):3078–3087, 1996.

[42] S. Dixon, C. Edwards, and S. B. Palmer. Texture measurements of metal sheets using wideband electromagnetic acoustic transducers. *J. Phys. D: Appl. Phys.*, 35:816–824, 2002.

[43] D. W. Eades, E. M. Hawkes, and S. A. Lockyer. Ratcliffe Boiler 1: Failure of Cold Form Bend RS7/4. Technical report, E.ON UK Plc, 2006. PT/06/BB386/R.

[44] Jimmy Fong. *A study of curvature effects on guided elastic waves*. PhD thesis, University of London, 2005.

[45] A. Freedman. On the 'overlapping resonances' concept of acoustic transmission through an elastic plate. i - an examination of properties. *J. Sound Vib.*, 82:181–195, 197–213, 1982.

[46] P. Fromme, P. Wilcox, M. J. S. Lowe, and P. Cawley. A guided ultrasonic wave array for structural integrity monitoring. In D. O. Thompson and D. E. Chimenti, editors, *Review of Progress in Quantitative NDE 24*, pages 1780–1787. AIP, Plenum, New York, 2005.

[47] H. M. Frost. Electromagnetic-ultrasound transducers: principles, practice, and applications. In H. M. Mason and R. N. Thurston, editors, *Physical Acoustics XIV*, pages 179–275. New York: Academic Press, 1979.

[48] A. Galvagni and P. Cawley. The reflection of guided waves from simple supports in pipes. *J. Acoust. Soc. Am.*, 129(4):1869–1880, 2011.

[49] J. Gauthier, V. Mustafa, A. Chabbaz, and D. R. Hay. EMAT generation of horizontally polarized guided shear waves for ultrasonic pipe inspection. In *ASME Int. Pipeline Conf. 1*, pages 327–334, 1998.

[50] L. Gavric. Computation of propagative waves in free rail using a finite element technique. *J. Sound Vib.*, 185(3):531–543, 1995.

[51] D. Gazis. Three dimensional investigation of the propagation of waves in hollow circular cylinders. *J. Acoust. Soc. Am.*, 31:568–578, 1959.

[52] D. C. Gazis. Exact analysis of the plane-strain vibrations of thick-walled hollow cylinders. *J. Acoust. Soc. Am.*, 30(8):786–794, 1958.

[53] T. Hayashi, K Kawashima, Z. Sun, and J. L. Rose. Analysis of flexural mode focusing by a semianalytical. *J. Acoust. Soc. Am.*, 113(3):1241–1248, 2003.

[54] T. Hayashi and M. Murase. Defect imaging with guided waves in a pipe. *J. Acoust. Soc. Am.*, 117(4):2134–2140, 2005.

[55] P. Hőller and A. Wilbrand. Electromagnetic ultrasonic testing. *Traitement du Signal*, 2 (5):459–464, 1985.

[56] M. Hirao and H. Ogi. An SH-wave EMAT technique for gas pipeline inspection. *NDT & E International*, 32(3):127–132, 1999.

[57] C. Holmes, B. Drinkwater, and P. Wilcox. The post-processing of ultrasonic data using the total focusing method. *Insight*, 46(11):677–680, 2004.

[58] D. Howe. Private communication, 2012.

[59] M. Karaman, P-C. Li, and M. O'Donnell. Synthetic aperture imaging for small scale systems. *IEEE Trans. Ultrason. Ferroelectr. Freq. Control*, 42(3):429–442, 1995.

[60] J. Krautkramer and H. Krautkramer. *Ultrasonic testing of materials*. Springer, 1977.

[61] H. Kwun, S. Y. Kim, M. S. Choi, and S. M. Walker. Torsional guided-wave attenuation in coal-tar-enamel-coated, buried piping. *NDT & E International*, 37(8):663–665, 2004.

[62] H. Kwun, S-Y. Kim, and G. M. Light. Long-range guided wave inspection of structures using the magnetostrictive sensor. *J. Korean Soc. NDT*, 2001.

[63] H. Kwun, S. Y. Kim, and G. M. Light. The magnetostrictive sensor technology for long range guided wave testing and monitoring of structures. *Mat. Eval.*, 61:80–84, 2003.

[64] H. Lamb. On waves in an elastic plate. *Proc. R. Soc. London. Ser. A*, pages 114–128, 1917.

[65] V. M. N. Ledesma, E. Perez-Baruch, A. Demma, and M. J. S. Lowe. Guided wave testing of an immersed gas pipeline. *Mat. Eval.*, 67(2):102–115, 2009.

[66] J. Li and J. L. Rose. Implementing guided wave mode control by use of a phased transducer array. *IEEE Trans. Ultrason. Ferroelectr. Freq. Control*, 49(12):1720–1729, 2001.

[67] J. Li and J. L. Rose. Natural beam focusing of non-axisymmetric guided waves in large-diameter pipes. *Ultrasonics*, 44:35–45, 2006.

[68] M. J. S. Lowe. Matrix techniques for modelling ultrasonic waves in multilayered media. *IEEE Trans. Ultrason. Ferroelectr. Freq. Control*, 42(4):525–542, 1995.

[69] M. J. S. Lowe, D. N. Alleyne, and P. Cawley. The mode conversion of a guided wave by a part-circumferential notch in a pipe. *J. Appl. Mech.*, 65:649–656, 1998.

[70] M. J. S. Lowe and P. Cawley. Long range guided wave inspection usage - current commercial capabilities and research directions. Technical report, Department of Mechanical Engineering, Imperial College London, 2006. can be found at: http://www3.imperial.ac.uk/pls/portallive/docs/1/55745699.pdf.

[71] M. J. S. Lowe, P. Cawley, J-Y. Kao, and O. Diligent. The low frequency reflection characteristics of the fundamental antisymmetric Lamb wave A0 from a rectangular notch in a plate. *J. Acoust. Soc. Am.*, 112(6):2612–2622, 2002.

[72] M. J. S. Lowe and O. Diligent. Low-frequency reflection characteristics of the S0 Lamb wave from a rectangular notch in a plate. *J. Acoust. Soc. Am.*, 111(1):64–74, 2001.

[73] Guided Ultrasonics Ltd. *Wavemaker G3 Level 1 Training Pack*. Guided Ultrasonics Ltd, 17 Doverbeck Close, Ravenshead, Nottingham, May 2007.

[74] L. E. Malvern. *Introduction to the mechanics of a continuous medium*. Prentice-Hall, 1969.

[75] *Matlab ®7*. The MathWorks Inc., The MathWorks Inc., 3 Apple Hill Drive, Natick, Ma, 01760-2098, 7 edition, 2009. www.mathworks.com.

[76] W. Mohr and P. Hőller. On inspection of thin-walled tubes for transverse and longitudinal flaws by guided ultrasonic waves. *IEEE Trans. Sonics Ultrason.*, 23(5):369–374, 1976.

[77] P. M. Morse and H. Feshbach. *Methods of theoretical physics*. McGraw-Hill Book Company, 1953.

[78] P. J. Mudge. Field application of the Teletest® long-range ultrasonic testing technique. *Insight*, 43(2):74–77, 2001.

[79] D. Murray. Private communication, 2012.

[80] K. Nagai. A new synthetic-aperture focusing method for ultrasonic B-scan imaging by the Fourier transform. *IEEE Trans. Sonics Ultrason.*, 32:531–536, 1985.

[81] BBC News. Accident shuts down power station. Internet article, 2006. http://news.bbc.co.uk/1/hi/england/nottinghamshire/5153024.stm.

[82] F. Niese, H-J. Salzburger, and J. Zenner. Scannende prüfung auf aussenkorrosion an rohrleitungen mittels umlaufender geführter wellen. Technical report, Fraunhofer IZFP,

2007. can be found at http://publica.fraunhofer.de/starweb/ep09/servlet.starweb (as of 2011).

[83] M. Onoe, H. D. McNiven, and R. D. Mindlin. Dispersion of axially symmetric waves in elastic rods. *J. Appl. Mech.*, 29(4):729–734, 1962.

[84] Y. H. Pao and R. D. Mindlin. Dispersion of flexural waves in an elastic, circular cylinder. *J. Appl. Mech.*, 27(3):513–520, 1960.

[85] B. N. Pavlakovic. *Leaky guided ultrasonic waves in NDT*. PhD thesis, University of London, 1998.

[86] B. N. Pavlakovic, M. J. S. Lowe, D. N. Alleyne, and P. Cawley. Disperse: A general purpose program for creating dispersion curves. In D. O. Thompson and D. E. Chimenti, editors, *Review of Progress in Quantitative NDE 16*, pages 185–192. AIP, Plenum, New York, 1997.

[87] P. Rajagapol and M. J. S. Lowe. Short range scattering of the fundamental shear horizontal guided wave mode normally incident at a through-thickness crack in an isotropic plate. *J. Acoust. Soc. Am*, 122(3):1527–1538, 2007.

[88] P. Rajagapol and M. J. S. Lowe. Angular influence on the scattering of fundamental shear horizontal guided waves by a through-thickness crack in an isotropic plate. *J. Acoust. Soc. Am.*, 124(4):2021–2030, 2008.

[89] P. Rajagapol and M. J. S. Lowe. Scattering of the fundamental shear horizontal guided wave by a part-thickness crack in an isotropic plate. *J. Acoust. Soc. Am.*, 124(5): 2895–2904, 2008.

[90] M. Ratassepp, S. Fletcher, and M. J. S. Lowe. Scattering of the fundamental torsional mode at an axial crack in a pipe. *J. Acoust. Soc. Am.*, 127(2):730–740, 2010.

[91] M. Ratassepp, M. J. S. Lowe, P. Cawley, and A. Klauson. Scattering of the fundamental shear horizontal mode in a plate when incident at a through crack aligned in the propagation direction of the mode. *J. Acoust. Soc. Am.*, 124(5):2873–2882, 2008.

[92] F. Ravenscroft, R. Hill, C. Duffill, and D. Buttle. A new ultrasonic method for rapid screening of pipe, plate and inaccessible geometries. *J. Nondestruct. Test. Ultrason. (Germany)*, 3(10):103, 1998.

[93] Lord Rayleigh. On waves propagating along the plane surfaces of an elastic solid. *Proc. London Math. Soc.*, 17(1):4–11, 1885.

[94] Lord Rayleigh. On the free vibrations of an infinite plate of homogeneous isotropic elastic matter. *Proc. London Math. Soc.*, 20(1):225–237, 1888.

[95] J. L. Rose, M. J. Avioli, and Y Cho. Elastic wave analysis for broken rail detection. In D. O. Thompson and D. E Chimenti, editors, *AIP Conference Proceedings*, pages 1806–1812. AIP, 2002.

[96] J. L. Rose and P. J. Mudge. Flexural mode focusing in a pipe. In *8th European Conference on Non-Destructive Testing (ECNDT)*, 2002.

[97] J. L. Rose and X. Zhao. Anomaly throughwall depth measurement potential with shear horizontal guided waves. *Mat. Eval.*, 59(10):1234–1238, 2001.

[98] C. B. Scruby and L. E. Drain. *Laser ultrasonics: techniques and applications*. Adam Hilger, Bristol, 1990.

[99] M. G. Silk and K. F. Bainton. The propagation in metal tubing of ultrasonic wave modes equivalent to Lamb waves. *Ultrasonics*, 17:11–19, 1979.

[100] F. Simonetti and P. Cawley. On the nature of shear horizontal wave propagation in elastic plates coated with viscoelastic materials. *Proc. Royal Soc. Lond.: Mathematical, Physical and Engineering Sciences*, 460:2197–2221, 2004.

[101] S. B. Spurr. Development of inspection methods that reduce preparation requirements for plant. review of electromagnetic acoustic transducers (emat) for the thickness measurement of boiler tubing. Technical report, Powergen, 2002. PT/02/BB2413/R.

[102] R. N. Thomson. Transverse and longitudinal resolution of the synthetic aperture focusing technique. *Ultrasonics*, 22(1):9–15, 1984.

[103] C. Valle, M. Neithammer, J. Qu, and L. Jacobs. Crack characterisation using guided circumferential waves. *J. Acoust. Soc. Am.*, 110(3):1282–1290, 2001.

[104] C. Valle, J. Qu, and L. Jacobs. Guided circumferential waves in layered cylinders. *Int. J. Eng. Sci.*, 37:1369–1387, 1999.

[105] I. A. Victorov. *Rayleigh and Lamb Waves*. Plenum Press, 1970.

[106] P. Wilcox, M. Evans, B. Pavlakovic, D. Alleyne, K. Vine, P. Cawley, and M. Lowe. Guided wave testing of rail. *Insight*, 45:413–420, 2003.

[107] P. Wilcox, M. Lowe, and P. Cawley. The effect of dispersion on long-range inspection using ultrasonic guided waves. *NDT & E International*, 34(1):1–9, 2001.

[108] P. Wilcox, M. Lowe, and P. Cawley. Omnidirectional guided wave inspection of large metallic plate structures using an emat array. *IEEE Trans. Ultrason. Ferroelectr. Freq. Control*, 52:653–665, 2005.

[109] P. D. Wilcox, M. J. S. Lowe, and P. Cawley. Long range Lamb wave inspection: the effect of dispersion and modal selectivity. In D. Thompson and D. Chimenti, editors, *Review of Progress in Quantitative NDE 18*, pages 151–158. AIP, Plenum, New York, 1999.

[110] Paul Wilcox. *Lamb wave inspection of large structures using permanently attached transducers*. PhD thesis, University of London, 1998.

[111] D. C. Worlton. Experimental confirmation of Lamb waves at megacycle frequencies. *J. Appl. Phys.*, 32(6):967–971, 1961.

[112] W. Zhu. An FEM simulation for guided elastic wave generation and reflection in hollow cylinders with corrosion defects. *Journal of Pressure Vessel Technology*, 124(1):107–117, 2002.

List of Publications

[P1] M. Ratassepp, S. Fletcher, M. Lowe. Scattering of the fundamental torsional mode at an axial crack in a pipe. *J. Acoust. Soc. Am.*, 127(2):730-740, 2010.

[P2] S. Fletcher, M. J. S. Lowe, M. Ratassepp and C. Brett. Detection of axial cracks in pipes using focused guided waves. *J. Nondestruct. Eval.*, 2011 *Accepted*